Electrochemical and Optical Sensors for Ion Sensing

Jansod, Sutida

UNIVERSITÉ DE GENÈVE
Section de chimie et biochimie
Département de chimie analytique et minérale

FACULTE DES SCIENCES
Professeur Eric Bakker

Electrochemical and Optical Sensors for Ion Sensing

THÈSE

Présentée à la Faculté des Sciences de l'Université de Genève
pour obtenir le grade de Docteur ès sciences, mention chimie

par
Sutida JANSOD
De Thaïlande

Thèse N° 5534

GENÈVE
Atelier d'impression ReproMail
2021

UNIVERSITÉ DE GENÈVE
FACULTÉ DES SCIENCES

DOCTORAT ÈS SCIENCES, MENTION CHIMIE

Thèse de Madame Sutida JANSOD

intitulée :

«Electrochemical and Optical Sensors for Ion Sensing»

La Faculté des sciences, sur le préavis de Monsieur E. BAKKER, professeur ordinaire et directeur de thèse (Département de chimie minérale et analytique), Monsieur R. MILTON, professeur assistant (Département de chimie minérale et analytique) et Monsieur H. GIRAULT, professeur (Laboratoire d'électrochimie physique et analytique, École Polytechnique Fédérale de Lausanne, Suisse), autorise l'impression de la présente thèse, sans exprimer d'opinion sur les propositions qui y sont énoncées.

Genève, le 4 janvier 2021

Thèse - 5534 -

Le Doyen

N.B. - La thèse doit porter la déclaration précédente et remplir les conditions énumérées dans les "Informations relatives aux thèses de doctorat à l'Université de Genève".

Abstract

Sensing platforms based on optical sensors have been growing rapidly owing to their simple readout, ease of miniaturization and the fact that they do not require an external power source. However, major limitations of traditional optical sensors (e.g., optical interferences and the effect of ionic strength on the sensor readout) need to be improved. Potentiometric sensors based on polymeric membrane ion-selective electrodes (ISEs) are well-established tools for measuring ion activities in various electrolytes (e.g., blood, serum). They have been important in the fields of clinical diagnosis, environmental monitoring and pharmaceuticals. Recently, attention has been significantly drawn to integrated sensing devices. The combination of sensing tools allows us to obtain additional analytical information and/or improve the performance characteristics of the sensors (e.g., sensitivity, selectivity, robustness). Recently, the readout of ISEs has been expanded to a broad range of electrochemical techniques such as chronopotentiometry, voltammetry and coulometry. It has also included optical sensing methods where colorimetric probes or/and materials are utilized as optical displays. However, the ISE has not yet been coupled into an optical redox indicator to directly read out the potential change of the sensing probe.

The main goals of this thesis have been development and fabrication of integrated devices by coupling an optical redox indicator and the potentiometric sensor into a closed bipolar electrode platform, where the detection compartment is physically separated from the sample solution. This platform may overcome some major limitations of the traditional optical sensors: (i) colored/turbid samples do not interfere with optical sensing, (ii) extra-thermodynamic assumptions that deviate from potentiometric sensing probes are no longer required in the proposed integrated sensors, and (iii) the optical readout is not affected by ionic strength. A water-soluble 1,10-phenanthroline iron (II) complex (Chapter 3 – 4) and electrochromic Prussian Blue (PB) film (Chapter 5) have been exploited as the optical displays in the detection compartment. In the bipolar electrode system, the cell potential is kept constant by the assistance of an external power source (e.g., potentiostat). The potential change, triggered by the change in ion activity in the sample solution, is compensated by the potential of the optical redox indicator. This results in a transient current at the bipolar electrode, which results in a color change of the colorimetric redox indicator. The tunable color readout is analyzed at zero current once the new equilibrium is established. The working range of the system can be electrochemically altered by the potentiostat. The optical signals (e.g., hue from HSV (hue, saturation, value), and absorbance from RGB (red, green, blue) color patterns) serve as the analytical signals and are recorded by a digital camera. The images are computed by converting the colors into sensing numbers.

Moreover, we have shown the simultaneous optical readout of a potentiometric sensor array using Prussian Blue films as the redox indicator in the detection compartment (Chapter 5). The simultaneous

detection of multiple analytes in colored fruit juice samples is achieved. Furthermore, we have demonstrated a self-powered colorimetric absorbance-based PB array of potentiometric ISEs in a short circuited system without the use of the external power supply (Chapter 6). The sufficient energy generated by the ISE in the sample compartment directly triggers the color change of the PB film in the detection compartment. The working range can be chemically modulated by changing the composition of inner filling solution of the ISE, membrane composition and electrolyte in contact with PB film. We have found that the response time is faster compared to the case where the cell potential is dictated by the external power source.

Apart from the integrated sensing devices described above we have introduced a lipophilic Os(II)/Os(III) dinonyl bipyridyl complex, which is explored as an ion-to-electron transducer in thin layer ion transfer voltammetry (Chapter 2). The ratio of Os(II) complex and cation exchanger in the thin membrane can promote either cation transfer or anion transfer. The addition of tetraalkylammonium additive gives near-ideal voltammetric behavior, which suggest that it acts as an important phase transfer catalyst. This new Os(II) mediator could avoid electrochemical irreversibility problems of other commonly used conducting polymer based mediators (e.g., poly(3-octylthiophene) (POT), ferrocene).

The thesis has been divided into six chapters. Each on demonstrates the fundamental and developmental aspects of the associated topic.

Chapter 1 presents a basic overview of electrochemical and optical sensors for ion-sensing. This includes the fundamental background and discussion of the ISEs, dynamic electrochemistry, ion-transfer principle, optical sensors, colorimetric analysis, electrochemical and optical sensing arrays, bipolar electrode sensors and self-powered sensors based on ISEs.

Chapter 2 Introduces a new redox buffer of lipophilic Os(II)/Os(III) dinonyl bipyridyl complex as a molecular ion-to-electron transducing probe in polymeric thin film. This probe is replaced and overcomes some limitations of conducing polymers (e.g., poly(3-octylthiophene) (POT)). This redox buffer is directly dissolved in the sensing thin film for the mediation of ion-transfer at a membrane-sample interface by using ion-transfer voltammetry. A particular ratio between the concentration of the redox probe and cation exchanger is found to be a key for the fabrication of either cation or anion sensors.

Chapter 3 shows a proof of concept of a tunable optical readout using the ISE as the potentiometric sensing probe with closed-bipolar electrode configuration, which overcomes some drawbacks of traditional optical sensors. A potential change at the potentiometric probe in the sample is compensated by the potential change of water-soluble redox indicator (ferroin) in a thin layer detection compartment. This results in a modulation of oxidized/reduced forms of the indicator. A chloride responsive Ag/AgCl electrode and a liquid membrane-based calcium-selective membrane electrode are successfully

demonstrated. The optical signals are computed into hue value based on colorimetric analysis. This principle is readily expanded to determine other ionic species with conventional liquid-contact ISEs. A working range is electrochemically modulated by a potentiostat.

Chapter 4 explores the theoretical response mechanism of bipolar ion-selective optical sensors based on the traditional plasticized polymeric membranes for determination of a variety of ions. This approach was used to successfully measure potassium content in colored samples by using ferroin indicator as the colorimetric readout.

Chapter 5 exhibits the simultaneous optical readout of a potentiometric sensor array of ionophore-based ISEs. An electrochromic Prussian Blue (PB)/Prussian White (PW) thin film replaced the water-soluble redox ferroin indicator in the detection compartment. A multiple cation-bipolar electrode array achievably measures potassium, sodium and calcium in colored fruit juices. This chapter contains theoretical aspects of the principle of operation of the multiple bipolar sensing array, equilibrium theory, electrochemical and absorbance-based colorimetric behaviors of PB films.

Chapter 6 shows the state-of-the-art self-powered optical sensor array empowered by the ISEs in a short circuited cell without the use of an external supply. The potentiometric response of the ISE serves as a power generator and directly powers the potential of the electrochromic PB film. A working range is chemically tuned by varying the concentration of inner filling solution of the ISE, membrane composition and electrolyte in contact with the PB film in the detection compartment. Theoretical aspects are described and correlate well with the experimental results.

Résumé

Les plates-formes de capteurs opto-chimiques ont connu une croissance rapide en raison de leur lecture simple, de leur facilité de miniaturisation et de leurs sources d'alimentation externes non requises. Cependant, les limitations majeures des capteurs optiques traditionnels (par exemple, interférences optiques, effet de force ionique) doivent être améliorées. Les capteurs potentiométriques basés sur des électrodes ion-sélectives à membrane polymère (ISE) sont des outils bien établis pour mesurer les activités ioniques dans divers électrolytes (par exemple, le sang, le sérum). Ils ont joué un rôle important dans les domaines du diagnostic clinique, de la surveillance environnementale et des produits pharmaceutiques. Récemment, l'attention a été fortement attirée sur les dispositifs de détection intégrés. La combinaison d'outils de détection nous permet d'obtenir des informations analytiques supplémentaires et / ou d'améliorer les caractéristiques de performance des capteurs (par exemple, sensibilité, sélectivité, robustesse). Le principe de lecture potentiométrique a été étendu à une large gamme de techniques électrochimiques telles que la chronopotentiométrie, la voltamétrie et la coulométrie. De plus, il a couvert les procédés de détection optique, dans lesquels les sondes colorimétriques ou / et les matériaux ont été utilisés comme affichages optiques. Cependant, l'ISE n'a jamais été traduit en un indicateur redox optique.

Les principaux objectifs de cette thèse ont été le développement et la fabrication de dispositifs intégrés en couplant un indicateur redox optique et des systèmes de détection potentiométrique dans une plate-forme d'électrode bipolaire fermée, au niveau de laquelle le compartiment de détection est physiquement séparé de la solution échantillon. Cette plate-forme a surmonté certaines limitations majeures des capteurs optiques traditionnels tels que: (i) les échantillons colorés / troubles n'interfèrent pas avec la détection optique, (ii) les hypothèses extra-thermodynamiques n'étaient pas nécessaires dans les capteurs intégrés proposés, et (iii) le la lecture optique n'est pas affectée par la force ionique. Un complexe de 1,10-phénanthroline fer (II) soluble dans l'eau (chapitre 3-4) et un film de bleu de Prusse électrochrome (PB) (chapitre 5) ont été exploités comme afficheurs optiques dans le compartiment de détection. Dans le système d'électrodes bipolaires, le potentiel de la cellule est maintenu constant par une assistance d'une source d'alimentation externe (par exemple, un potentiostat). Le changement de potentiel, en fonction du changement du niveau d'activité ionique dans la solution échantillon, est compensé par le potentiel de l'indicateur redox optique. Il en résulte un courant transitoire dans l'électrode bipolaire, ce qui nécessite le changement de couleur de l'indicateur redox colorimétrique. La lecture de la couleur réglable est analysée, au cours de laquelle le nouvel équilibre est établi (courant nul). La plage de travail du système peut être modifiée électrochimiquement par le potentiostat. Les signaux optiques (par exemple, la teinte de HSV (teinte, saturation, valeur) et l'absorbance des motifs de couleur RVB (rouge, vert, bleu)), ont

servi de signaux analytiques sont suivis par un appareil photo numérique. Les images enregistrées sont calculées en convertissant les couleurs en nombres de détection.

De plus, nous avons montré la lecture optique simultanée pour un réseau de capteurs potentiométriques en utilisant les films PB comme indicateur redox dans le compartiment de détection (chapitre 5). La détection simultanée de plusieurs analytes dans des échantillons de jus de fruits colorés est obtenue. En outre, nous avons démontré un tableau PB basé sur l'absorbance colorimétrique auto-alimenté d'ISE potentiométriques dans un système en court-circuit sans l'utilisation de l'alimentation externe (chapitre 6). L'énergie suffisante générée par l'ISE dans le compartiment à échantillon déclenche directement le changement de couleur du film PB dans le compartiment de détection. La plage de travail peut être modulée chimiquement en changeant la composition de la solution de remplissage interne de l'ISE, la composition de la membrane et l'électrolyte en contact avec le film PB. Nous avons constaté que le temps de réponse est plus rapide par rapport à un, où le potentiel de la cellule est dicté par la source d'alimentation externe.

Outre les capteurs intégrés, nous avons introduit un complexe lipophile de dinonyl bipyridyl Os(II)/Os(III), qui est exploité comme transducteur ion-électron en voltamétrie de transfert d'ions en couche mince (chapitre 2). Les différents processus de transfert d'ions sont interrogés en utilisant la voltamétrie cyclique. Le rapport du complexe Os (II) et de l'échangeur de cations dans la membrane mince peut favoriser soit le transfert de cations, soit le transfert d'anions. L'addition d'additif tétralkylammonium donne un comportement voltammétrique presque idéal, ce qui suggère qu'il agit comme un catalyseur de transfert de phase important. Ce nouveau médiateur Os (II) pourrait éviter les problèmes d'irréversibilité électrochimique d'autres médiateurs à base de polymère conducteur couramment utilisés (par exemple, poly (3-octylthiophène) (POT), ferrocène).

La thèse est divisée en six chapitres. Chacun démontre les aspects fondamentaux et développementaux.

Le chapitre 1 présente un aperçu de base des capteurs électrochimiques et optiques pour la détection d'ions. Il inclut le contexte fondamental et la discussion des ISE, l'électrochimie dynamique, le principe de transfert d'ions, les capteurs optiques, l'analyse colorimétrique, les réseaux de détection électrochimique et optique, les capteurs d'électrodes bipolaires et les senseurs auto-alimentés basés sur les ISE.

Le chapitre 2 présente un nouveau tampon redox basé sur le complexe lipophile dinonyl bipyridyl Os (II)/Os (III) comme sonde de transduction moléculaire ion-à-électron dans un film polymérique fin. Cette sonde est remplacée et surmonte certaines limitations des polymères conducteurs (par exemple le poly (3-octylthiophène) (POT)). Ce tampon redox est directement dissous dans le film fin de détection pour permettre la médiation du transfert d'ions à l'interface membrane-échantillon en utilisant la voltammétrie

à transfert d'ions. Un rapport précis entre la concentration de la sonde redox et de l'échangeur de cations s'avère être clé pour la fabrication de capteurs de cations ou d'anions.

Le chapitre 3 montre la démonstration de faisabilité d'une lecture optique modulable utilisant l'ISE comme sonde de détection potentiométrique avec une configuration d'électrode bipolaire fermée, qui surmonte certains inconvénients des capteurs optiques traditionnels. Un changement de potentiel au niveau de la sonde potentiométrique dans l'échantillon est compensé par le changement de potentiel de l'indicateur redox soluble dans l'eau (ferroïne) dans un compartiment de détection à couche mince. Il en résulte une modulation des formes oxydées/réduites de l'indicateur. Une électrode Ag/AgCl sensible aux chlorures et une électrode sélective au calcium basée une membrane polymérique avec solution interne de référence sont démontrées avec succès. Les signaux optiques sont calculés en valeur de teinte sur la base d'une analyse colorimétrique. Ce principe de détermination peut être facilement étendu à d'autres espèces ioniques avec des ISE conventionnelles utilisant une solution interne de référence. L'étendue de fonctionnement est modulée électrochimiquement par un potentiostat.

Le chapitre 4 explore le mécanisme de réponse théorique des capteurs optiques bipolaires à sélectivité ionique basés sur des membranes polymériques plastifiées traditionnelles pour la détermination de différents ions. Cette approche mesure avec succès les teneurs en potassium dans des échantillons colorés en utilisant la de ferroïne comme indicateur de lecture colorimétrique.

Le chapitre 5 présente la lecture optique simultanée d'un réseau de capteurs potentiométriques composé d'ISE à base d'ionophores. L'indicateur ferroïne redox soluble dans l'eau est remplacé par un film électrochrome fin à base de bleu de Prusse (PB)/blanc de Prusse (PW) dans le compartiment de détection. Un réseau multiple d'électrodes bipolaires sélectives aux cations mesure le potassium, le sodium et le calcium dans les jus de fruits colorés. Ce chapitre inclut les aspects théoriques du fonctionnement du principe du réseau de détection bipolaire multiple, la théorie de l'équilibre et les comportements colorimétriques basés sur l'électrochimie et l'absorbance des films de PB.

Le chapitre 6 montre un réseau de capteurs optiques auto-alimenté de pointe, alimenté par les ISE dans un système court-circuité sans l'utilisation d'une alimentation externe. Une réponse potentiométrique suffisante de l'ISE sert de générateur d'énergie et alimente directement le potentiel du film électrochrome à base de PB. L'étendue de fonctionnement est réglée chimiquement en faisant varier la concentration de la solution de remplissage interne de l'ISE, la composition de la membrane et l'électrolyte en contact avec le film de PB dans le compartiment de détection. Les aspects théoriques sont bien corrélés aux résultats expérimentaux.

List of Publications

1. **Jansod, S.**; Bakker, E., Self-powered colorimetric sensing array based on ion-selective electrodes. (submitted).

2. **Jansod, S.**; Cherubini, T.; Soda, Y.; Bakker, E., Optical sensing with a potentiometric sensing array by Prussian blue film integrated closed bipolar electrodes. *Anal. Chem.* **2020**, *92*, 9138-9145.

3. **Jansod, S.**; Bakker, E., Tunable Optical Sensing with PVC Membrane Based Ion-Selective Bipolar Electrodes. *ACS Sens.* **2019**, *4*, 1008-1016.

4. **Jansod, S.**; Cuartero, M.; Cherubini, T.; Bakker, E., Colorimetric Readout for Potentiometric Sensors with Closed Bipolar Electrodes. *Anal. Chem.* **2018**, *90*, 6376-6379.

5. **Jansod, S.**; Wang, L.; Cuartero, M.; Bakker, E., Electrochemical ion transfer mediated by a lipophilic Os(ii)/Os(iii) dinonyl bipyridyl probe incorporated in thin film membranes. *Chem. Commun.* **2017**, *53*, 10757-10760.

6. **Jansod, S.**; Ghahraman Afshar, M.; Crespo, G. A.; Bakker, E., Alkalinization of Thin Layer Samples with a Selective Proton Sink Membrane Electrode for Detecting Carbonate by Carbonate-Selective Electrodes. *Anal. Chem.* **2016**, *88*, 3444-3448.

7. **Jansod, S.**; Afshar, M. G.; Crespo, G. A.; Bakker, E., Phenytoin speciation with potentiometric and chronopotentiometric ion-selective membrane electrodes. *Biosens. Bioelectron.* **2016**, *79*, 114-120.

Acknowledgements

I would like to express my gratitude and appreciation to Prof. Eric Bakker for all of his guidance, dedication, patience, understanding and encouragement during my four year journey. He has inspired me and showed me how beautiful electrochemistry is. I really enjoy doing my PhD here and I extremely appreciate his personality and his warm smiles.

I am very grateful to Prof. Hubert Girault from the Ecole Polytechnique Fédérale de Lausanne (EPFL) and Prof. Ross Milton from the University of Geneva for having accepted the request to review my thesis and join the jury for my defense.

I am really thankful to Prof. Thawatchai Tuntulani, who was my advisor during my master's study at Chulalongkorn University in Thailand. I appreciated his kind support and I thank him again for putting me in touch with my supervisor Prof. Eric Bakker.

I am thankful to Thomas Cherubini, Stephane Jeanneret, Serge Rodak and Guy Lecoulte for their technical assistance and support. I very much thank Magali Cissokho for her administrative management and kindness.

I special thank Dr. Maria Cuartero, Ass. Prof. Gaston Crespo and Asst. Prof. Majid Afshar for our successful collaboration, especially their encouragement and support when I did an internship here in 2015 and during my first year of my PhD study.

I would like to thank for my friends, current and former colleagues for their helps and meaningful conversations during my study here: Marie-Lou Tercier-Waeber, Pitchnaree Kraikeaw, Yoshiki Soda, Canwei Mao, Elena Zdrachek, Polina Damala, Sunil Sailapu, Melina Abduo, Nadezda Pankratova, Suphasinee Sateanchok, Supacha Wirojsaengthong, Zdenka Jarolimova, Wenyue Gao, Lu wang, Dajing Yuan, Stefan Meeuwisse. Especially thanks my close friends: Dr. Narongrit Ritjoho and Loic de Sybourg who are always with me through thick and thin and all my friends in Switzerland and Thailand.

I thank Romain Mercerat and Tara Forrest for thesis language correction in French and Dr. Kye Robinson for English language suggestion.

I would like to specially acknowledge the Swiss Government Excellence Scholarship for financial support throughout my PhD study in Switzerland.

Last but not least, I gratefully thank my kindest parents Thassapong and Winya Jansod, my sweetest sisters Jutathip and Surapat Jansod for all unconditional love and giving me the best support that I cannot be more thankful. I would not have been able to reach to this point without them. I am truly overwhelmed.

Contents

Abstract **1**

Résumé **4**

List of Publications **7**

Acknowledgements **8**

Chapter 1: Introduction **11**

1.1 Chemical sensors 11
1.2 Electrochemical sensors 11
1.2.1 Potentiometric sensors 11
1.2.2 Dynamic electrochemistry 14
1.2.2.1 Voltammetry 16
1.2.2.2 Ion-transfer voltammetry 18
1.3 Optical sensors 19
1.3.1 Absorbance-based spectrophotometric devices 20
1.3.2 Absorbance-based digital images devices 22
1.4 Sensor arrays 23
1.4.1 Potentiometric sensor arrays 23
1.4.2 Optical sensor arrays 23
1.5 Bipolar sensing electrode platform 24
1.6 Self-powered sensors 25
1.7 References 27

Chapter 2: Electrochemical Ion Transfer Mediated by a Lipophilic Os(II)/Os(III) Dinonyl Bipytidyl Probe Incorporated in Thin Membranes **33**

2.1 Abstract 33
2.2 Introduction 34
2.3 Experimental Details 35
2.4 Results and Discussion 35
2.5 Conclusions 41
2.6 Acknowledgements 41
2.7 Supporting Information 42
2.7 References 50

Chapter 3: Colorimetric Readout for Potentiometric sensors with Closed Bipolar Electrodes **51**

3.1 Abstract 51
3.2 Introduction 52
3.3 Experimental Details 52
3.4 Results and Discussion 54
3.5 Conclusions 57
3.6 Acknowledgements 58
3.7 Supporting Information 58
3.8 References 60

Chapter 4: Tunable Optical Sensing with PVC-Membrane-Based Ion-Selective Bipolar Electrodes **61**

4.1 Abstract 61
4.2 Introduction 62
4.3 Theory of the Bipolar Ion Sensor 63
4.4 Experimental Details 65
4.5 Results and Discussion 67
4.6 Conclusions 73

4.7 Acknowledgements 73
4.8 Supporting Information 74
4.9 References 79

Chapter 5: Optical Sensing with a Potentiometric Sensing Array by Prussian Blue Film Integrated Closed Bipolar Electrodes 80

5.1 Abstract 80
5.2 Introduction 81
5.3 Principle of operation 82
5.4 Experimental Section 85
5.5 Results and Discussion 87
5.6 Conclusions 92
5.7 Acknowledgements 93
5.8 Supporting Information 94
5.9 References 103

Chapter 6: Self-powered colorimetric sensing array based on ion-selective electrodes 105

6.1 Abstract 105
6.1 Introduction 106
6.2 Results and Discussion 108
6.3 Conclusion 113
6.4 Acknowledgements 113
6.5 Supporting information 113
6.6 References 119

Chapter 7: Conclusions and Outlook 120

Chapter 1: Introduction

1.1 Chemical sensors

Chemical sensors are often utilized for detecting and monitoring various substances. They are widely exploited for measurement of analytes or ionic species by using different mechanisms of molecule-recognition and numerous chemical transducers for transforming their chemical or physical properties into an analytical output.[1–3] The recognition element or host molecule selectively interacts with the guest or target analyte,[4] which later produces a measurable signal where the chemical output can be observed in a form of electrical response (e.g. colorimetric readout and thermometric signal) (scheme 1). The transducer converts the signal of the interaction between receptor/analyte into a physically measurable signal. These chemical sensors can be classified depending on the type of transducer, which may be correlated to the analyte concentrations. Therefore, quantitative analysis can be achieved.

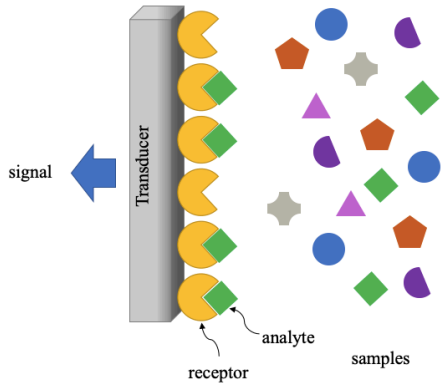

Scheme 1. Illustration of a chemical sensor.

1.2 Electrochemical sensors

The electrochemical sensors employ the electrochemical transducers to transform the chemical information into the electrical signals such as potential, current, charge, impedance. Electrochemical sensors are robust, easy to miniaturize and give attractive detection limits with high sensitivity. Numerous transducers are exploited to fabricate the sensors in order to measure the specific analyte, at which the concentration of the analyte is proportional to the observed electrical output. There are two major groups of electrochemical sensors; i) thermodynamic electrochemistry such as potentiometry and ii) dynamic electrochemistry such as amperometry, voltammetry, coulometry. These sensors have been widely applied in environmental, clinical, pharmaceutical and industrial analyses.

1.2.1 Potentiometric sensors

Potentiometric sensors have been traditionally defined as a zero current method and the most extensively used in practical applications for many decades due to their simplicity, low cost, great selectivity and sensitivity.[5–8] There

are three general groups of potentiometric devices; i) ion-selective electrodes (ISEs), ii) coated wire electrodes (CWEs) and iii) field effect transistors (FETs).[9] While the ISEs based on different matrices, potentiometric sensors based on polymeric or liquid membrane materials are the most widely used as the sensing layer, which physically separates the liquids between an aqueous inner filling solution and sample solution. The ion-selective membranes (ISMs) are employed in the polymeric membrane (e.g. poly(vinylchloride) (PVC)[10–12], polyurethanes (PU)[13–15], polystyrene (PS)[16,17], silicone rubbers[18,19]) and are utilized to construct the ISE. The ISEs have been widely exploited for being capable of selective ionic species including cations (e.g. potassium, sodium, calcium, pH)[20–25], anions (e.g. chloride, nitrite, nitrate, thiocyanate, bicarbonate/carbonate)[20,21,26–29] and polycation (e.g. heparin[30,31] and protamine[32–34]). The ISM must be permselective toward the target analyte or primary ion. Examples of the ISEs based on different matrices include the glass membranes for pH measurement, solid state membranes (e.g. LaF_3 membrane for fluoride detection), precipitates of insoluble salts in polymer matrices (e.g. AgCl, AgBr, AgI, Ag_2S, CuS, CdS, PbS).[35] More typically, the polymeric-based ISM contains a selective receptor (ionophore) (e.g. tridodecylamine for measurement of pH value[36,37], valinomycin for potassium detection), an ionic additive (e.g. sodium tetrakis[3,5-bis(trifluoromethyl)phenyl]borate (NaTFPB), tridodecylmethylammonium chloride (TDMACl) and a plasticizer (e.g. 2-nitrophenyl octyl ether (*o*-NPOE), dioctyl sebacate (DOS)). A lipophilic inert electrolyte (e.g. tetradodecylammonium tetrakis(4-chlorophenyl)borate (ETH500)) is alternatively used to reduce membrane resistance[38] and improve the selectivity by influence of activity coefficient in the membrane phase.[39]

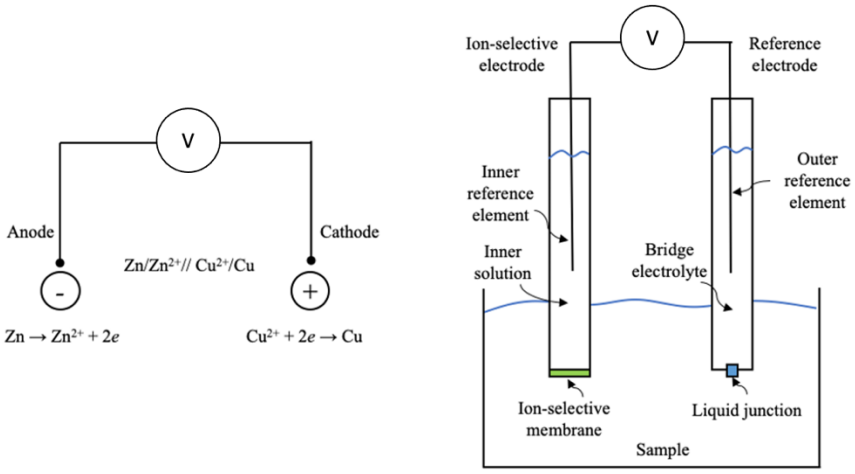

Figure 1. Galvanic cell (left), two-electrode system used for potentiometry (right).[7,40,41]

The potentiometric technique is based on measuring the potential difference (electromotive force, EMF) between the ISE and a reference electrode (e.g. an Ag/AgCl element, double junction reference electrode (Ag/AgCl/KCl, 3M), Hg/Hg_2Cl_2).[41] The potential at the reference electrode must be constant and independent of sample concentration/composition. This is based on a galvanic cell, where the reactions spontaneously occur at the electrodes when they are externally coupled by a conductor (Figure 1, left).[41] A determination in potentiometry is conducted in a two electrode galvanic cell under zero current conditions. Potentiometric sensors basically contain the ISE (cathode, indicator electrode) and reference electrode (anode) (Figure 1, right).[7,8] The potential difference at the membrane/sample interface is measured using a high impedance voltmeter in order to ensure there is no

current flow in the electrochemical cell.[7,8,40,41] Since the potential of the reference electrode remains constant, the potential difference (cell potential) is correlated to the activity of the target analyte or the ion of interest. The ideal relationship between the EMF response and the ion activity is described by the Nernst equation (eq. 1)[7,8,41] as shown below:

$$E_i = E^0 + \frac{RT}{z_i F} ln a_i \qquad \text{eq. 1}$$

where E_i is the potential or EMF readout. R, T and F are the universal gas constant (8.314 J mol^{-1} K^{-1}), absolute temperature (K) and the Faraday constant (96,485 C mol^{-1}), respectively. a_i is an activity of primary ion i in sample solution, z_i is a charge of the primary ion i, E^0 is a constant potential value. At room temperature (298 K), eq. 1 may be written as follows (eq. 2):

$$E_i = E^0 + \frac{s}{z_i} log a_i \qquad \text{eq. 2}$$

where s is the Nernstian slope, typically is 59.2 mV for monovalent cation and 29.6 mV for divalent cation in the absence of interfering ion. If the sample contains other interfering ions with the same charge as the primary ion, these ions may be replaced the primary ion in the ion-selective membrane.[7,8] This results in a deviation from the Nernstian equation. The Nicolsky equation is used as extension of eq. 2 to describe this behavior, as shown in eq. 3.[7,8,40]

$$E_i = E^0 + \frac{s}{z_i} log\left(a_i + \sum_{j \neq i} K_{i,j}^{pot} a_j\right) \qquad \text{eq. 3}$$

where $K_{i,j}^{pot}$ is the selectivity coefficient. a_i and a_j are the activities of primary ion i and interfering ion j in the mixed sample solution, respectively. The smaller value of $K_{i,j}^{pot}$ gives better selectivity of the primary ion over the interfering ion. If the primary and interfering ion have different charges. The eq. 3 is expanded in a semi-empirical manner and to describe the potential change. Eq. 4 is called the Nicolsky-Eisenman equation:[7,8,40]

$$E_i = E^0 + \frac{s}{z_i} log\left(a_i + \sum_{j \neq i} K_{i,j}^{pot} a_j^{z_i/z_j}\right) \qquad \text{eq. 4}$$

The most important characteristic of ISEs is its selectivity. The selectivity coefficients can be measured experimentally by the separate solution method (SSM) and the fixed interference method (FIM) method. The SSM requires individual calibration curves of primary and interfering ion in separate solutions. The selectivity coefficient is calculated by using potential readouts and two activities of primary and interfering ions, which lie on the Nernstian slope of each curve. The selectivity coefficient can be measured based on Nicolski equation, which may be written as shown by eq. 5.[7,40,42]

$$K_{i,j}^{pot} = -\frac{z_i(E_i - E_j)}{s} + log \frac{a_i}{a_j^{z_i/z_j}} \qquad \text{eq. 5}$$

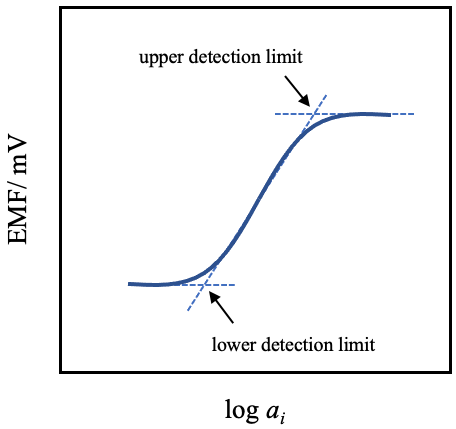

Figure 2. Measurement of upper and lower detection limits of the ion-selective electrode, according to the IUPAC recommendations.[43]

The FIM, however, is the technique where the calibration curve of the primary ion is established in a fixed concentration of interfering ion in the sample solution. The selectivity coefficient can be obtained from the lower detection limit (LDL) of the calibration curve. According to the recommendation of the IUPAC, the lower or upper detection limits are given by the intersection of the two extrapolated linear segments of the calibration curve (Figure 2).[7,42,43]

$$K_{i,j}^{pot} = \frac{a_i(LDL)}{\frac{z_i}{a_j}^{z_j}} \qquad \text{eq. 6}$$

The lowest detection limit of the polymeric membrane-based ISEs is often observed around 1 μM.[7,44–46] This may be caused by limited selectivity or because the ion flux in the inner filling solution (e.g. 10 – 100 mM primary ion) is introduced to the membrane side, resulting in the primary ion leaching into the sample solution. This can be improved by using a small amount of ion exchange in the membrane, which may be the origin of the primary ion leaching into the sample[47] and using a diluted concentration of the primary ion in the inner filling solution or with ion buffers.[25,41,44] The primary ion flux can also be reduced by applying a bias current that counteracts the ion flux, which helps to improve the detection limit to ultra-trace levels.[48] The upper detection limit of the ISEs is defined similarly to the lower detection limit. This may be caused by a breakdown in permselectivity of the ISE membrane (i.e. Donnan exclusion failure).[49–51] An increase of analyte concentration, or an excessive binding affinity between ionophore and analyte, increases the concentration of complexed ionophores in the membrane. Eventually, the membrane begins to act as ion-exchanger and results in a co-extraction of counter ions into the sensing membrane.

1.2.2 Dynamic electrochemistry

Dynamic electrochemistry is different from the thermodynamic electrochemistry (e.g. potentiometric sensors). The electrochemical reaction, which is often related to the oxidation/reduction reaction is measured under non-equilibrium condition and is used to drive a non-spontaneous electrochemical reaction,[41,52] unlike potentiometry where the electrochemical cell is measure under equilibrium or zero current condition (spontaneous reaction). The dynamic electrochemical cell allows one to measure e.g. current, potential, capacitance, charge as a function of an independent variable. This is widely used to classify the electrochemical methods. An electrode

process is a heterogenous reaction, which occurs at the electrode/electrolyte interface. Then, the rate reaction is dependent of mass transfer to electrode and electrode surface effects. The reaction rates are often described by eq. 7.[41]

$$\text{Rate (mol } s^{-1}cm^{-2}) = \frac{i}{nFA} = \frac{j}{nF} \qquad \text{eq. 7}$$

Where i is the current, F is the faraday constant, A is surface area of the working electrode and j is the current density (A/cm^2). This electrode reaction gives information by determining the current as a function of applied potential (i-E curve). The polarization is the departure of cell potential (electrode potential) from an equilibrium value upon passing a Faradaic current.[41,52] The polarization curves are obtained under steady-state conditions. The ideal polarization electrode exhibits a wide change of potential (Figure 3, left). The reference electrode used in the dynamic electrochemical system should be a non-polarizable electrode (Figure 3, right), where its potential is known and constant.

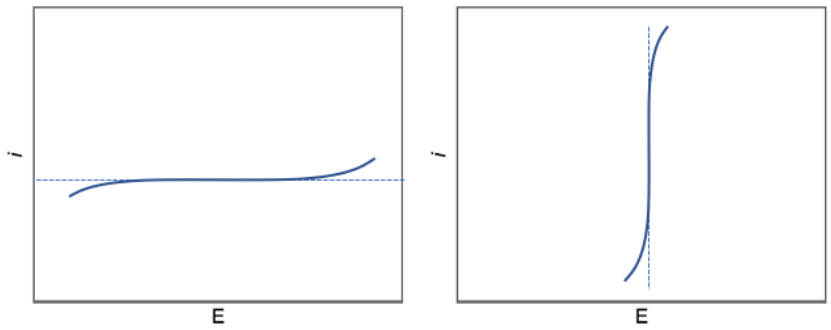

Figure 3. Current-potential curves of ideal (left) polarizable electrode and (right) non-polarizable electrode.

A two-electrode system consists of the working (as the anode) and counter electrodes (as the cathode). The reference electrode provides the reference potential but equally acts as the auxiliary or counter electrode (Scheme 2, left). In this case, the counter electrode is usually larger (surface area) than the working electrode to ensure that the half-reaction taken place at the counter electrode is not limiting the reaction at the working electrode.[41] In this way the current is limited by the working electrode only. This two-electrode system may be used when the electrochemical cell contains a very small ohmic potential drop (iR value of 1-2 mV)[41] and sometimes in classical polarography, where the working electrode is a dropping mercury electrode (DME). An ultramicroelectrode is an example for using this mode as the working electrode gives currents at the nA level.[40,53] Otherwise, the large currents passing between the working and reference electrodes may cause potential changes at the reference electrode and may give rise to limiting currents at the reference electrode.[41]

To overcome the limits stated above, a three-electrode system containing the working electrode, reference electrode, auxiliary or counter electrode (Scheme 2, right) may instead be used in order to prevent the iR drop (or may observe such very small value) between the working and reference electrode.[40,41] Since the current passing through the reference electrode is negligible, the counter electrode allows all the current to pass that is observed at the working electrode. The potential difference at the electrode/electrolyte interface at the working electrode is imposed by the potentiostat/external power supply.

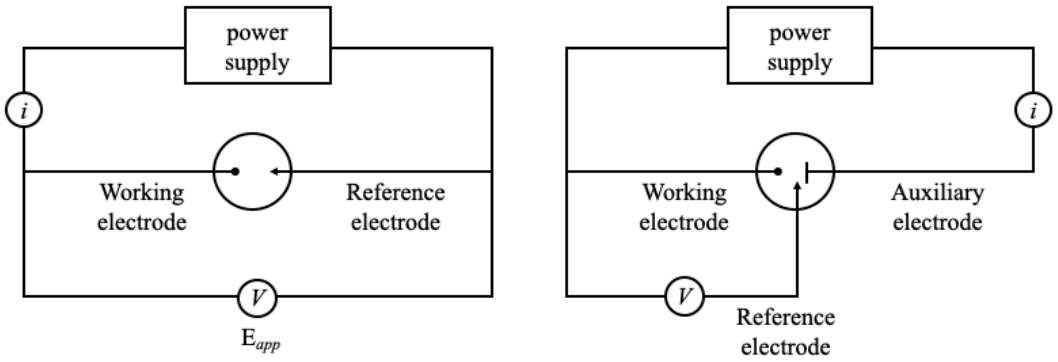

Scheme 2. Electrochemical cell of two-electrode system (left) and three-electrode system (right).[41]

The overall electrode reaction (O + ne ⇌ R) contains a series of steps that cause the conversion of a dissolved oxidized (O) form to a reduced form (R) also in the solution (Scheme 3).[41,52,54] The current is generated by the rate of the process. Generally, the O from bulk solution is transported to the electrode surface by mass transfer. Once it is really near the electrode surface, an electron transfer occurs.[41] There are the chemical reactions and surface reactions in this electrode process. The slowest step becomes a rate limiting (e.g. mass transfer, chemical reaction, charge transfer).

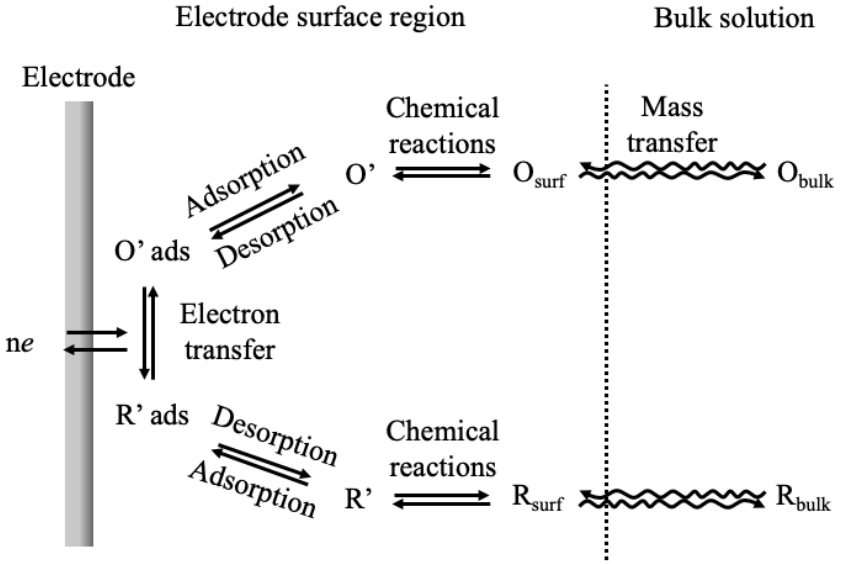

Scheme 3. Pathway of a general electrode reaction.

1.2.2.1 Voltammetry

Voltammetry is a subclass of amperometry, in which the current is typically measured as a function of applied electrode potential,[55] allowing one in some cases to obtain speciation information. They are widely employed for the quantitative analysis of broad organic and inorganic analytes in a variety of matrices. The effects of this applied potential and the behavior of the redox current can be described by either the Nernst equation[41,54] (e.g. concentrations of redox species at electrode surface) as shown in eq. 8 or for limited electron transfer kinetics by

the Butler-Volmer equation. The different voltammetric techniques are classified by their waveform, in which the potential is varied as the function of time (e.g. linear sweep voltammetry, staircase voltammetry, squarewave voltammetry, cyclic voltammetry, chronoamperometry, cathodic/anodic stripping voltammetry, normal pulse voltammetry, differential pulse voltammetry, polarography, adsorptive stripping voltammetry and others).[35,41]

Cyclic voltammetry is widely utilized to study redox processes, intermediate reactions and the stability of the redox probes.[35,41,54] The waveform of the applied potential at the working electrode for the cyclic voltammetry is in forward and backward directions at a constant scan rate (Figure 4a) while measuring the current (Figure 4b). Peak potentials (E_{pc}, E_{pa}) and peak currents (i_{pc}, i_{pa}) of the cathodic and anodic peaks, respectively are important parameters (Figure 4b). A redox indicator (i.e., oxidation-reduction indicator) is an optical indicator that changes color at specific potential difference. It possesses of a reduced (Ind_{red}) and oxidized (Ind_{ox}) form with different colors. The redox process must be reversible, and the oxidation-reduction equilibrium need to be established quickly. The ratio of the redox species is modulated if the potential is changed in order to satisfy eq. 8 and can be measured as shown:[35,41,54]

$$E = E^0 - \frac{RT}{nF} ln \frac{[Ind_{red}]}{[Ind_{ox}]} \qquad \text{eq. 8}$$

Where E^0 is the standard reduction potential of the redox couple. Ind_{red} and Ind_{ox} are the relative concentrations of the reduced and oxidized forms of the redox indicator, respectively, at the electrode surface.

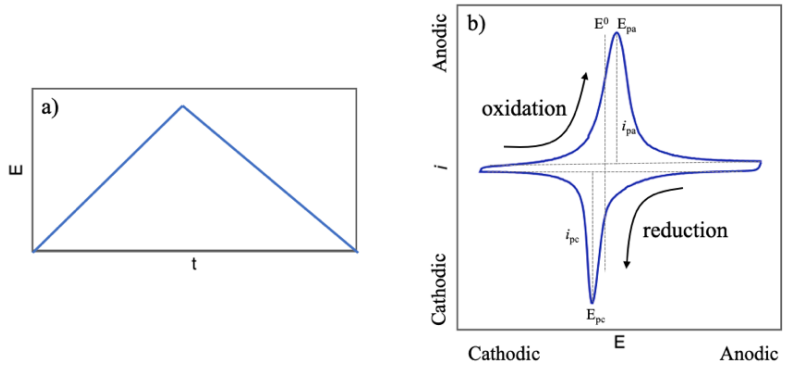

Figure 4. a) Cyclic voltammetry potential waveform and b) the resulting voltammogram of a reversible redox couple for an exhaustive conversion (confined on the electrode surface or in a thin solution layer).

If the electron transfer process is faster than other processes (e.g. diffusion), the reaction is called reversible. The peak separation (ΔE_p) can be described by eq. 9.[35,40,41,54]

$$\Delta E_p = |E_{pa} - E_{pc}| = 0.0592/n \qquad \text{eq. 9}$$

Therefore, for a reversible redox process at 25 °C, where n=1 (one electron transfer), the ideal ΔE_p is 59.2 mV. On the other hand, if the reaction is irreversible due to a much slower the electron transfer process ΔE_p would be larger than 59.2 mV. The formal reduction potential (E^0) of the reversible redox probe is described be eq. 10.[40,41]

$$E^0 = (E_{pa} + E_{pc})/2 \qquad \text{eq. 10}$$

1.2.2.2 Ion-transfer voltammetry

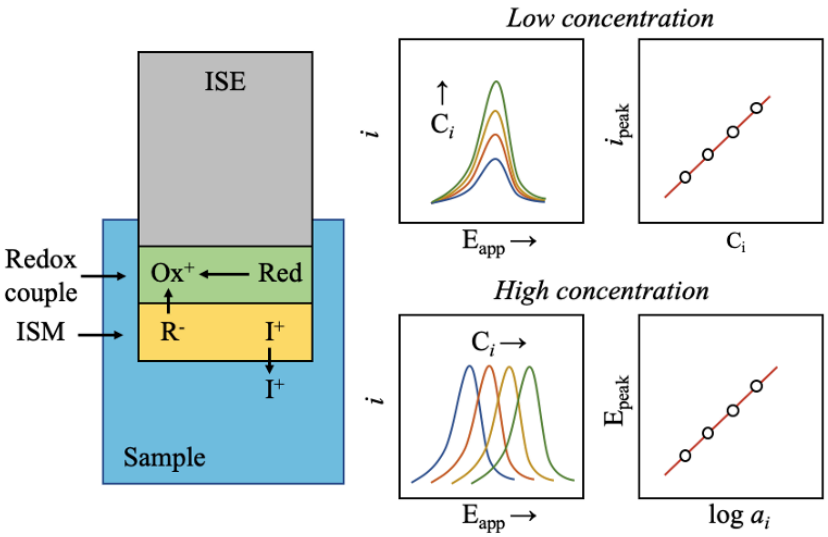

Figure 5. Ion-transfer at the interface of the membrane/solution induced by the oxidation/reduction of the redox couple, which lies between the sensing membrane and the working electrode.[6]

Ion-transfer voltammetry is observed at the membrane/solution interface. It has recently been studied as an alternative readout of the ISEs.[56–63] The potential provides the required potential to polarize the interface and then transfer ions from one phase to another.[55,64] This results in a linear increase of the faradaic current if the concentration level of the analyte is low (Figure 5, top). One the hand, at high concentration level of the analyte, the peak position demonstrates a Nernstian shift with analyte activity change (Figure 4, bottom).[6] The mechanism of the ion-transfer process is shown in Figure 5 (left). If the redox couple is oxidized (Ox^+), the anionic additive (R^-) is stabilized the product of the reaction, while the cation (I^+) is expelled to the solution at the characteristic potential.[65–67] Yuan et al. predicted the voltametric current and peak position in these two concentration regions by using a model where the mass transport at the membrane/solution interface was considered.[68,69] Cuartero et al. reported the ion-transfer process of three different analytes (Li^+, Na^+, K^+), where a thin membrane (about 200 nm) contained multiple ionophores and ion exchanger.[70] This sensing membrane was deposited on top of a conducting polymer layer (poly(3-octylthiophene), POT). When the transducer layer was oxidized, the oxidized form (POT^+) of the transducer layer was stabilized by anionic additive in the membrane, while the cation was expelled from the membrane to the solution at the characteristic potential. The ion-transfer mediated by the oxidation/reduction process can be observed in the cyclic voltammogram. This allows one to simultaneously and selectively measure up to three different analyte activities, where the peak position served as an analytical signal. This technique is in many ways analogous to the potentiometric method. Other conducting polymers (e.g. poly(3,4-ethylenedioxythiophene) (PEDOT),[71,72] polyaniline (PANI)[73,74]), the molecular lipophilic redox probe dispersed in the polymeric membranes (e.g. cobalt(II) porphyrin/cobalt(III) corrole complex[75]) were successfully utilized as the electrochemical transducers for inducing ion-transfer processes at the interface of the membrane/solution.

1.3 Optical sensors

Colorimetry is one of the oldest class of analytical techniques.[76] In principle, colorimetric sensors contain a light source, a wavelength selector and detector, which is sensitive at the selected wavelength of interest (Scheme 5). Optical sensors often use ultraviolet (10 – 390 nm) or visible light (390 – 700 nm) and infrared radiation (780 nm - 1 mm) to sense chemical reactions at liquid or solid interfaces.[77] They utilize optical transducers to convert electromagnetic radiation into an electrical quantity. This replies on a change of their optical properties and can be classified as absorption, emission (e.g. fluorescence, phosphorescence and chemiluminescence), scattering, reflection or refraction.[78,79] Due to their high sensitivity, selectivity, low-cost, portability (e.g. they allow one to permit remote sensing), dynamic range and miniatured scales (e.g. approach into inaccessible locations), optical sensors have been extensively reported for many decades for application in a wide range of quantitative areas. Especially for measuring pH, which may be concerned in life sciences (e.g. seawater, river, lake, tap water and urine).[80–85] Other examples include biological samples (e.g. sucrose, glucose and fructose)[86–88], environmental samples (Na^+, K^+)[89,90] and clinical samples (e.g. in blood and serum).[91–94]

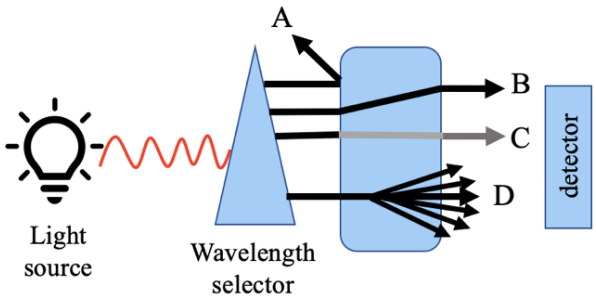

Scheme 5. A general spectroscopic setup consists of a light source, a wavelength selection device (e.g. filters, monochromators) and the detector. (A) light reflection, (B) light refraction, (C) light absorption, (D) fluorescent emission.[79,95]

In spectrophotometry, hundreds of color channels and wavelengths with nm resolution are selected for interrogation for analysis. In principle, the transmittance of a surface, solution or object is described as the part of the light passes through the other side of the objective. It can be reflected, refracted, absorbed or/and emitted (Scheme 5A-D). Some applications use transmittance as the analytical signals (e.g. water pollutants[96], powdered and pharmaceutical tablets[97,98]). When the light passes through the solution, some is reflected from the surface of the object while some amount of light may be absorbed by the solution. The remaining light goes passes to the other side of the object (Scheme 6) and can be measured by eq. 11.

$$T = I/I_0 \qquad \text{eq. 11}$$

where I_0 and I are the intensity of the light source and the remaining light intensity that has traveled though the sample, respectively. The absorbance can be calculated from the transmittance, T. The relationship between the absorbance and the transmittance is described by Beer-Lambert law (Beer's law). The wavelength-dependent absorbance, A, is given by eq. 12.[99,100]

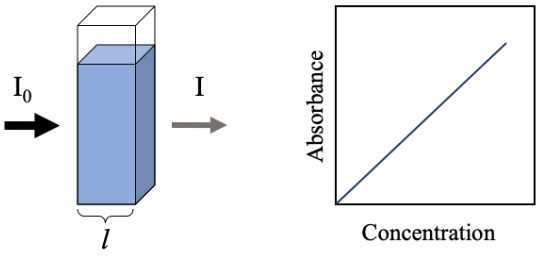

Scheme 6. Schematic illustration of light intensity from the light source before (I_0) and after (I) passes through the sample solution. *l* is the length of the object (left). Absorbance-based calibration (right).

$$A = -\log_{10}(I/I_0) = \varepsilon l c \qquad \text{eq. 12}$$

Where *A* is the absorbance, ε is the molar extinction coefficient. *l* is the length of sample through which the light source passes. c is the concentration of the analyte of interest. A complement color wheel can be used to estimate the wavelength of light the sample solution absorbs the most.[100] Ideally, the absorbance is directly proportional to analyte concentration. This absorbance is traditionally exploited as the analytical signal for optical sensors.

1.3.1 Absorbance-based spectrophotometric devices

Absorption spectrophotometer has been extensively utilized as an analytical tool to determine absorbed light intensity as a function of wavelength. An appropriated light source (e.g. UV and/or visible light) is passed through a prism or diffraction grating monochromator. The selected light passes through the sample before reaching to a detector. There are two groups of spectrometers (single and double beam). In a double beam spectrophotometer (scheme 7B), the light source is split into two separate beams or light paths after passing through a monochromator. One goes to the reference solution and another one goes to the sample. The intensities of both beams are measured simultaneously by two detectors. Whereas, a single beam spectrophotometer (scheme 7A) determines the relative light intensity of the beam, which requires to measure a reference solution separately.[101,102]

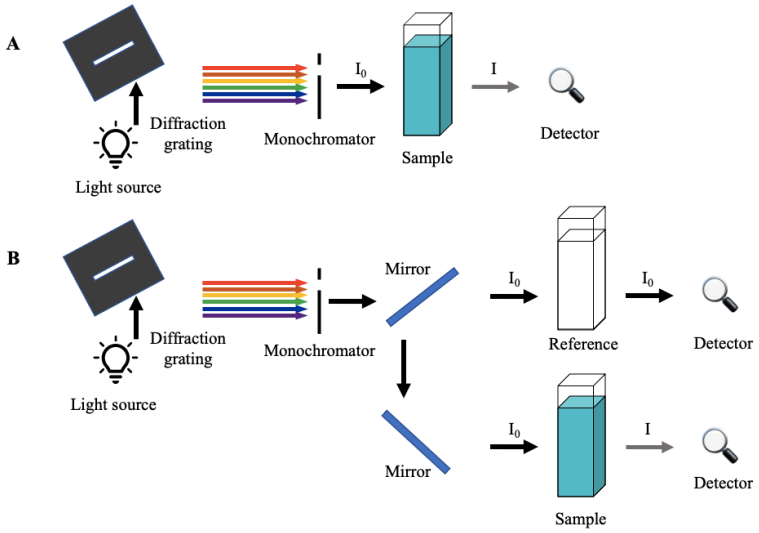

Scheme 7. Optical layout of an absorption spectrophotometer: A) single beam spectrophotometer and B) double beam spectrophotometer.[101]

UV-visible absorbance has been broadly used for quantitative and qualitative information. Absorbance-based thin films prepared by polymeric materials and conducing polymers have been utilized for optical readout. Wang et al. fabricated anion-selective optical sensors by using plasticized polymeric membranes (e.g. PVC, PU) doped with metalloporphyrins (e.g. Mn(III) and In(III)) as the ionophore and chromophore.[103] The films based on Mn(III) tetraphenylporphyrins alone simultaneously served as the ionophore and chromophore. When iodide ions were extracted into the membrane phase. The metal center was coordinated axially by the iodide and resulted in a change of molar absorptivity of the porphyrin. This mechanism was based on ion-exchange between iodide in solution and chloride in membrane phase. While In(III) octaethylporphyrin required a pH-sensitive dye to enhance optical absorbance change in the presence of nitrite and chloride ions. Anion was inducted into the membrane phase by the In(III) octaethylporphyrin. In a meantime, a proton was co-extracted into the sensing membrane in order to maintain charge balance. This allowed one to observe the absorbance change of the pH-sensitive dye. However, the samples were modified by buffering at pH <5. Instead of using a pH indicator immobilized in polymeric materials, Marco et al. used a thin polypyrrole (PPr) film prepared by oxidative polymerization of pyrrole on the walls of polystyrene cuvette.[104] This film was used as the optical sensors for measuring pH between 6 – 12. The absorbance spectrum of the PPr film (p*K*a ~8.6) was shifted to shorter wavelength when the pH increased from 6 – 12 (color changed from dark brown to green). The pH dependent spectral variations of PPr film were explained by the transformation from protonated to deprotonated form. This sensing film needed to be treated in 0.1 M HCl, otherwise resulted in an irreversible film before use. Other organic conducting polymer such as polyaniline (PANI) and Prussian blue (PB) were also exploited as the optical sensor.[105,106]

Other absorbance-based materials such as gold nanoparticles have been widely utilized in biosensors. One of the main advantages of using nanoparticles as sensing material is the size and surface characteristics which greatly affect to the performance of electrochemical sensors (e.g. high selectivity and sensitivity).[107] Nath et al. exploited colloidal surface plasmon resonance of immobilized and self-assembled gold nanoparticles on the transparent material.[108] High affinity of gold colloids on the surface was used to bind thiol and amine functional groups. The glass surface was transformed into an optical sensing chip by self-assembly of gold nanoparticles to form a reactive monolayer. The biomolecular binding at the surface of the functionalized gold monolayer was transduced to a colorimetric output, which was resulted by a shift in peak wavelength and increase in intensity of the absorbance. This was because the refractive index of the immobilized gold nanoparticles was changed after the protein binding on the surface. This label-free colorimetric biosensor quantitatively determined biomolecule (streptavidin) interactions in real time in a commercial UV-VIS spectrophotometer and an optical scanner by observing a change in the absorbance spectrum. The limit detection was found as 16 nM. This sensor may be not robust because the absorbance was dependent on the size of colloid and surface density. Also, the gold nanoparticles were deposited on glass, which may be fragile. Furthermore, Date et al. used a miniaturized microfluidic device to determine concentration of heavy metals based on absorbance measurement using gold nanoparticle-labelled antibodies.[109] Heavy metal samples (cadmium, chromium and lead) were modified by mixing for >30 min with gold nanoparticle-labelled antibody, ethylenediaminetetraacetic acid (EDTA) and Tris buffer (pH 7.5). This equilibrium sample was flowed to a main channel and passed rapidly to a detection area (T-junction), at which an antigen-immobilized solid phase was packed in detection area. Free antibody was selectively captured and accumulated on the surface of the solid phase in detection area, while uncaptured antibody was washout with PBS-BSA (phosphate buffered

saline-bovine serum albumin). The amount of antibody captured in detection area was optically determined by the absorbance. The observed absorbance was proportional to the metal concentration. This microfluidic device exhibited a rapid, low-cost, selective and sensitive performance and was successfully extended to microfluidic immunoassays. Malcik et al. reported a microchip-based fiber optic measurement for clinical analysis of calcium ions in urine.[110] The absorbance was observed when the analyte interacted with arsenazo III (5 mM) to form the complex. Arsenazo III exhibited a high affinity for unbound divalent and trivalent metal ions. In the presence of calcium, arsenazo III formed a Ca^{2+}-arsenazo III complex and caused a shift of an absorbance spectrum of the arsenazo III. This allowed one to determine calcium concentration range from 0.125 – 2.50 mM in biological samples with a wide pH range from 4 – 12 and required a small volume of the sample. The interferences (e.g. magnesium range of 0.38 – 0.54 mM, Na^+ and K^+ in blood) were found not to interrupt the sensor. Only if the concentration of Mg^{2+} ion was five times higher than Ca^{2+} concentration. Other monovalent cationic species (e.g. Na^+, K^+) in blood and serum were not found to interfere because the arsenazo III was not selective to the monovalent cations. Several drawbacks of this technique include i) the absorbance in the microchip was dependent on a short path-length (*l*) based on Beer law. This may limit the sensitivity of the sensor. The microchip was needed to be well-designed in order to enhance the absorbance intensity. ii) the sensor may not be robust because the bottom plate of the microchip was fabricated in borosilicate float glass, iii) Ca^{2+}-arsenazo III complex was irreversible. The regeneration of the sensor may need to rinse with HCl (0.23 M) and required 5 min before reusing again, iv) This approach was not ready to measure the samples without modification because the urine sample was modified by mixing in a borate buffer (pH 9) together with arsenazo III solution. Most of microfluidic sensors may not be robust for a number of reasons because the performances of the sensors were dependent on a fluidic viscosity and a fluidic resistance of the microchannel. These drawbacks are very challenging for the researchers. Moreover, numerous of applications of the sensors have been developed and many of them exploited the absorbance-based UV-visible spectrophotometry as a reference technique to compare the quantitative information with state-of-the-art sensors.

1.3.2 Absorbance-based digital images devices

Digital imaging methods, where the colorimetric image can be captured by digital cameras, webcams, scanners and smart phones have been extensively introduced for quantitative information.[111,112] These simple analytical sensors utilizing digital images have in some applications replaced classical spectrophotometric instruments. Most digital image-based methods use the RGB color pattern using the primary colors (red (R), green (G), blue (B)) to carry out quantitative analysis, where more than 16 million colors can be extracted from these RGB data.[113] Kohl et al. reported that the absorbance may be investigated by using the digital color image analysis, where the resulting absorbance from the digital image was proportional to the concentration of the analyte and was correlated to Beer-Lambert's law.[114] Benedetti et al. used the digital image from spot-test reactions, which captured by using the camera to quantify the concentration of ethanol in drinks.[115] The absorbance provided by the red (R) channel exhibited linearity with ethanol concentration. The results were in close accordance with one using the spectrophotometric method. Tajee et al. followed the color change of hue (H) value by using the HSV color pattern, H (hue), S (saturate) and V (value). This hue-based optical signal was utilized to indicate the endpoint of a colorimetric titration, at which the images were captured by the digital camera and computed by Mathematica

software. This optical signal was successfully used to measure potassium contents in environmental and clinical sample (human serum) with good agreement with a reference method (atomic emission spectroscopy).[116] Soda et al. exploited the RGB or HSV data for colorimetric measurement and the optical readout for paper-based analytical devices by using image analysis.[66] The image color data were computed into the absorbance values and were found to be correlated well to the spectrophotometry after elimination of grammar correction, which is normally applied in camera to make image more realistic to the human eye. This approach was successfully utilized for quantitative analysis.

1.4 Sensor arrays

Array-based sensing is inspired by mammalian olfactory system (e.g. chemical and or electronic nose and tongue).[117–122] In the sensing array platform, the response signals from all the target analytes are collected and analyzed like a fingerprint analysis.[123] The sensor array based on pattern-recognition platform have been intensively enabled to separate a tiny change of extremely similar signals over a broad range of analytes and allow one to discriminate the overlapping sensitivity profiles between similar analytes within complex mixtures.[117,121,124,125] This sensing array allows one to obtain the full chemical profiles of multi-analytes being measured. The number of these applications have been increasingly introduced using the electrochemical and/or optical strategies for measurement of the analytes of interest. Examples cover *in situ* monitoring of dopamine,[126,127] pH,[128–137] DNA,[138] insulin,[139,140] water pollution,[141–143] glucose[144–147], dissolved oxygen concentrations.[148]

1.4.1 Potentiometric sensor arrays

Simultaneous analysis is very attractive because it significantly reduces time-consuming and expense. Pankratova et al. measured nutrients and chemical species relevant to the carbon cycle in freshwater ecosystems by using potentiometric sensing array based on the ISEs. This sensor array was successfully exploited for continuous monitoring nitrate, carbonate, calcium and pH.[36] The sensor allowed one to observe analyte concentration profiles with time. The development of potentiometric sensing array has been extended into intensive diagnostic areas. Examples include creatinine together with K^+, Na^+, NH_4^+ and Ca^{2+} in urine,[149] heavy metals of Cu^{2+}, Pb^{2+} and Cd^{2+} in digested wine,[150] physiological measurement of K^+, Na^+, Cl^- and pH in human colon epithelium cell line.[151] amino acids such as phenylalanine, tyrosine, ornithine and glutamic acid.[152] The potentiometric sensing arrays are not only utilized for simultaneous determinations of analytes. Some were used to increase the sensitivity of the sensors. Zdrachek et al. integrated multi-ISEs into a sensing array platform.[153] This allowed one to enlarge the potentiometric response and increase sensitivity by using the combined electrochemical cell consisted of several identical ISEs and immersed into separate sample solutions of equal composition. The associated potentiometric response of an individual Nernstian slope in one electrochemical cell was amplified by *n* times, depending on the number of ISEs (*n* electrodes). This increased the number of membrane/sample phase boundaries in a shared electrochemical cell, where the small change of the analyte concentration was sensitively detected. This approach was successfully utilized for measurement concentration of potassium, sodium and carbonate.

1.4.2 Optical sensor arrays

Traditional sensing employing "lock-and-key" molecular receptor is selectively to just one target analyte.[117,154] However, diverse analytes may be simultaneously measured by merging the traditional sensing mode into the sensing array platform. A cross-reactive technique incorporated into the optical sensor array is inspired by mammalian olfactory and taste system.[117–122] This makes an important contribution to the fabrication of elegant and simultaneous sensors. Optical array widely expands the range of molecular specificity.[117] They contain a facile, sensitive and efficient strategies for rapid determination and discrimination of wide ranges of analytes based on colorimetric change. They may be quantitatively monitored by digital imaging.[155–157] An active center in the optical sensor array strongly interacted with the target analytes, resulting in the colorimetric change.[117] A variety of chemoresponsive colorants have been used as a diverse array and fabricate the pattern of optical fingerprint for detection of a mixture of odorants.[158,159] Other examples include the sensing array-based molecular imprinted polymer (MIP), which differentiated seven structurally similar amines with high accuracy.[160] Colorimetric sensor array utilized triple-channel properties (RGB color) for measurement of biothiols.[161] Fiber gene optic array was used to screen unlabeled DNA by monitoring a fluorescence change.[162] Bead-based fiber optical arrays, at which each bead independently probed the target analyte (e.g. DNA target) was also reported.[163]

1.5 Bipolar sensing electrode platform

A bipolar electrode (BPE) is typically an electron conductor based on the polarization of conducting objects in electrolyte solution.[164–166] This polarization generates the potential different between two ends. When a sufficient potential is provided, the oxidation and reduction reactions may be simultaneously promoted at the two poles.[166] The BPE setup is constructed without the direct connection of an external power supply, which is different from the traditional three-electrode system (Scheme 2). The BPE setup allows simultaneous control multiple electrodes, which provides access to various new categories of the experiments.[167] The combination of the BPE and other alternative optical techniques (e.g. electrochemiluminescence (ECL),[168–171] light emitting diode (LED)[172], fluorescence,[173–175] and electrochromic electrodes/films[176–179]) have extensively promoted as a new and powerful route to perform the analytical measurement. Jaworska et al. showed the quantitative optical output of potentiometric responses from ISEs based on bipolar electrode system.[180] A polypyrrole (PPr)-based solid-contact ISE, where a potassium ion-selective membrane was cast on top was connected to the zinc (Zn) wire, which immersed in the same solution. An increase of potassium ion activity in sample induced a reduction of PPr-based transducing layer. This resulted in an oxidation of Zn wire, at which the accumulated Zinc ions in the solution later enhanced a fluorescence emission intensity.

Potentiometric-based ISEs have recently been utilized to translate the potential change into the coulometric readout (e.g. using conducting polymers (PEDOT)[181,183,184] and electronic capacitor[182,185]) and optical readout (e.g. ECL,[186] LEDs[187] and fluorescent probe[180]). Bobacka's group introduced a coulometric readout based on a redox process for solid-contact ISEs by imposing a constant potential to the electrochemical cell with the use of the potentiostat (Figure 5a).[181,183] A potential change at the membrane/sample interface was compensated by a change in potential of the capacitive solid-contact layer. This chemically resulted in a current spike, where the charge was integrated and used as the analytical signal. The capacitance, C may be quantitatively calculated by eq. 13.[182,184]

$$Q = C\frac{s}{z_i} log \frac{a_i(initial)}{a_i(final)} \quad \text{eq. 13}$$

where Q is a measured charge. C is capacitance, z_i is a charge of a primary ion. a_i (initial) and a_i (final) are the activity of the detected primary ion *i* before and after a change of sample composition. Recently, Kraikeaw et al. replaced the capacitive transducing layer by using a commercially electronic capacitor.[182] The electronic capacitor, ranging from 4.7 to 470 µF was placed in series to the ISE probe (Figure 5b). This approach allowed one to rapidly measure ultrasensitive pH down to 0.001 pH units in seawater samples. Moreover, with coulometric-based ISEs using an electronic capacitor it was found that the charging transient reach equilibrium in just less than 10 s.[185] This response time was dramatically quicker than one with the use of the capacitive transducing layer.

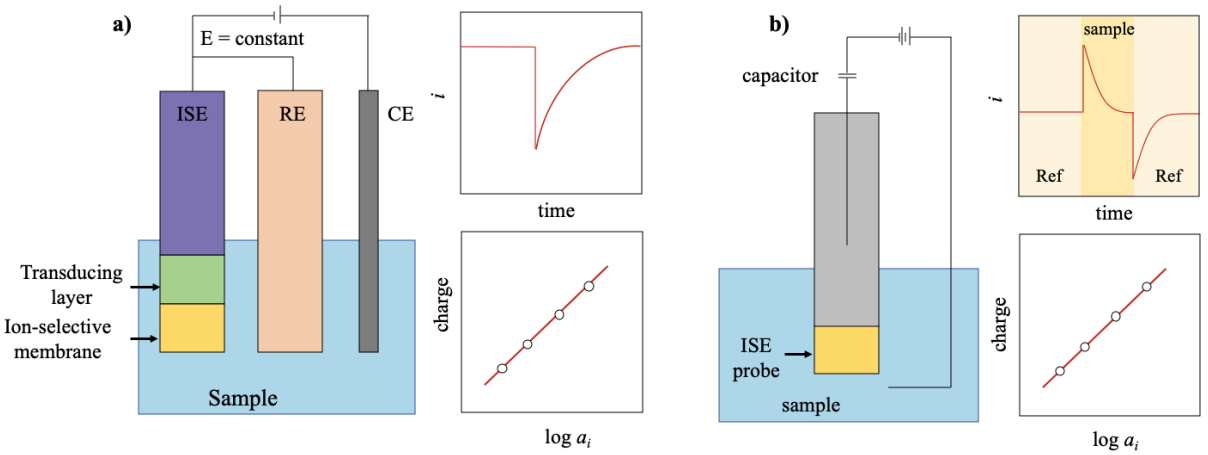

Figure 5. Coulometric measurements: a) conducting polymer-based solid-contact ISE, at which a transducing layer was deposited between electrode surface and sensing membrane.[181,6] b) Solid contact ISE, at which the transducing layer was replaced by an electronic capacitor. The commercial capacitor was placed in series to the ISE probe (Ref was a reference solution).[182]

1.6 Self-powered sensors

Traditional electrochemical sensors contain recognition sensing element, transducer, signaling electronic amplifier and external power supply.[188,189] However, self-powered sensors are not required the battery or external power sources.[190] They harvest power/energy in the environment and self-supply of the energy for sensing the analytes. Self-powered systems were first exploited for nuclear sensing and later transformed to the chemical and biological sensors.[189,191]

There are typically three different types of fuel cells, which relate to the oxidation/reduction at anode and cathode, respectively to produce energy for the sensors (Scheme 6).[190] An enzymatic fuel cell (Scheme 6a) utilizes enzymes as catalysts to generate electrons by oxidation of fuel at anode. The electrons move to the cathode through an external circuit. Meantime, the oxidants (e.g. O_2 and H_2O_2) receive the electrons to satisfy the reduction process by catalysis of another enzyme-immobilized at the cathode.[190,192–194] This may produce electricity, which was for example exploited to obtain power for a wearable self-powered sensor to measure lactate in human sweat.[195] Hanashi et al. showed that a capacitor can be charged and discharged as a function of enzyme reaction at the anode, which was obtained by glucose concentration.[196] In the presence of glucose, this bio-capacitor generated electricity

as the power source for operation of a stepper motor for using as a drug delivery/pumping device based on self-powered sensor. Pinyou et al. miniaturized the biofuel cell for self-powered glucose sensing measured by optical readout.[197] The oxidation reaction of the enzyme glucose dehydrogenase at the anode triggered the reduction of an electrochromic reporter (modified methylene green) at the cathode. This resulted in a discoloration of the optical indicator, which allowed one to determine glucose concentration. A microbial fuel cell (Scheme 6b) generally uses microorganisms to convert chemical power into electrical energy.[190,198] In an aerobic condition, the organics in the anodic chamber are decomposed by microorganism to release electrons and protons from the oxidation reaction at the anode. The electrons flow through the external circuit to the cathode, while the protons are transferred through the proton exchange membrane (PEM) to the cathode to form with the oxidant (e.g. O_2) to generate water.[199–201] A photocatalytic fuel cell (Scheme 6c) is an advanced oxidation process. The photogenerated electrons and holes are produced in the conducing band and valence band of the semiconductor (e.g. TiO_2) when promoted by light.[190,202,203] The strong oxidation ability of the holes powerfully oxidizes most of organic substates and transforms this chemical energy into electrical power.[190,204]

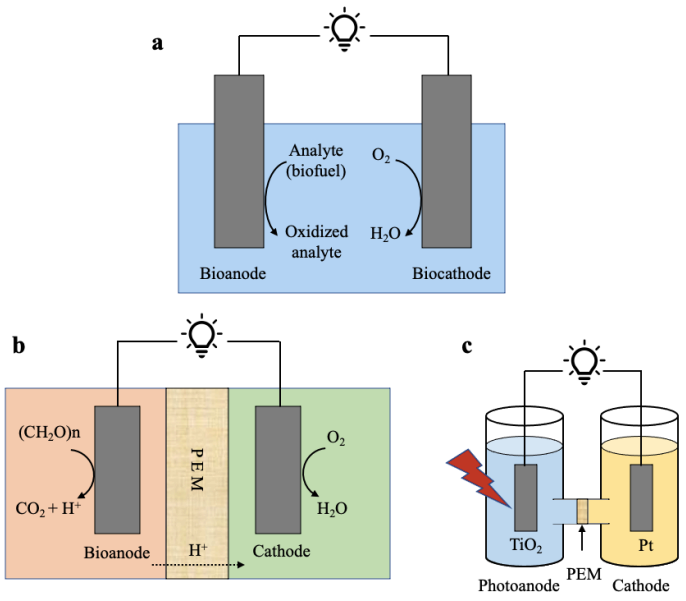

Scheme 6. General diagram of a) enzymatic biofuel cell (EBFC), b) microbial fuel cell (MFC) and c) photocatalytic fuel cell (PFC).[190] PEM stands for proton exchange membrane.

Self-powered sensors have received attention for a few decades. Katz and Willner introduced self-powered biosensors for chemical and biological sensing.[205] They fabricated the self-powered biosensor for glucose determination by employing an enzymatic biofuel cell with glucose oxidase at an anode and cytochrome *c* oxidase at a cathode. This system utilized glucose as the fuel, at which the glucose was oxidized at the anode while oxygen was reduced at the cathode. The open-circuit voltage, current and power were only observed in the presence of glucose concentration. Miyake et al. fabricated the fructose sensing devices consisting of the enzymatic biofuel cell coupled to the LED system by using the capacitor as the transducer.[206] The LED served as the self-powered indicator in grape fruit. This allowed one to determine the fructose concentration by the blink interval of the LED. Recently, Jawarska et al. reported a self-powered electrochemical-optical sensor based on a cascade bipolar electrode platform.[207] The sensors contained two bipolar electrodes. One was used to source (driving circuit) the

required energy to trigger the spontaneous charge transfer process at another electrode (sensing circuit). This resulted in an observed fluorescence intensity, which served as the analytical signal without the requirement of an external power source. Sailapu et al. proposed self-powered potentiometric sensors, where the energy can be harvested and collected during the sensing process into an electronic capacitor and later readout without the use of the external power device.[208] This approach successfully measured potassium concentration in artificial sweat samples and is promising for fabrication of portable devices especially in point of care applications.

1.7 References

(1) Peter Gründler. *Chemical Sensors*; Springer Berlin Heidelberg: Berlin, Heidelberg, 2007.
(2) Janata, J. *Principles of Chemical Sensors*; Springer US: Boston, MA, 2009.
(3) Bănică, F.-G. *Chemical Sensors and Biosensors: Fundamentals and Applications*; John Wiley & Sons, Ltd: Chichester, UK, 2012.
(4) Bandodkar, A. J.; Wang, J. Non-Invasive Wearable Electrochemical Sensors: A Review. *Trends Biotechnol.* **2014**, *32* (7), 363–371.
(5) Bakker, E.; Pretsch, E. Modern Potentiometry. *Angew. Chem. Int. Ed.* **2007**, *46* (30), 5660–5668.
(6) Zdrachek, E.; Bakker, E. Potentiometric Sensing. *Anal. Chem.* **2019**, *91* (1), 2–26.
(7) Bakker, E.; Bühlmann, P.; Pretsch, E. Carrier-Based Ion-Selective Electrodes and Bulk Optodes. 1. General Characteristics. *Chem. Rev.* **1997**, *97* (8), 3083–3132.
(8) Lindner, E.; Pendley, B. D. A Tutorial on the Application of Ion-Selective Electrode Potentiometry: An Analytical Method with Unique Qualities, Unexplored Opportunities and Potential Pitfalls; Tutorial. *Anal. Chim. Acta* **2013**, *762*, 1–13.
(9) Miyahara, Y.; Simon, W. Comparative Studies between Ion-Selective Field Effect Transistors and Ion-Selective Electrodes with Polymeric Membranes. *Electroanalysis* **1991**, *3* (4–5), 287–292.
(10) Lindner, Erno.; Graf, Etelka.; Niegreisz, Zsuzsa.; Toth, Klara.; Pungor, Erno.; Buck, R. P. Responses of Site-Controlled, Plasticized Membrane Electrodes. *Anal. Chem.* **1988**, *60* (4), 295–301.
(11) Ma, S. C.; Chaniotakis, N. A.; Meyerhoff, M. E. Response Properties of Ion-Selective Polymeric Membrane Electrodes Prepared with Aminated and Carboxylated Poly(Vinyl Chloride). *Anal. Chem.* **1988**, *60* (20), 2293–2299.
(12) Cosofret, V. V.; Buck, R. P.; Erdosy, Miklos. Carboxylated Poly(Vinyl Chloride) as a Substrate for Ion Sensors: Effects of Native Ion Exchange on Responses. *Anal. Chem.* **1994**, *66* (21), 3592–3599.
(13) Cho, Y. A.; Lee, H. S.; Cha, G. S.; Lee, Y. T. Fabrication of Butyrylcholinesterase Sensor Using Polyurethane-Based Ion-Selective Membranes. *Biosens. Bioelectron.* **1999**, *14* (4), 435–438.
(14) Berrocal, M. J.; Badr, I. H. A.; Gao, D.; Bachas, L. G. Reducing the Thrombogenicity of Ion-Selective Electrode Membranes through the Use of a Silicone-Modified Segmented Polyurethane. *Anal. Chem.* **2001**, *73* (21), 5328–5333.
(15) Górski, Ł.; Malinowska, E. Fluoride-Selective Sensors Based on Polyurethane Membranes Doped with Zr(IV)-Porphyrins. *Anal. Chim. Acta* **2005**, *540* (1), 159–165.
(16) Dabrowska, S.; Migdalski, J.; Lewenstam, A. A Breakthrough Application of a Cross-Linked Polystyrene Anion-Exchange Membrane for a Hydrogencarbonate Ion-Selective Electrode. *Sensors* **2019**, *19* (6), 1268.
(17) Singh, A. K.; Saxena, P. Silver(I)-Selective Electrode Based on [Bz2Oxo4(18)DieneS4] Tetrathia Macrocyclic Carrier. *Anal. Bioanal. Chem.* **2006**, *385* (1), 90–95.
(18) Shin, J. H.; Sakong, D. S.; Nam, H.; Cha, G. S. Enhanced Serum Carbon Dioxide Measurements with a Silicone Rubber-Based Carbonate Ion-Selective Electrode and a High-PH Dilution Buffer. *Anal. Chem.* **1996**, *68* (1), 221–225.
(19) Yoon, I. J.; Lee, D. K.; Nam, H.; Cha, G. S.; Strong, T. D.; Brown, R. B. Ion Sensors Using One-Component Room Temperature Vulcanized Silicone Rubber Matrices. *J. Electroanal. Chem.* **1999**, *464* (2), 135–142.
(20) Cuartero, M.; Pankratova, N.; Cherubini, T.; Crespo, G. A.; Massa, F.; Confalonieri, F.; Bakker, E. In Situ Detection of Species Relevant to the Carbon Cycle in Seawater with Submersible Potentiometric Probes. *Environ. Sci. Technol. Lett.* **2017**, *4* (10), 410–415.
(21) Paczosa-Bator, B.; Cabaj, L.; Piech, R.; Skupień, K. Potentiometric Sensors with Carbon Black Supporting Platinum Nanoparticles. *Anal. Chem.* **2013**, *85* (21), 10255–10261.
(22) Pankratova, N.; Ghahraman Afshar, M.; Yuan, D.; Crespo, G. A.; Bakker, E. Local Acidification of Membrane Surfaces for Potentiometric Sensing of Anions in Environmental Samples. *ACS Sens.* **2016**, *1* (1), 48–54.
(23) Garcia, C. A. B.; Júnior, L. R.; Neto, G. de O. Determination of Potassium Ions in Pharmaceutical Samples by FIA Using a Potentiometric Electrode Based on Ionophore Nonactin Occluded in EVA Membrane. *J. Pharm. Biomed. Anal.* **2003**, *31* (1), 11–18.
(24) Mortimer, R. Potentiometric Determination of Potassium Cations Using a Nickel(II) Hexacyanoferrate-Modified Electrode. *Talanta* **1999**, *49* (2), 271–275.
(25) Moody, G. J.; Saad, B. B.; Thomas, J. D. R. Studies on Bis(Crown Ether)-Based Ion-Selective Electrodes for the Potentiometric Determination of Sodium and Potassium in Serum. *Analyst* **1989**, *114* (1), 15.
(26) Pankratova, N.; Cuartero, M.; Cherubini, T.; Crespo, G. A.; Bakker, E. In-Line Acidification for Potentiometric Sensing of Nitrite in Natural Waters. *Anal. Chem.* **2017**, *89* (1), 571–575.
(27) Jansod, S.; Ghahraman Afshar, M.; Crespo, G. A.; Bakker, E. Alkalinization of Thin Layer Samples with a Selective Proton Sink Membrane Electrode for Detecting Carbonate by Carbonate-Selective Electrodes. *Anal. Chem.* **2016**, *88* (7), 3444–3448.
(28) Cuartero, M.; Bakker, E. Environmental Water Analysis with Membrane Electrodes. *Curr Opin Electrochem* **2017**, *3* (1), 97–105.
(29) Afshar, M. G.; Crespo, G. A.; Bakker, E. Thin-Layer Chemical Modulations by a Combined Selective Proton Pump and PH Probe for Direct Alkalinity Detection. *Angew. Chem. Int. Ed.* **2015**, *54* (28), 8110–8113.
(30) Mathison, S.; Bakker, E. Renewable PH Cross-Sensitive Potentiometric Heparin Sensors with Incorporated Electrically Charged H^+ Ionophores. *Anal. Chem.* **1999**, *71* (20), 4614–4621.
(31) Chen, Y.; Ding, J.; Qin, W. Polycation-Sensitive Membrane Electrode for Determination of Heparin Based on Controlled Release of Protamine. *Analyst* **2012**, *137* (8), 1944
(32) Ayranci, E. Binding of Iodide to Bovine Serum Albumin and Protamine Studied with an Ion-Selective Electrode. *Food Chem.* **1995**, *54* (2), 173–175.

(33) Yun, J. H.; Meyerhoff, M. E.; Yang, V. C. Protamine-Sensitive Polymer Membrane Electrode: Characterization and Bioanalytical Applications. *Anal. Biochem.* **1995**, *224* (1), 212–220.
(34) Ramamurthy, N.; Baliga, N.; Wakefield, T. W.; Andrews, P. C.; Yang, V. C.; Meyerhoff, M. E. Determination of Low-Molecular-Weight Heparins and Their Binding to Protamine and a Protamine Analog Using Polyion-Sensitive Membrane Electrodes. *Anal. Biochem.* **1999**, *266* (1), 116–124.
(35) Crouch, S, S., D. A. ;. West, D. M. ;. Holler, F. J. *Fundamentals of Analytical Chemistry, Ninth Edition*; Mary Finch: Belmont, CA, USA, 2014.
(36) Pankratova, N.; Crespo, G. A.; Afshar, M. G.; Crespi, M. C.; Jeanneret, S.; Cherubini, T.; Tercier-Waeber, M.-L.; Pomati, F.; Bakker, E. Potentiometric Sensing Array for Monitoring Aquatic Systems. *Environ. Sci.: Processes Impacts* **2015**, *17* (5), 906–914.
(37) Opdycke, W. N.; Parks, S. J.; Meyerhoff, M. E. Polymer-Membrane PH Electrodes as Internal Elements for Potentiometric Gas-Sensing Systems. *Anal. Chim. Acta* **1983**, *155*, 11–20.
(38) Ammann, D.; Pretsch, E.; Simon, W.; Lindner, E.; Bezegh, A.; Pungor, E. Lipophilic Salts as Membrane Additives and Their Influence on the Properties of Macro- and Micro-Electrodes Based on Neutral Carriers. *Anal. Chim. Acta* **1985**, *171*, 119–129.
(39) Nägele, M.; Mi, Y.; Bakker, E.; Pretsch, E. Influence of Lipophilic Inert Electrolytes on the Selectivity of Polymer Membrane Electrodes. *Anal. Chem.* **1998**, *70* (9), 1686–1691.
(40) Eric Bakker. *Fundamentals of Electroanalysis Electrochemistry of Ion and Electron Transfer Processes*; Eric Bakker: Geneva, Switzerland, 2014.
(41) Larry R . Faulkner, A. J. B. *ELECTROCHEMICAL METHODS Fundamentalsand Applications*, 2nd Edition.; John Wiley & Sons: New York.
(42) Thomas, J. D. R.Thomas, J. D. R.Thomas, J. D. R.Thomas, J. D. R.aa, G., G. G. ;. Durst, R. A. ;. Frant, M. S. ;. Freiser, H. ;. Hansen, E. H. ;. Light, T. S. ;. E. Pungor; Rechnitz, G. ;. Rice, N. M. ;. Rohm, T. J. ;. Simon, W. ; Recommendations for Nomenclature of ION-Selective Electrodes. *Pure and Applied Chemistry* **1976**, *48* (1), 127–132.
(43) Buck, R. P.; Lindner, E. Recommendations for Nomenclature of Ionselective Electrodes (IUPAC Recommendations 1994). *Pure and Applied Chemistry* **1994**, *66* (12), 2527–2536.
(44) Johnson, R. D.; Bachas, L. G. Ionophore-Based Ion-Selective Potentiometric and Optical Sensors. *Anal. Bioanal. Chem.* **2003**, *376* (3), 328–341.
(45) Maj-Zurawska, M. Interpretation of the Selectivity and Detection Limit of Liquid Ion-Exchanger Electrodes. *Talanta* **1988**, *35* (4), 281–286.
(46) Sokalski, T.; Zwickl, T.; Bakker, E.; Pretsch, E. Lowering the Detection Limit of Solvent Polymeric Ion-Selective Electrodes. 1. Modeling the Influence of Steady-State Ion Fluxes. *Anal. Chem.* **1999**, *71* (6), 1204–1209.
(47) Bühlmann, P.; Yajima, S.; Tohda, K.; Umezawa, K.; Nishizawa, S.; Umezawa, Y. Studies on the Phase Boundaries and the Significance of Ionic Sites of Liquid Membrane Ion-Selective Electrodes. *Electroanalysis* **1995**, *7* (9), 811–816.
(48) Höfler, L.; Bedlechowicz, I.; Vigassy, T.; Gyurcsányi, R. E.; Bakker, E.; Pretsch, E. Limitations of Current Polarization for Lowering the Detection Limit of Potentiometric Polymeric Membrane Sensors. *Anal. Chem.* **2009**, *81* (9), 3592–3599.
(49) Buck, R. P.; Toth, K.; Graf, E.; Horvai, G.; Pungor, E. Donnan Exclusion Failure in Low Anion Site Density Membranes Containing Valinomycin. *J. electroanal. chem. interfacial electrochem.* **1987**, *223* (1–2), 51–66.
(50) Yajima, S.; Tohda, K.; Bühlmann, P.; Umezawa, Y. Donnan Exclusion Failure of Neutral Ionophore-Based Ion-Selective Electrodes Studied by Optical Second-Harmonic Generation. *Anal. Chem.* **1997**, *69* (10), 1919–1924.
(51) Bühlmann, P.; Amemiya, S.; Yajima, S.; Umezawa, Y. Co-Ion Interference for Ion-Selective Electrodes Based on Charged and Neutral Ionophores: A Comparison. *Anal. Chem.* **1998**, *70* (20), 4291–4303.
(52) Ana Maria Oliveira Brett, C. M. A. B. *Electrochemistry: Principles, Methods, and Applications*; Oxford University Press: Oxford, United Kingdom, 1993.
(53) Buitenweg, J. R.; Rutten, W. L. C.; Marani, E. Nano-Ampere Stimulation Window for Cultured Neurons on Micro-Electrode Arrays. In *2001 Conference Proceedings of the 23rd Annual International Conference of the IEEE Engineering in Medicine and Biology Society*; IEEE: Istanbul, Turkey, 2001; Vol. 1, pp 725–728.
(54) Elgrishi, N.; Rountree, K. J.; McCarthy, B. D.; Rountree, E. S.; Eisenhart, T. T.; Dempsey, J. L. A Practical Beginner's Guide to Cyclic Voltammetry. *J. Chem. Educ.* **2018**, *95* (2), 197–206.
(55) Crespo, G. A.; Bakker, E. Dynamic Electrochemistry with Ionophore Based Ion-Selective Membranes. *RSC Adv.* **2013**, *3* (48), 25461.
(56) Jarolímová, Z.; Bosson, J.; Labrador, G. M.; Lacour, J.; Bakker, E. Ion Transfer Voltammetry in Polyurethane Thin Films Based on Functionalised Cationic [6]Helicenes for Carbonate Detection. *Electroanalysis* **2018**, *30* (7), 1378–1385.
(57) Jarolímová, Z.; Bosson, J.; Labrador, G. M.; Lacour, J.; Bakker, E. Ion Transfer Voltammetry at Thin Films Based on Functionalized Cationic [6]Helicenes. *Electroanalysis* **2018**, *30* (4), 650–657.
(58) Langmaier, J.; Skopalová, J.; Navrátil, T.; Samec, Z. Detection of Antimuscarinic Agents Tolterodine and Fesoterodine and Their Metabolite 5-Hydroxymethyl Tolterodine by Ion Transfer Voltammetry at a Polarized Room-Temperature Ionic Liquid Membrane. *Electrochim. Acta* **2019**, *304*, 54–61.
(59) Ding, J.; Cherubini, T.; Yuan, D.; Bakker, E. Paper-Supported Thin-Layer Ion Transfer Voltammetry for Ion Detection. *Sens. Actuator B-Chem.* **2019**, *280*, 69–76.
(60) Poltorak, L.; Sudhölter, E. J. R.; de Smet, L. C. P. M. Effect of Charge of Quaternary Ammonium Cations on Lipophilicity and Electroanalytical Parameters: Task for Ion Transfer Voltammetry. *J. Electroanal. Chem.* **2017**, *796*, 66–74.
(61) Olmos, J. M.; Laborda, E.; Ortuño, J. Á.; Molina, Á. Characterization of Inclusion Complexes of Organic Ions with Hydrophilic Hosts by Ion Transfer Voltammetry with Solvent Polymeric Membranes. *Talanta* **2017**, *164*, 636–644.
(62) Molina, A.; Serna, C.; Ortuño, J. A.; Gonzalez, J.; Torralba, E.; Gil, A. Differential Pulse Voltammetry for Ion Transfer at Liquid Membranes with Two Polarized Interfaces. *Anal. Chem.* **2009**, *81* (11), 4220–4225.
(63) Langmaier, J.; Samec, Z. Cyclic Voltammetry of Ion Transfer across a Room Temperature Ionic Liquid Membrane Supported by a Microporous Filter. *Electrochem. commun.* **2007**, *9* (10), 2633–2638.
(64) Samec, Z. Electrochemistry at the Interface between Two Immiscible Electrolyte Solutions (IUPAC Technical Report). *Pure Appl. Chem.* **2004**, *76* (12), 2147–2180.
(65) Cuartero, M.; Acres, R. G.; De Marco, R.; Bakker, E.; Crespo, G. A. Electrochemical Ion Transfer with Thin Films of Poly(3-Octylthiophene). *Anal. Chem.* **2016**, *88* (13), 6939–6946.
(66) Cuartero, M.; Crespo, G. A.; Bakker, E. Polyurethane Ionophore-Based Thin Layer Membranes for Voltammetric Ion Activity Sensing. *Anal. Chem.* **2016**, *88* (11), 5649–5654.
(67) Crespo, G. A.; Cuartero, M.; Bakker, E. Thin Layer Ionophore-Based Membrane for Multianalyte Ion Activity Detection. *Anal. Chem.* **2015**, *87* (15), 7729–7737.

(68) Yuan, D.; Cuartero, M.; Crespo, G. A.; Bakker, E. Voltammetric Thin-Layer Ionophore-Based Films: Part 1. Experimental Evidence and Numerical Simulations. *Anal. Chem.* **2017**, *89* (1), 586–594.
(69) Yuan, D.; Cuartero, M.; Crespo, G. A.; Bakker, E. Voltammetric Thin-Layer Ionophore-Based Films: Part 2. Semi-Empirical Treatment. *Anal. Chem.* **2017**, *89* (1), 595–602.
(70) Cuartero, M.; Crespo, G. A.; Bakker, E. Ionophore-Based Voltammetric Ion Activity Sensing with Thin Layer Membranes. *Anal. Chem.* **2016**, *88* (3), 1654–1660.
(71) Kim, Y.; Rodgers, P. J.; Ishimatsu, R.; Amemiya, S. Subnanomolar Ion Detection by Stripping Voltammetry with Solid-Supported Thin Polymeric Membrane. *Anal. Chem.* **2009**, *81* (17), 7262–7270.
(72) Greenawalt, P. J.; Amemiya, S. Voltammetric Mechanism of Multiion Detection with Thin Ionophore-Based Polymeric Membrane. *Anal. Chem.* **2016**, *88* (11), 5827–5834.
(73) Liu, C.; Jiang, X.; Zhao, Y.; Jiang, W.; Zhang, Z.; Yu, L. A Solid-Contact Pb 2+ - Selective Electrode Based on Electrospun Polyaniline Microfibers Film as Ion-to-Electron Transducer. *Electrochim. Acta* **2017**, *231*, 53–60.
(74) Bobacka, Johan.; Lindfors, Tom.; McCarrick, Mary.; Ivaska, Ari.; Lewenstam, Andrzej. Single-Piece All-Solid-State Ion-Selective Electrode. *Anal. Chem.* **1995**, *67* (20), 3819–3823.
(75) Jaworska, E.; Naitana, M. L.; Stelmach, E.; Pomarico, G.; Wojciechowski, M.; Bulska, E.; Maksymiuk, K.; Paolesse, R.; Michalska, A. Introducing Cobalt(II) Porphyrin/Cobalt(III) Corrole Containing Transducers for Improved Potential Reproducibility and Performance of All-Solid-State Ion-Selective Electrodes. *Anal. Chem.* **2017**, *89* (13), 7107–7114.
(76) Nassau, K. The Fifteen Causes of Color: The Physics and Chemistry of Color. *Color Res. Appl.* **1987**, *12* (1), 4–26.
(77) Zaera, F. Probing Liquid/Solid Interfaces at the Molecular Level. *Chem. Rev.* **2012**, *112* (5), 2920–2986.
(78) Anzenbacher, Jr., P.; Lubal, P.; Buček, P.; Palacios, M. A.; Kozelkova, M. E. A Practical Approach to Optical Cross-Reactive Sensor Arrays. *Chem. Soc. Rev.* **2010**, *39* (10), 3954.
(79) Askim, J. R.; Mahmoudi, M.; Suslick, K. S. Optical Sensor Arrays for Chemical Sensing: The Optoelectronic Nose. *Chem. Soc. Rev.* **2013**, *42* (22), 8649.
(80) Clarke, J. S.; Achterberg, E. P.; Rérolle, V. M. C.; Abi Kaed Bey, S.; Floquet, C. F. A.; Mowlem, M. C. Characterisation and Deployment of an Immobilised PH Sensor Spot towards Surface Ocean PH Measurements. *Anal. Chim. Acta* **2015**, *897*, 69–80.
(81) Clarke, J. S.; Achterberg, E. P.; Connelly, D. P.; Schuster, U.; Mowlem, M. Developments in Marine PCO2 Measurement Technology; towards Sustained in Situ Observations. *Trends Anal. Chem* **2017**, *88*, 53–61.
(82) Liu, X.; Wang, Z. A.; Byrne, R. H.; Kaltenbacher, E. A.; Bernstein, R. E. Spectrophotometric Measurements of PH In-Situ: Laboratory and Field Evaluations of Instrumental Performance. *Environ. Sci. Technol.* **2006**, *40* (16), 5036–5044.
(83) Staudinger, C.; Strobl, M.; Fischer, J. P.; Thar, R.; Mayr, T.; Aigner, D.; Müller, B. J.; Müller, B.; Lehner, P.; Mistlberger, G.; Fritzsche, E.; Ehgartner, J.; Zach, P. W.; Clarke, J. S.; Geißler, F.; Mutzberg, A.; Müller, J. D.; Achterberg, E. P.; Borisov, S. M.; Klimant, I. A Versatile Optode System for Oxygen, Carbon Dioxide, and PH Measurements in Seawater with Integrated Battery and Logger: *A Versatile Optode System for O_2, CO_2, and PH*. *Limnol. Oceanogr. Methods* **2018**, *16* (7), 459–473.
(84) Al-Qaysi, W. W.; Duerkop, A. Sensor and Sensor Microtiterplate with Expanded PH Detection Range and Their Use in Real Samples. *Sens. Actuator B-Chem.* **2019**, *298*, 126848.
(85) Staudinger, C.; Strobl, M.; Breininger, J.; Klimant, I.; Borisov, S. M. Fast and Stable Optical PH Sensor Materials for Oceanographic Applications. *Sens. Actuator B-Chem.* **2019**, *282*, 204–217.
(86) Vosburgh, W. C. THE OPTICAL ROTATION OF MIXTURES OF SUCROSE, GLUCOSE AND FRUCTOSE. *J. Am. Chem. Soc.* **1921**, *43* (2), [219]-232.
(87) Hieu, H. C.; Li, H.; Miyauchi, Y.; Mizutani, G.; Fujita, N.; Nakamura, Y. Wetting Effect on Optical Sum Frequency Generation (SFG) Spectra of d-Glucose, d-Fructose, and Sucrose. *Spectrochim. Acta A* **2015**, *138*, 834–839.
(88) Adeel, M.; Rahman, Md. M.; Caligiuri, I.; Canzonieri, V.; Rizzolio, F.; Daniele, S. Recent Advances of Electrochemical and Optical Enzyme-Free Glucose Sensors Operating at Physiological Conditions. *Biosensors and Bioelectronics* **2020**, *165*, 112331.
(89) Giovannitti, A.; Nielsen, C. B.; Rivnay, J.; Kirkus, M.; Harkin, D. J.; White, A. J. P.; Sirringhaus, H.; Malliaras, G. G.; McCulloch, I. Sodium and Potassium Ion Selective Conjugated Polymers for Optical Ion Detection in Solution and Solid State. *Adv. Funct. Mater.* **2016**, *26* (4), 514–523.
(90) Wang, E.; Zhu, L.; Ma, L.; Patel, H. Optical Sensors for Sodium, Potassium and Ammonium Ions Based on Lipophilic Fluorescein Anionic Dye and Neutral Carriers. *Anal. Chim. Acta* **1997**, *357* (1–2), 85–90.
(91) Haes, A. J.; Chang, L.; Klein, W. L.; Van Duyne, R. P. Detection of a Biomarker for Alzheimer's Disease from Synthetic and Clinical Samples Using a Nanoscale Optical Biosensor. *J. Am. Chem. Soc.* **2005**, *127* (7), 2264–2271.
(92) Nagel, T.; Ehrentreich-Förster, E.; Singh, M.; Schmitt, K.; Brandenburg, A.; Berka, A.; Bier, F. F. Direct Detection of Tuberculosis Infection in Blood Serum Using Three Optical Label-Free Approaches. *Sens. Actuator B-Chem.* **2008**, *129* (2), 934–940.
(93) Qi, D.; Berger, A. J. Chemical Concentration Measurement in Blood Serum and Urine Samples Using Liquid-Core Optical Fiber Raman Spectroscopy. *Appl. Opt.* **2007**, *46* (10), 1726.
(94) Singh, V.; Rodenbaugh, C.; Krishnan, S. Magnetic Optical Microarray Imager for Diagnosing Type of Diabetes in Clinical Blood Serum Samples. *ACS Sens.* **2016**, *1* (4), 437–443.
(95) Jeronimo, P.; Araujo, A.; Conceicaobsmmontenegro, M. Optical Sensors and Biosensors Based on Sol–Gel Films. *Talanta* **2007**, *72* (1), 13–27.
(96) Carreres-Prieto, D.; García, J. T.; Cerdán-Cartagena, F.; Suardiaz-Muro, J. Performing Calibration of Transmittance by Single RGB-LED within the Visible Spectrum. *Sensors* **2020**, *20* (12), 3492.
(97) Eustaquio, A.; Blanco, M.; Jee, R. D.; Moffat, A. C. Determination of Paracetamol in Intact Tablets by Use of near Infrared Transmittance Spectroscopy. *Anal. Chim. Acta* **1999**, *383* (3), 283–290.
(98) Merckle, P.; Kovar, K.-A. Assay of Effervescent Tablets by Near-Infrared Spectroscopy in Transmittance and Reflectance Mode: Acetylsalicylic Acid in Mono and Combination Formulations. *J. Pharm. Biomed. Anal.* **1998**, *17* (3), 365–374.
(99) Ricci, R. W.; Ditzler, M.; Nestor, L. P. Discovering the Beer-Lambert Law. *J. Chem. Educ.* **1994**, *71* (11), 983.
(100) Kuntzleman, T. S.; Jacobson, E. C. Teaching Beer's Law and Absorption Spectrophotometry with a Smart Phone: A Substantially Simplified Protocol. *J. Chem. Educ.* **2016**, *93* (7), 1249–1252.
(101) Nilapwar, S. M.; Nardelli, M.; Westerhoff, H. V.; Verma, M. Absorption Spectroscopy. In *Methods in Enzymology*; Elsevier, 2011; Vol. 500, pp 59–75.
(102) Cosimo A. De Caro. *UV/VIS Spectrophotometry - Fundamentals and Applications*; Mettler-Toledo: Sonnenbergstrasse 74 CH-8603 Schwerzenbach, Switzerland, 2015.
(103) Wang, E.; Meyerhoff, M. E. Anion Selective Optical Sensing with Metalloporphyrin-Doped Polymeric Films. *Anal. Chim. Acta* **1993**, *283* (2), 673–682.

(104) de Marcos, S.; Wolfbeis, O. S. Optical Sensing of PH Based on Polypyrrole Films. *Anal. Chim. Acta* **1996**, *334* (1–2), 149–153.
(105) Grummt, U.-W.; Pron, A.; Zagorska, M.; Lefrant, S. Polyaniline Based Optical PH Sensor. *Anal. Chim. Acta* **1997**, *357* (3), 253–259.
(106) Koncki, R.; Wolfbeis, O. S. Composite Films of Prussian Blue and N-Substituted Polypyrroles: Fabrication and Application to Optical Determination of PH. *Anal. Chem.* **1998**, *70* (13), 2544–2550.
(107) Xie, Z.; Ramakrishnam Raju, M. V.; Stewart, A. C.; Nantz, M. H.; Fu, X.-A. Imparting Sensitivity and Selectivity to a Gold Nanoparticle Chemiresistor through Thiol Monolayer Functionalization for Sensing Acetone. *RSC Adv.* **2018**, *8* (62), 35618–35624.
(108) Nath, N.; Chilkoti, A. A Colorimetric Gold Nanoparticle Sensor To Interrogate Biomolecular Interactions in Real Time on a Surface. *Anal. Chem.* **2002**, *74* (3), 504–509.
(109) Date, Y.; Terakado, S.; Sasaki, K.; Aota, A.; Matsumoto, N.; Shiku, H.; Ino, K.; Watanabe, Y.; Matsue, T.; Ohmura, N. Microfluidic Heavy Metal Immunoassay Based on Absorbance Measurement. *Biosens. Bioelectron.* **2012**, *33* (1), 106–112.
(110) Malcik, N.; Ferrance, J. P.; Landers, J. P.; Caglar, P. The Performance of a Microchip-Based Fiber Optic Detection Technique for the Determination of Ca2+ Ions in Urine. *Sens. Actuator B-Chem.* **2005**, *107* (1), 24–31.
(111) Yam, K. L.; Papadakis, S. E. A Simple Digital Imaging Method for Measuring and Analyzing Color of Food Surfaces. *J. Food Eng.* **2004**, *61* (1), 137–142.
(112) Oliveira, L. F.; Canevari, N. T.; Guerra, M. B. B.; Pereira, F. M. V.; Schaefer, C. E. G. R.; Pereira-Filho, E. R. Proposition of a Simple Method for Chromium (VI) Determination in Soils from Remote Places Applying Digital Images: A Case Study from Brazilian Antarctic Station. *Microchem. J.* **2013**, *109*, 165–169.
(113) Silvalyra, W.; Dossantos, V.; Dionizio, A.; Martins, V.; Almeida, L.; Nobregagaiao, E.; Diniz, P.; Silva, E.; Araujo, M. Digital Image-Based Flame Emission Spectrometry. *Talanta* **2009**, *77* (5), 1584–1589.
(114) Kohl, S. K.; Landmark, J. D.; Stickle, D. F. Demonstration of Absorbance Using Digital Color Image Analysis and Colored Solutions. *J. Chem. Educ.* **2006**, *83* (4), 644.
(115) Benedetti, L. P. dos S.; dos Santos, V. B.; Silva, T. A.; Filho, E. B.; Martins, V. L.; Fatibello-Filho, O. A Digital Image-Based Method Employing a Spot-Test for Quantification of Ethanol in Drinks. *Anal. Methods* **2015**, *7* (10), 4138–4144.
(116) Thajee, K.; Wang, L.; Grudpan, K.; Bakker, E. Colorimetric Ionophore-Based Coextraction Titrimetry of Potassium Ions. *Anal. Chim. Acta* **2018**, *1029*, 37–43.
(117) Askim, J. R.; Mahmoudi, M.; Suslick, K. S. Optical Sensor Arrays for Chemical Sensing: The Optoelectronic Nose. *Chem. Soc. Rev.* **2013**, *42* (22), 8649.
(118) Capelli, L.; Sironi, S.; Del Rosso, R. Electronic Noses for Environmental Monitoring Applications. *Sensors* **2014**, *14* (11), 19979–20007.
(119) Montuschi, P.; Mores, N.; Trové, A.; Mondino, C.; Barnes, P. J. The Electronic Nose in Respiratory Medicine. *Respiration* **2013**, *85* (1), 72–84.
(120) Röck, F.; Barsan, N.; Weimar, U. Electronic Nose: Current Status and Future Trends. *Chem. Rev.* **2008**, *108* (2), 705–725.
(121) Ciosek, P.; Wróblewski, W. Sensor Arrays for Liquid Sensing – Electronic Tongue Systems. *Analyst* **2007**, *132* (10), 963.
(122) Winquist, F.; Wide, P.; Lundström, I. An Electronic Tongue Based on Voltammetry. *Anal. Chim. Acta* **1997**, *357* (1–2), 21–31.
(123) Bigdeli, A.; Ghasemi, F.; Golmohammadi, H.; Abbasi-Moayed, S.; Nejad, M. A. F.; Fahimi-Kashani, N.; Jafarinejad, S.; Shahrajabian, M.; Hormozi-Nezhad, M. R. Nanoparticle-Based Optical Sensor Arrays. *Nanoscale* **2017**, *9* (43), 16546–16563.
(124) Jurs, P. C.; Bakken, G. A.; McClelland, H. E. Computational Methods for the Analysis of Chemical Sensor Array Data from Volatile Analytes. *Chem. Rev.* **2000**, *100* (7), 2649–2678.
(125) Wright, A. T.; Anslyn, E. V. Differential Receptor Arrays and Assays for Solution-Based Molecular Recognition. *Chem. Soc. Rev.* **2006**, *35* (1), 14–28.
(126) Senel, M.; Dervisevic, M.; Alhassen, S.; Alachkar, A.; Voelcker, N. H. Electrochemical Micropyramid Array-Based Sensor for *In Situ* Monitoring of Dopamine Released from Neuroblastoma Cells. *Anal. Chem.* **2020**, *92* (11), 7746–7753.
(127) Leng, Y.; Xie, K.; Ye, L.; Li, G.; Lu, Z.; He, J. Gold-Nanoparticle-Based Colorimetric Array for Detection of Dopamine in Urine and Serum. *Talanta* **2015**, *139*, 89–95.
(128) Liao, Y.-H.; Chou, J.-C. Preparation and Characteristics of Ruthenium Dioxide for PH Array Sensors with Real-Time Measurement System. *Sens. Actuator B-Chem.* **2008**, *128* (2), 603–612.
(129) Rahimi, R.; Ochoa, M.; Parupudi, T.; Zhao, X.; Yazdi, I. K.; Dokmeci, M. R.; Tamayol, A.; Khademhosseini, A.; Ziaie, B. A Low-Cost Flexible PH Sensor Array for Wound Assessment. *Sens. Actuator B-Chem.* **2016**, *229*, 609–617.
(130) Zhao, R.; Xu, M.; Wang, J.; Chen, G. A PH Sensor Based on the TiO2 Nanotube Array Modified Ti Electrode. *Electrochim. Acta* **2010**, *55* (20), 5647–5651.
(131) Liu, Y.-H.; Dam, T. H.; Pantano, P. A PH-Sensitive Nanotip Array Imaging Sensor. *Anal. Chim. Acta* **2000**, *419* (2), 215–225.
(132) Safavi, A.; Maleki, N.; Rostamzadeh, A.; Maesum, S. CCD Camera Full Range PH Sensor Array. *Talanta* **2007**, *71* (1), 498–501.
(133) Zhou, Y.; Huang, W.; He, Y. PH-Induced Silver Nanoprism Etching-Based Multichannel Colorimetric Sensor Array for Ultrasensitive Discrimination of Thiols. *Sens. Actuator B-Chem.* **2018**, *270*, 187–191.
(134) Yeow, T. C. W.; Haskard, M. R.; Mulcahy, D. E.; Seo, H. I.; Kwon, D. H. A Very Large Integrated PH-ISFET Sensor Array Chip Compatible with Standard CMOS Processes. *Sens. Actuator B-Chem.* **1997**, *44* (1–3), 434–440.
(135) Carofiglio, T.; Fregonese, C.; Mohr, G. J.; Rastrelli, F.; Tonellato, U. Optical Sensor Arrays: One-Pot, Multiparallel Synthesis and Cellulose Immobilization of PH and Metal Ion Sensitive Azo-Dyes. *Tetrahedron* **2006**, *62* (7), 1502–1507.
(136) Capel-Cuevas, S.; Cuéllar, M. P.; de Orbe-Payá, I.; Pegalajar, M. C.; Capitán-Vallvey, L. F. Full-Range Optical PH Sensor Array Based on Neural Networks. *Microchem. J.* **2011**, *97* (2), 225–233.
(137) Martinez-Olmos, A.; Capel-Cuevas, S.; López-Ruiz, N.; Palma, A. J.; de Orbe, I.; Capitán-Vallvey, L. F. Sensor Array-Based Optical Portable Instrument for Determination of PH. *Sens. Actuator B-Chem.* **2011**, *156* (2), 840–848.
(138) Harandizadeh, Z.; Ito, T. Block Copolymer-Derived Recessed Nanodisk-Array Electrodes as Platforms for Folding-Based Electrochemical DNA Sensors. *ChemElectroChem* **2019**, *6* (22), 5627–5632.
(139) Singh, V. Quantum Dot Decorated Multi-Walled Carbon Nanotube Modified Electrochemical Sensor Array for Single Drop Insulin Detection. *Mater. Lett.* **2019**, *254*, 415–418.
(140) Rafati, A.; Zarrabi, A.; Abediankenari, S.; Aarabi, M.; Gill, P. Sensitive Colorimetric Assay Using Insulin G-Quadruplex Aptamer Arrays on DNA Nanotubes Coupled with Magnetic Nanoparticles. *R. Soc. open sci.* **2018**, *5* (3), 171835.
(141) Abu-Ali, H.; Nabok, A.; Smith, T. J.; Al-Shanawa, M. Development of a Novel Electrochemical Inhibition Sensor Array Based on Bacteria Immobilized on Modified Screen-Printed Gold Electrodes for Water Pollution Detection. *BioNanoSci.* **2019**, *9* (2), 345–355.
(142) Huang, Y.; Cheng, P.; Tan, C. Visual Artificial Tongue for Identification of Various Metal Ions in Mixtures and Real Water Samples: A Colorimetric Sensor Array Using off-the-Shelf Dyes. *RSC Adv.* **2019**, *9* (47), 27583–27587.
(143) Minami, T.; Emami, F.; Nishiyabu, R.; Kubo, Y.; Anzenbacher, P. Quantitative Analysis of Modeled ATP Hydrolysis in Water by a Colorimetric Sensor Array. *Chem. Commun.* **2016**, *52* (50), 7838–7841.

(144) Li, Y.; He, X.; Guo, M.; Lin, D.; Xu, C.; Xie, F.; Sun, X. Porous NiTe2 Nanosheet Array: An Effective Electrochemical Sensor for Glucose Detection. *Sens. Actuator B-Chem.* **2018**, *274*, 427–432.
(145) Xie, F.; Cao, X.; Qu, F.; Asiri, A. M.; Sun, X. Cobalt Nitride Nanowire Array as an Efficient Electrochemical Sensor for Glucose and H2O2 Detection. *Sens. Actuator B-Chem.* **2018**, *255*, 1254–1261.
(146) Liu, W.; Ding, F.; Wang, Y.; Mao, L.; Liang, R.; Zou, P.; Wang, X.; Zhao, Q.; Rao, H. Fluorometric and Colorimetric Sensor Array for Discrimination of Glucose Using Enzymatic-Triggered Dual-Signal System Consisting of Au@Ag Nanoparticles and Carbon Nanodots. *Sens. Actuator B-Chem.* **2018**, *265*, 310–317.
(147) Jia, M.-Y.; Wu, Q.-S.; Li, H.; Zhang, Y.; Guan, Y.-F.; Feng, L. The Calibration of Cellphone Camera-Based Colorimetric Sensor Array and Its Application in the Determination of Glucose in Urine. *Biosens. Bioelectron.* **2015**, *74*, 1029–1037.
(148) Han, J.-H.; Kim, S.; Choi, J.; Kang, S.; Pak, Y. K.; Pak, J. J. Development of Multi-Well-Based Electrochemical Dissolved Oxygen Sensor Array. *Sens. Actuator B-Chem.* **2020**, *306*, 127465.
(149) Magalhães, J. M. C. S.; Machado, A. A. S. C. Array of Potentiometric Sensors for the Analysis of Creatinine in Urine Samples. *Analyst* **2002**, *127* (8), 1069–1075.
(150) Rudnitskaya, A.; Costa, A. M. S.; Delgadillo, I. Calibration Update Strategies for an Array of Potentiometric Chemical Sensors. *Sens. Actuator B-Chem.* **2017**, *238*, 1181–1189.
(151) Toczyłowska-Mamińska, R.; Kloch, M.; Zawistowska-Deniziak, A.; Bala, A. Design and Characterization of Novel All-Solid-State Potentiometric Sensor Array Dedicated to Physiological Measurements. *Talanta* **2016**, *159*, 7–13.
(152) Jańczyk, M.; Kutyła-Olesiuk, A.; Cetó, X.; del Valle, M.; Ciosek, P.; Wróblewski, W. Resolution of Amino Acid Mixtures by an Array of Potentiometric Sensors Based on Boronic Acid Derivative in a SIA Flow System. *Sens. Actuator B-Chem.* **2013**, *189*, 179–186.
(153) Zdrachek, E.; Bakker, E. Potentiometric Sensor Array with Multi-Nernstian Slope. *Anal. Chem.* **2020**, *92* (4), 2926–2930.
(154) Albert, K. J.; Lewis, N. S.; Schauer, C. L.; Sotzing, G. A.; Stitzel, S. E.; Vaid, T. P.; Walt, D. R. Cross-Reactive Chemical Sensor Arrays. *Chem. Rev.* **2000**, *100* (7), 2595–2626.
(155) Anker, J. N.; Hall, W. P.; Lyandres, O.; Shah, N. C.; Zhao, J.; Van Duyne, R. P. Biosensing with Plasmonic Nanosensors. *Nature Mater* **2008**, *7* (6), 442–453.
(156) Jeon, S.; Ahn, S.-E.; Song, I.; Kim, C. J.; Chung, U.-I.; Lee, E.; Yoo, I.; Nathan, A.; Lee, S.; Ghaffarzadeh, K.; Robertson, J.; Kim, K. Gated Three-Terminal Device Architecture to Eliminate Persistent Photoconductivity in Oxide Semiconductor Photosensor Arrays. *Nature Mater* **2012**, *11* (4), 301–305.
(157) Lu, Y.; Peng, S.; Luo, D.; Lal, A. Low-Concentration Mechanical Biosensor Based on a Photonic Crystal Nanowire Array. *Nat Commun* **2011**, *2* (1), 578.
(158) Rakow, N. A.; Suslick, K. S. A Colorimetric Sensor Array for Odour Visualization. *Nature* **2000**, *406* (6797), 710–713.
(159) Lim, S. H.; Feng, L.; Kemling, J. W.; Musto, C. J.; Suslick, K. S. An Optoelectronic Nose for the Detection of Toxic Gases. *Nature Chem* **2009**, *1* (7), 562–567.
(160) Greene, N. T.; Shimizu, K. D. Colorimetric Molecularly Imprinted Polymer Sensor Array Using Dye Displacement. *J. Am. Chem. Soc.* **2005**, *127* (15), 5695–5700.
(161) Li, X.; Li, S.; Liu, Q.; Cui, Z.; Chen, Z. A Triple-Channel Colorimetric Sensor Array for Identification of Biothiols Based on Color RGB (Red/Green/Blue) as Signal Readout. *ACS Sustainable Chem. Eng.* **2019**, *7* (20), 17482–17490.
(162) Steemers, F. J.; Ferguson, J. A.; Walt, D. R. Screening Unlabeled DNA Targets with Randomly Ordered Fiber-Optic Gene Arrays. *Nat. Biotechnol.* **2000**, *18* (1), 91–94.
(163) Walt, D. R. MOLECULAR BIOLOGY:Bead-Based Fiber-Optic Arrays. *Science* **2000**, *287* (5452), 451–452.
(164) Zhang, X.; Zhai, Q.; Xing, H.; Li, J.; Wang, E. Bipolar Electrodes with 100% Current Efficiency for Sensors. *ACS Sens.* **2017**, *2* (3), 320–326.
(165) Loget, G.; Kuhn, A. Shaping and Exploring the Micro- and Nanoworld Using Bipolar Electrochemistry. *Anal. Bioanal. Chem.* **2011**, *400* (6), 1691–1704.
(166) Mavré, F.; Anand, R. K.; Laws, D. R.; Chow, K.-F.; Chang, B.-Y.; Crooks, J. A.; Crooks, R. M. Bipolar Electrodes: A Useful Tool for Concentration, Separation, and Detection of Analytes in Microelectrochemical Systems. *Anal. Chem.* **2010**, *82* (21), 8766–8774.
(167) Kuhn, A.; Crooks, R. M.; Inagi, S. A Compelling Case for Bipolar Electrochemistry. *ChemElectroChem* **2016**, *3* (3), 351–352.
(168) Zhan, W.; Alvarez, J.; Crooks, R. M. Electrochemical Sensing in Microfluidic Systems Using Electrogenerated Chemiluminescence as a Photonic Reporter of Redox Reactions. *J. Am. Chem. Soc.* **2002**, *124* (44), 13265–13270.
(169) Mavré, F.; Chow, K.-F.; Sheridan, E.; Chang, B.-Y.; Crooks, J. A.; Crooks, R. M. A Theoretical and Experimental Framework for Understanding Electrogenerated Chemiluminescence (ECL) Emission at Bipolar Electrodes. *Anal. Chem.* **2009**, *81* (15), 6218–6225.
(170) Shi, H.-W.; Zhao, W.; Liu, Z.; Liu, X.-C.; Wu, M.-S.; Xu, J.-J.; Chen, H.-Y. Joint Enhancement Strategy Applied in ECL Biosensor Based on Closed Bipolar Electrodes for the Detection of PSA. *Talanta* **2016**, *154*, 169–174.
(171) Wu, M.; Xu, N.; Qiao, J.; Chen, J.; Jin, L. Bipolar Electrode-Electrochemiluminescence (ECL) Biosensor Based on a Hybridization Chain Reaction. *Analyst* **2019**, *144* (15), 4633–4638.
(172) Zhang, X.; Chen, C.; Yin, J.; Han, Y.; Li, J.; Wang, E. Portable and Visual Electrochemical Sensor Based on the Bipolar Light Emitting Diode Electrode. *Anal. Chem.* **2015**, *87* (9), 4612–4616.
(173) Bouffier, L.; Doneux, T.; Goudeau, B.; Kuhn, A. Imaging Redox Activity at Bipolar Electrodes by Indirect Fluorescence Modulation. *Anal. Chem.* **2014**, *86* (8), 3708–3711.
(174) Xu, W.; Ma, C.; Bohn, P. W. Coupling of Independent Electrochemical Reactions and Fluorescence at Closed Bipolar Interdigitated Electrode Arrays. *ChemElectroChem* **2016**, *3* (3), 422–428.
(175) Xing, H.; Zhang, X.; Zhai, Q.; Li, J.; Wang, E. Bipolar Electrode Based Reversible Fluorescence Switch Using Prussian Blue/Au Nanoclusters Nanocomposite Film. *Anal. Chem.* **2017**, *89* (7), 3867–3872.
(176) Zhang, X.; Zhang, L.; Zhai, Q.; Gu, W.; Li, J.; Wang, E. Self-Powered Bipolar Electrochromic Electrode Arrays for Direct Displaying Applications. *Anal. Chem.* **2016**, *88* (5), 2543–2547.
(177) Xu, W.; Fu, K.; Bohn, P. W. Electrochromic Sensor for Multiplex Detection of Metabolites Enabled by Closed Bipolar Electrode Coupling. *ACS Sens.* **2017**, *2* (7), 1020–1026.
(178) Yu, X.; Liang, J.; Yang, T.; Gong, M.; Xi, D.; Liu, H. A Resettable and Reprogrammable Keypad Lock Based on Electrochromic Prussian Blue Films and Biocatalysis of Immobilized Glucose Oxidase in a Bipolar Electrode System. *Biosens. Bioelectron.* **2018**, *99*, 163–169.
(179) Xu, W.; Fu, K.; Ma, C.; Bohn, P. W. Closed Bipolar Electrode-Enabled Dual-Cell Electrochromic Detectors for Chemical Sensing. *Analyst* **2016**, *141* (21), 6018–6024.
(180) Jaworska, E.; Michalska, A.; Maksymiuk, K. Fluorimetric Readout of Ion-Selective Electrode Potential Changes. *Electrochimica Acta* **2018**, *284*, 321–327.

(181) Vanamo, U.; Hupa, E.; Yrjänä, V.; Bobacka, J. New Signal Readout Principle for Solid-Contact Ion-Selective Electrodes. *Anal. Chem.* **2016**, *88* (8), 4369–4374.
(182) Kraikaew, P.; Jeanneret, S.; Soda, Y.; Cherubini, T.; Bakker, E. Ultrasensitive Seawater PH Measurement by Capacitive Readout of Potentiometric Sensors. *ACS Sens.* **2020**, *5* (3), 650–654.
(183) Hupa, E.; Vanamo, U.; Bobacka, J. Novel Ion-to-Electron Transduction Principle for Solid-Contact ISEs. *Electroanalysis* **2015**, *27* (3), 591–594.
(184) Jarolímová, Z.; Han, T.; Mattinen, U.; Bobacka, J.; Bakker, E. Capacitive Model for Coulometric Readout of Ion-Selective Electrodes. *Anal. Chem.* **2018**, *90* (14), 8700–8707.
(185) Kraikaew, P.; Sailapu, S. K.; Bakker, E. Rapid Constant Potential Capacitive Measurements with Solid-Contact Ion-Selective Electrodes Coupled to Electronic Capacitor. *Anal. Chem.* **2020**, acs.analchem.0c03254.
(186) Crespo, G. A.; Mistlberger, G.; Bakker, E. Electrogenerated Chemiluminescence for Potentiometric Sensors. *J. Am. Chem. Soc.* **2012**, *134* (1), 205–207.
(187) Zhai, J.; Yang, L.; Du, X.; Xie, X. Electrochemical-to-Optical Signal Transduction for Ion-Selective Electrodes with Light-Emitting Diodes. *Anal. Chem.* **2018**, *90* (21), 12791–12795.
(188) Mehrotra, P. Biosensors and Their Applications – A Review. *J Oral Biol Craniofac Res* **2016**, *6* (2), 153–159.
(189) Arechederra, R. L.; Minteer, S. D. Self-Powered Sensors. *Anal. Bioanal. Chem.* **2011**, *400* (6), 1605–1611.
(190) Chen, Y.; Ji, W.; Yan, K.; Gao, J.; Zhang, J. Fuel Cell-Based Self-Powered Electrochemical Sensors for Biochemical Detection. *Nano Energy* **2019**, *61*, 173–193.
(191) Gai, P.; Gu, C.; Hou, T.; Li, F. Integration of Biofuel Cell-Based Self-Powered Biosensing and Homogeneous Electrochemical Strategy for Ultrasensitive and Easy-To-Use Bioassays of MicroRNA. *ACS Appl. Mater. Interfaces* **2018**, *10* (11), 9325–9331.
(192) Kumar, A.; Sharma, S.; Pandey, L. M.; Chandra, P. Nanoengineered Material Based Biosensing Electrodes for Enzymatic Biofuel Cells Applications. *Mater. Sci. Technol.* **2018**, *1* (1), 38–48.
(193) Meredith, M. T.; Minteer, S. D. Biofuel Cells: Enhanced Enzymatic Bioelectrocatalysis. *Annual Rev. Anal. Chem.* **2012**, *5* (1), 157–179.
(194) Wen, D.; Eychmüller, A. Enzymatic Biofuel Cells on Porous Nanostructures. *Small* **2016**, *12* (34), 4649–4661.
(195) Xu, Z.; Liu, Y.; Williams, I.; Li, Y.; Qian, F.; Wang, L.; Lei, Y.; Li, B. Flat Enzyme-Based Lactate Biofuel Cell Integrated with Power Management System: Towards Long Term in Situ Power Supply for Wearable Sensors. *Appl. Energy* **2017**, *194*, 71–80.
(196) Hanashi, T.; Yamazaki, T.; Tanaka, H.; Ikebukuro, K.; Tsugawa, W.; Sode, K. The Development of an Autonomous Self-Powered Bio-Sensing Actuator. *Sens. Actuator B-Chem.* **2014**, *196*, 429–433.
(197) Pinyou, P.; Conzuelo, F.; Sliozberg, K.; Vivekananthan, J.; Contin, A.; Pöller, S.; Plumeré, N.; Schuhmann, W. Coupling of an Enzymatic Biofuel Cell to an Electrochemical Cell for Self-Powered Glucose Sensing with Optical Readout. *Bioelectrochemistry* **2015**, *106*, 22–27.
(198) Li, S.; Cheng, C.; Thomas, A. Carbon-Based Microbial-Fuel-Cell Electrodes: From Conductive Supports to Active Catalysts. *Adv. Mater.* **2017**, *29* (8), 1602547.
(199) Liu, J.; Qiao, Y.; Guo, C. X.; Lim, S.; Song, H.; Li, C. M. Graphene/Carbon Cloth Anode for High-Performance Mediatorless Microbial Fuel Cells. *Bioresour. Technol.* **2012**, *114*, 275–280.
(200) Wang, H.; Ren, Z. J. A Comprehensive Review of Microbial Electrochemical Systems as a Platform Technology. *Biotechnol. Adv.* **2013**, *31* (8), 1796–1807.
(201) Choudhury, P.; Uday, U. S. P.; Mahata, N.; Nath Tiwari, O.; Narayan Ray, R.; Kanti Bandyopadhyay, T.; Bhunia, B. Performance Improvement of Microbial Fuel Cells for Waste Water Treatment along with Value Addition: A Review on Past Achievements and Recent Perspectives. *Renew. Sust. Energ. Rev.* **2017**, *79*, 372–389.
(202) Zang, Y.; Fan, J.; Ju, Y.; Xue, H.; Pang, H. Current Advances in Semiconductor Nanomaterial-Based Photoelectrochemical Biosensing. *Chem. Eur. J.* **2018**, *24* (53), 14010–14027.
(203) Wang, Y.; Zhang, L.; Cui, K.; Xu, C.; Li, H.; Liu, H.; Yu, J. Solar Driven Electrochromic Photoelectrochemical Fuel Cells for Simultaneous Energy Conversion, Storage and Self-Powered Sensing. *Nanoscale* **2018**, *10* (7), 3421–3428.
(204) Zhu, Y.; Yan, K.; Liu, Y.; Zhang, J. Photovoltammetric Behavior and Photoelectrochemical Determination of P-Phenylenediamine on CdS Quantum Dots and Graphene Hybrid Film. *Anal. Chim. Acta* **2015**, *884*, 29–36.
(205) Katz, E.; Bückmann, A. F.; Willner, I. Self-Powered Enzyme-Based Biosensors. *J. Am. Chem. Soc.* **2001**, *123* (43), 10752–10753.
(206) Miyake, T.; Haneda, K.; Nagai, N.; Yatagawa, Y.; Onami, H.; Yoshino, S.; Abe, T.; Nishizawa, M. Enzymatic Biofuel Cells Designed for Direct Power Generation from Biofluids in Living Organisms. *Energy Environ. Sci.* **2011**, *4* (12), 5008.
(207) Jaworska, E.; Michalska, A.; Maksymiuk, K. Self-Powered Cascade Bipolar Electrodes with Fluorimetric Readout. *Anal. Chem.* **2019**, *91* (24), 15525–15531.
(208) Sailapu, S. K.; Kraikaew, P.; Sabaté, N.; Bakker, E. Self-Powered Potentiometric Sensor Transduction to a Capacitive Electronic Component for Later Readout. *ACS Sens.* **2020**, *5* (9), 2909–2914.

Chapter 2: Electrochemical Ion Transfer Mediated by a Lipophilic Os(II)/Os(III) Dinonyl Bipyridyl Probe Incorporated in Thin Membranes

This work has been published in: Jansod, S.; Wang, L.; Cuartero, M.; Bakker, E. *Chem. Commun*. **2017**, *53*, 10757-10760.

2.1 Abstract

A new lipophilic dinonyl bipyridyl Os(II)/Os(III) complex successfully mediates ion transfer processes across voltammetric thin membranes. Added lipophilic cation-exchanger may impose voltammetric anion or cation transfer waves of Gaussian shape that are reversible and repeatable. Peak potential is found to shift with ion concentration in agreement with the Nernst equation. The addition of tridodecylmethylammonium nitrate to the polymeric film dramatically reduces peak separation from 240 mV to 65 mV, and peak width to near-theoretical values of 85 mV, which agrees with a surface confined process. It is suggested that the cationic additive serves as phase transfer catalyst.

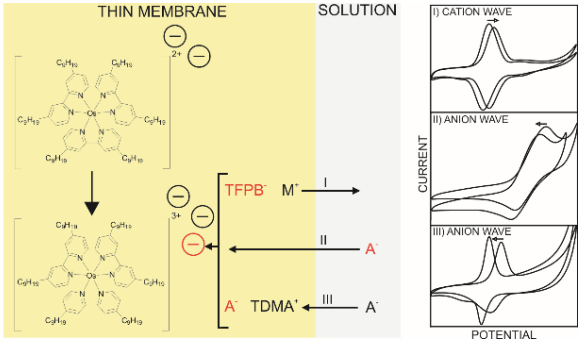

2.2 Introduction

The incorporation of conducting polymers (CPs) as ion-to-electron transducers in solid contact ion-selective electrodes (SC-ISE) has marked a significant step towards the fabrication of robust all solid state potentiometric sensors.[1] Subsequently, conducting polymers such as poly(3,4-ethylenedioxythiophene) (PEDOT) and poly(3-octylthiophene) (POT) were also introduced as electrochemical modulators in ion-transfer voltammetry at ion-selective membranes. Here, the oxidation/reduction of the buried CP film changes the ratio of CP/CP^+, and triggers the transfer of an ion across the sample–membrane interface to maintain electroneutrality.

Such all solid state voltammetric ion sensing probes were explored in stripping ion transfer voltammetry, exhibiting subnanomolar limits of detection.[2] Ion-selective membranes with PEDOT conducting polymer transducing layers that exhibited large redox capacities found their use in the exhaustive sensing/removal of ions from the sample for the realization of coulometric ion transfer sensing devices.[3] Moreover, multi-ionophore based ~230 nm thin membranes backside contacted with POT was used for triggering multiple exhaustive and selective cation transfer waves, each showing a reversible Gaussian voltammetric peak.[4]

Unfortunately, these ion-to-electron transducing materials are still not satisfactory. In this regard, POT exhibits very limited redox capacity since its oxidation wave is near 1 V (relative to Ag/AgCl electrode),[5] a potential where other sample species may interfere by redox reactivity. There are some literature reports on the detection of anions using either PEDOT or POT transducers.[2,6] However, cyclic voltammograms gave a lower cathodic current relative to the corresponding anodic one and, according to our knowledge, there exist no data that would explain this lack of reversibility. Also, the redox behavior of conducting polymers cannot easily be described theoretically, making it difficult to extract the underlying ion transfer wave from the voltammetric data. PEDOT is also known to exhibit a high polarity and there is the risk for water layer formation between the sensing membrane and the underlying electrode.[7]

Molecular redox probes dissolved in the sensing film or covalently attached to the polymer have been explored as alternative.[8] Unfortunately for the ubiquitous ferrocene, the oxidized ferrocenium is chemically unstable and results in deteriorating electrochemical behavior when confined to a thin film. In other work, complexes of a mixture of Co(II)/Co(III) were shown to act as reliable redox couple in potentiometry, but only in the absence of ionophore such as valinomycin,[9] as otherwise the Co(III) was gradually lost from the membrane by ionophore-mediated exchange with potassium ions. On the other hand, the use of a transducer layer based on Co(II)porphyrin/Co(III)corrole pair together with carbon nanotubes seems to be a promising tool towards a new generation of SC-ISEs.[10]

We explore here dinonyl dipyridyl complexes of Os(II)/Os(III) as molecular ion to electron transducing probes in thin voltammetric sensing layers. The approach was inspired by earlier work by Heller,[11] who demonstrated electrochemical reversibility of osmium complexes covalently attached to polymers confined to an electrode surface, giving a 20 mV peak separation and a peak width at half maximum of about 100 mV. Schuhmann more recently incorporated such redox probes into hydrogel materials.[12]

2.3 Experimental Details

Materials, reagents, and instruments

Sodium chloride (NaCl), sodium hexafluorophosphate ($NaPF_6$), sodium perchlorate ($NaClO_4$), sodium nitrate ($NaNO_3$), potassium chloride (KCl), lithium chloride (LiCl), magnesium chloride ($MgCl_2$), calcium chloride ($CaCl_2$), tridodecylmethylammonium nitrate ($TDMANO_3$), tetrabutylammonium chloride (TBACl, >97.0%), tetrahydrofuran (THF), sodium tetrakis[3,5-bis(trifluoromethyl)phenyl]-borate (NaTFPB), high molecular weight poly(vinyl chloride) (PVC) and bis(2-ethylhexyl)sebacate (DOS) were purchased from Sigma-Aldrich.

Glassy carbon (GC) electrode tip (6.1204.300) with an electrode diameter of 3.00 ± 0.05 mm were sourced from Metrohm (Switzerland). Cyclic voltammograms were recorded with a PGSTAT 101 (Metrohm Autolab B.V.) controlled by NOVA 1.8 software. A double-junction Ag/AgCl/3 M KCl/1 M LiOAc reference electrode (6.0726.100 model, Metrohm, Switzerland) and a platinum electrode (6.0331.010 model, Metrohm, Switzerland) were used in a three-electrode cell. A rotating disk electrode (Autolab, RDE, Metrohm Autolab B.V., Utrecht, The Netherlands) was used to spin coat the membranes on the electrode at 1500 rpm.

Electrode preparation

Different membrane cocktails were prepared by dissolving appropriate amounts of the components in 1 mL of THF (see Table S1 for the membrane compositions). A dilution of each cocktail (50 µL + 250 µL of THF) was prepared to be deposited on the electrode surface. Thin layer membrane was spin coated at 1500 rpm onto the GC electrode by dropping a volume of 25 µL of the diluted cocktail for 1 min.

2.4 Results and Discussion

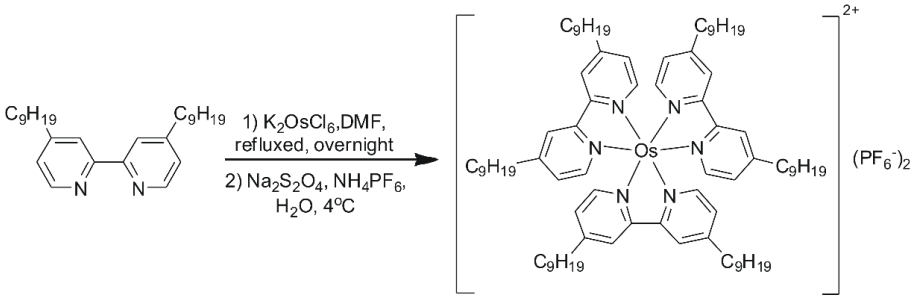

Scheme 1. Synthetic route for $(Os(II)(dnbpy)_3)\cdot(PF_6)_2$.

Scheme 1 presents the synthetic route designed to obtain $(Os(II)(dnbpy)_3)\cdot(PF_6)_2$. This is based on the substitution of chloride ligands in potassium hexachloroosmiate (K_2OsCl_6) by three bidentate ligands of 4,4' -dinonyl-2,2'-bipyridine (dnbpy), reducing the Os(IV) center to Os(II).

Cyclic voltammograms obtained for the synthesized compound in organic solution are shown in Figure S1. One reversible peak is displayed at 704 mV (vs. Ag/AgCl reference electrode) that corresponds to a one electron transfer process ($W_{1/2}$~100 mV, E_{pc}-E_{pa}=70 mV), suggesting that the wave corresponds to the Os(II)/Os(III)

oxidation/reduction process. It is assumed that the underlying electrochemical behavior is similar when moving from organic solution to a hydrophobic polymeric sensing film, as the polymer chiefly serves to gelify the organic solvent, mainly affecting mass transport properties.

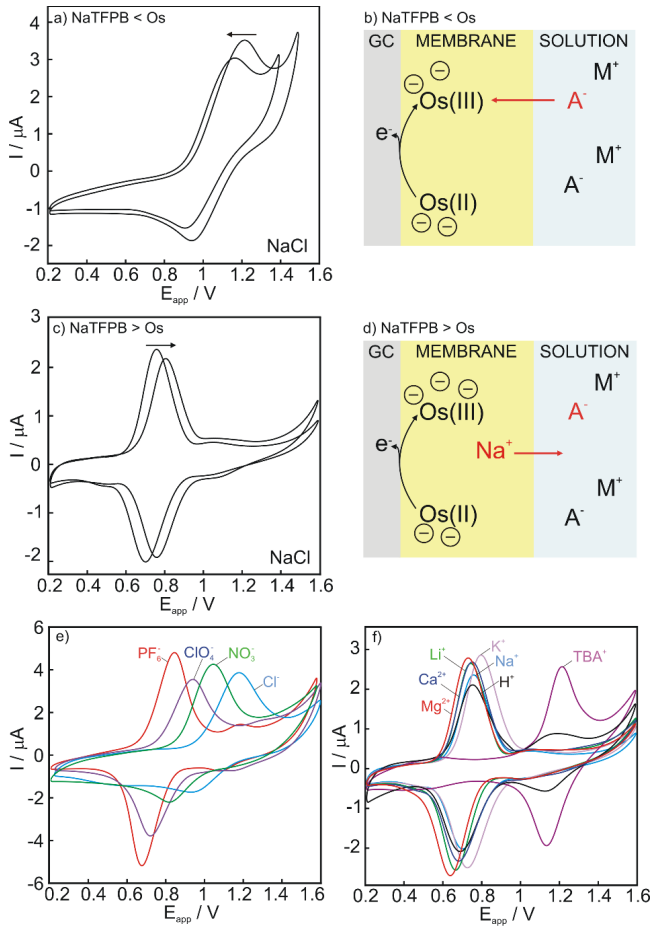

Figure 1. a) Voltammograms for 10 and 100 mM NaCl using a membrane containing NaTFPB:Os 10:100 mmol kg-1 (M1). b) Corresponding response mechanism. c) Voltammograms for 10 and 100 mM NaCl using a membrane containing NaTFPB:Os 200:75 mmol kg^{-1} (M3). d) Corresponding response mechanism. e) Voltammograms for different anions using a membrane with 100 mol kg^{-1} of Os (M2). f) Response towards different cations of a membrane with NaTFPB:Os 200:75 mmol kg^{-1}. Scan rate: 100 mV s^{-1}.

To compare with earlier work on conducting polymer based thin films,[4] a lower molar amount of the cation exchanger sodium tetrakis 3,5-bis(trifluoromethyl)phenyl borate (NaTFPB) with respect to the osmium based redox probe was selected with a membrane containing NaTFPB:Os 10:100 mmol kg^{-1} (M1, table S1). Figure 1a shows the observed thin layer voltammograms for increasing sample concentrations of NaCl. One may expect a cation wave as a consequence to the gradual oxidation of Os(II) to Os(III) that will be stabilized by the $TFPB^-$ in the membrane, therefore promoting Na^+ release to the aqueous solution, in analogy with POT based electrodes.[4] However, the observed wave shifted to less positive potentials instead (ΔE_{peak}= -55.1 mV), indicating that the membrane responds to chloride in agreement with the Nernst equation. The observed waves do not exhibit a Gaussian shape, and the 152 mV separation between cathodic and anodic peaks is larger than the 10 mV typically obtained with POT-based membrane electrodes.[4] Ohmic drop does not explain the peak separation, as it is calculated as just 17 mV (or 12% of the separation) from the experimentally determined resistance of 2.3 kΩ (Figure S2) and the peak current difference of 7.7 µA.

A thin membrane without NaTFPB (M2) exhibited the same anion sensing behavior (Figure S3), suggesting that Os(III) is stabilized by anions from the aqueous solution (Figure 1b). The two membranes, with and without NaTFPB, showed a response on the basis of the Hofmeister series for different anions (in the order of decreasing lipophilicity: $PF_6^- > ClO_4^- > NO_3^- > Cl^-$), see Figure S4 and Figure 1e respectively. The observed anion wave for this latter membrane is reproducible between scans, even for NO_3^- and Cl^- for which the cathodic waves show a smaller integrated charge than the cathodic wave (Figure S5).

The repeatability of the scans suggests that the electrochemical transformation of Os(II)/Os(III) is reversible. However, anions that enter the membrane to stabilize formed Os(III) are sourced from solution, which acts as a large reservoir of anions. A possible irreversibility of this ion transfer process (i.e. for NO_3^- and Cl^-) may therefore not necessarily affect consecutive scans. In contrast, in the case of PF_6^- the integrated charges from the anodic and cathodic waves are 7.41 and 7.92 μC respectively, showing a relatively small difference of 7%. The waves become sharper with increasing anion lipophilicity and the peak separation decreases (from 250 mV for Cl^- down to 150 mV for PF_6^-), see Figure 1e.

In order to observe the cation wave, a higher amount of NaTFPB was required in the thin membranes, thus promoting the stabilization of Os(III) by $TFPB^-$ instead of anions extracted from the aqueous solution. Accordingly, Figure 1c presents voltammograms in NaCl for a membrane containing NaTFPB:Os 200:75 mmol kg^{-1} (M3). The peaks now shift to more positive potentials for increasing concentrations (ΔE_{peak}= 57.6 mV), exhibiting a Nernstian response to cations as previously observed with POT based membranes.[4] Figure 1d schematically shows the suggested response mechanism for membranes containing a higher amount of NaTFPB than Os(II)/Os(III) complex, which is now in analogy to that previously described for POT based electrodes.[4]

As in the case of the anion wave observed above, the cation wave is reproducible between scans. For example, the integrated charges for the anodic and cathodic sodium transfer waves were 3.49 and 3.28 μC, respectively, giving a 5% difference. Peak separation was ~65 mV in all cases. Note that the charges associated with the anion and cation waves are not necessarily the same. In the case of cation transfer, the charge is dictated by the amount of the cation exchanger in the membrane[4] while for anion transfer it is given by excess Os(II) complex. Thin layer behavior was confirmed for this membrane, as evidenced by a linear dependence of peak current on the scan rate (Figure S6). The response towards different cations follows the expected lipophilicity order ($TBA^+ > K^+ > Na^+ \sim H^+ > Li^+ \sim Ca^{2+} > Mg^{2+}$), see Figure 1f.

According to the results shown above, the membrane composition may be tuned to observe the voltammetric wave corresponding to either cation or anion transfer. This is indeed demonstrated in Figure 2a, where voltammograms in NaCl samples are presented using membranes with a fixed amount of $(Os(II)(dnbpy)_3)\cdot(PF_6)_2$ (75 mmol kg^{-1}) and containing decreasing amounts of NaTFPB (M3–M6). In the first voltammogram (NaTFPB:Os molar ratio of 2.7, M3), there exists only a single wave corresponding to the transfer of cations. Here the amount of $TFPB^-$ in the membrane is sufficiently high to stabilize the formed Os(III) without the participation of other anions extracted from the sample.

When the amount of NaTFPB is decreased (NaTFPB:Os = 2, M4), three peaks are observed in the voltammogram. Increasing the NaCl concentration in the solution and observing the direction of the peak shift helps to identify the nature of the transferred ion. Consequently, peaks I and II in Figure 2a are associated with cation transfer while the third one (III) corresponds to anion transfer. Since there is less $TFPB^-$ available in the membrane, other anions present in the membrane (i.e. in the form of nanodroplets)[8] and those in the aqueous solution may additionally participate in the stabilization of Os(III) (Figure 2b). The presence of nanodroplets at the electrode/membrane buried interface has indeed been observed by other authors, including with thin membranes based on ferrocene derivatives.[8] We hypothesize therefore that NaCl containing nanodroplets may be responsible for peak II. If $TFPB^-$ is decreased more (M5) to the point of not being incorporated in the membrane (M6), a single wave appears that is related to anion transfer, as only the anions from the aqueous solutions are stabilizing Os(III) (Figure 2a).

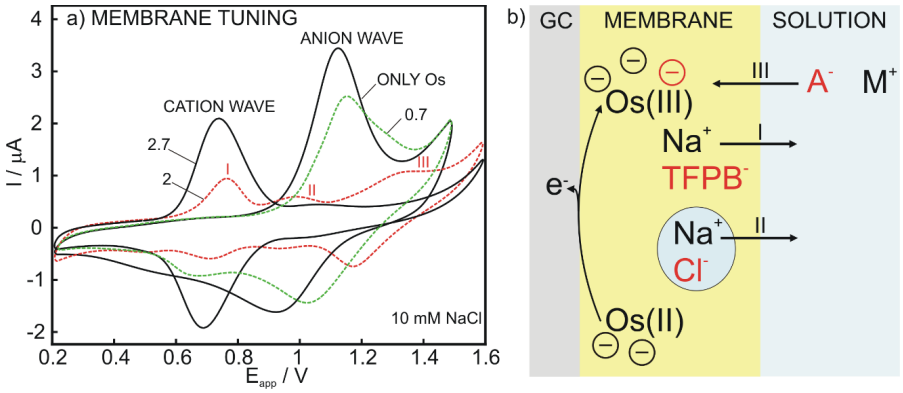

Figure 2. a) Cyclic voltammograms in 10 mM NaCl using membranes containing a fixed amount of $(Os(II)(dnbpy)_3)\cdot(PF_6)_2$ (75 mmol kg^{-1}) and a decreasing amount of NaTFPB. (NaTFPB:Os molar ratios are indicated in the figure for each voltammogram M3-6. Scan rate: 100 mV s^{-1}). b) Response mechanism for the membrane with NaTFPB:Os=2 (M4).

Considering now only membranes presenting a cation transfer wave, Figure 3a compares a voltammogram obtained for a thin membrane containing NaTFPB (M7), backside contacted with the traditional conducting polymer POT, with a corresponding membrane containing NaTFPB and Os(II) as molecular redox mediator (M3). The peak width is dramatically reduced with the Os(II) complex, but is still larger than the expected value for a surface confined one electron transfer process (~95 mV).[13]

In the case of POT electrodes, the larger peak width is associated with the non-ideal redox behavior of the polymer, i.e. POT/POT^+ conversion does not involve a molecular one electron transfer.[4,14] On the other hand, the Os(II) complex exhibited a one electron transfer in organic solution (Fig S1). The broadening in the membrane is thought to be related to either the stabilization of Os(III) by $TFPB^-$ or by a kinetic limitation of the cation transfer, and further work on this phenomenon is warranted.

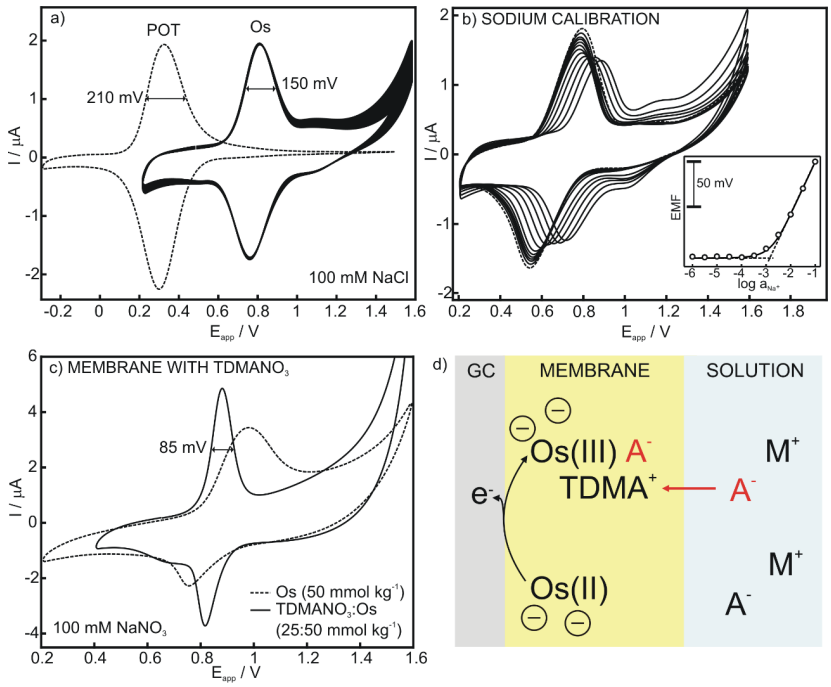

Figure 3. a) Voltammograms in 100 mM NaCl for a membrane containing 40 mmol kg^{-1} of NaTFPB (M7) backside contacted with POT and for a membrane containing Os:NaTFPB (75:200 mmol kg^{-1}, M3, n=25). b) Calibration graph for Na^+ (1 mM $MgCl_2$ background). c) Voltammograms obtained in 100 mM $NaNO_3$ using membranes with (M14) and without $TDMANO_3$ (M11). d) Response mechanism for membranes containing $TDMANO_3$, which appears to kinetically facilitate anion transfer. Scan rate: 100 mV s^{-1}.

A comparison of the optimal membrane composition used in the two systems (Figure 3a) shows that a larger amount of NaTFPB is required in thin membranes incorporating Os(II) compared to POT. Indeed, 200 mmol kg^{-1} used in this work exceeds that of common compositions used in traditional sensing membranes for potentiometry (~5-10 mmol kg^{-1}).[15] Note, however, that a reduction of the amount of redox probes while keeping the NaTFPB:Os ratio equal to 2.7 (M3,8-9) results in a deterioration of the ion transfer waves (Figure S7).

Figure 3b presents a calibration graph for sodium using the membrane composition M3. A Nernstian behavior was obtained between peak position and logarithmic ion concentration (slope = 58.3 mV) with a limit of detection of $2x10^{-3}$ M, which is typical for ion-selective electrodes based on membranes containing a lipophilic cation exchanger and also for voltammetric thin membranes backside contacted with POT.[4]

Considering membranes just exhibiting the anion transfer wave (in the absence of cation-exchanger), Nernstian behavior was confirmed for Cl^-, NO_3^-, ClO_4^- and PF_6^- using a membrane containing 100 mmol kg^{-1} of Os (M2). As an example, the calibration graph for PF_6^- is shown in Figure S8. The peak corresponding to the background electrolyte (red dotted line) decreases with increasing PF_6^- concentration and from a concentration of ~10^{-5} M a new peak appears and gradually grows with increasing concentration. The peak shifts to less positive potentials with the logarithmic anion concentration in agreement with the Nernst equation (slope = -60.1 mV).

Different amounts of Os(II) complex in this type of membranes were explored (M2,10-13, Figure S9). A least 25 mmol kg^{-1} of osmium probe is required to observe an acceptable peak shape. An increase in the amount of Os(II) gives higher peak currents, narrower waves and more reversible peaks. As a compromise between these

characteristics and the amount of the complex utilized for the membrane preparation, thin membranes containing 50 mmol kg^{-1} of the Os(II) complex were studied in more detail.

Additional anion exchanger tridodecylmethylammonium nitrate ($TDMANO_3$) was added to the membrane (M14), see Figure 3d for a scheme of the ion transfer process. Figure 3c compares voltammograms for thin membranes with and without $TDMANO_3$ (M14 and M11). We find that the addition of $TDMA^+$ results in a narrower ion transfer wave, with a $W_{1/2}$ corresponding to one electron transfer. Peak separation is also dramatically reduced from 240 to 65 mV, suggesting improved reversibility of the ion transfer process. The apparent value of E^0 from the experimental voltammograms, i.e. $E_{pa}+E_{pc}/2$, is practically the same in both membranes (849 and 855 mV with and without $TDMA^+$). This behavior suggests that $TDMA^+$ does not appreciably interact with the extracted anion, as evidenced by the lack of shift in the E^0 value, but acts as electrochemical catalyst, most likely for the phase transfer reaction.

Impedance experiments were conducted for membranes M14 and M11 with and without $TDMANO_3$ (Figure S10) showing that the incorporation of $TDMANO_3$ produces a slight decrease in the membrane resistance from 4.2 to 3.1 kΩ, being these values in the same order than those reported for PVC thin membranes backside contacted with POT.[5]

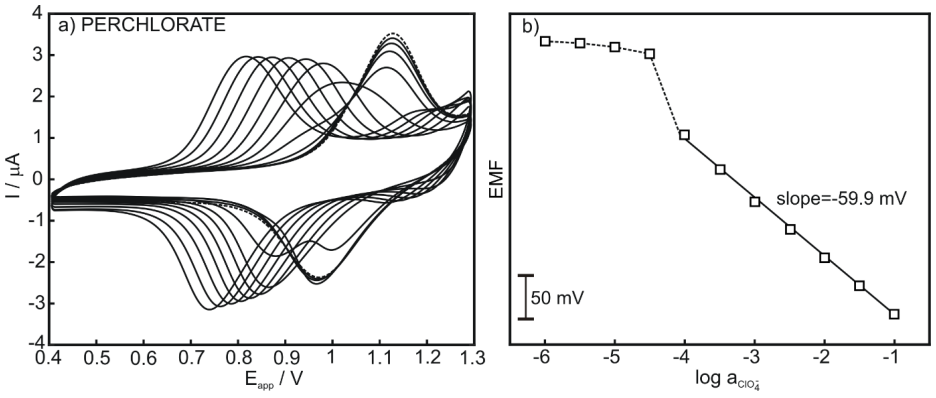

Figure 4. Calibration for ClO_4^- (1 mM $MgCl_2$ background, scan rate: 100 mV s^{-1}) using the membrane with $TDMANO_3$:Os 25:50 mmol kg^{-1} (M14).

Calibration graphs were recorded for membrane M14 with Cl^-, NO_3^-, ClO_4^- and PF_6^- (see Figure 4 for ClO_4^- as example), showing in all the cases Nernstian slopes. The observed limits of detection are lower compared with those obtained with membranes without $TDMANO_3$ (Figure S8, shown a comparison for PF_6^- calibration with M2 and M14).

Related to this, an initial super-Nernstian jump, typically obtained in potentiometric ion- selective electrodes of high selectivity, was obtained (Figure 4b and Figure S8c). The observed voltammograms were reproducible for consecutive scans (Figure S11) and thin layer behavior was again confirmed (Figure S12).

It is anticipated that Os(II) based redox probes may also be used for ion transfer stripping voltammetry in analogy to other electrodes reported in the literature, where a nanomolar detection limit was demonstrated for perchlorate with POT-based electrodes, although reproducibility and selectivity were not demonstrated in detail.[2]

Similar to PVC-based thin membranes, repetitive rinsing between measurements is not advisable as a gradual loss of response is observed as a consequence of component loss and/or membrane desorption. Here, polyurethane (PU) matrix provides much enhanced stability, even with samples as complex and lipophilic as serum.[4,5] While PVC has been chosen in this fundamental study, PU membranes will likely be preferred in practical applications.

2.5 Conclusions

A novel lipophilic Os(II) complex, $(Os(II)(dnbpy)_3)\cdot(PF_6)_2$, was synthesized that serves as ion transfer mediator when incorporated in voltammetric thin membranes. Tuning of the membrane composition gives rise to anion and cation transfer waves (and even both simultaneously). Importantly, electrochemical instabilities in anion detection when using POT based electrodes have been overcome. The addition of an asymmetric quaternary ammonium salt reduces peak separation and peak widths to theoretical expectations, suggesting a kinetic enhancement of the ion transfer process.

2.6 Acknowledgements

The authors thank the Swiss National Science Foundation for financial support. SJ gratefully thanks the Swiss government for a Swiss Government Excellence Scholarship.

2.7 Supporting Information

Osmium characterization

a) ^{1}H-NMR of $(Os(II)(dnbpy)_3)(PF_6)_2$:

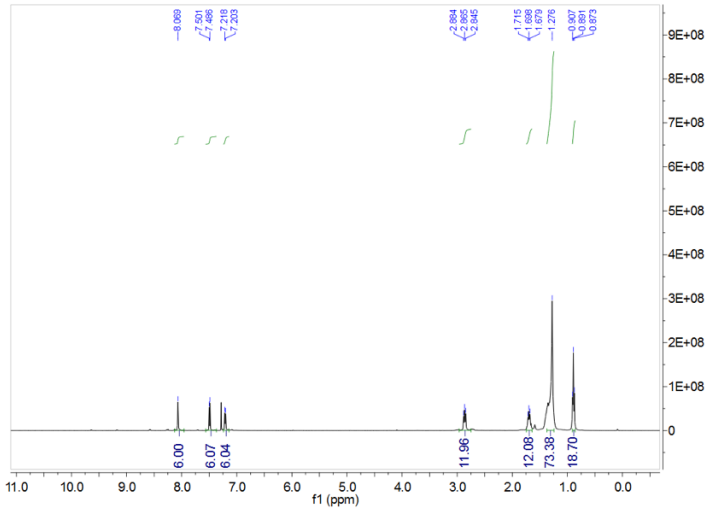

b) Electrospray–Mass Spectrum of $(Os(II)(dnbpy)_3)(PF_6)_2$:

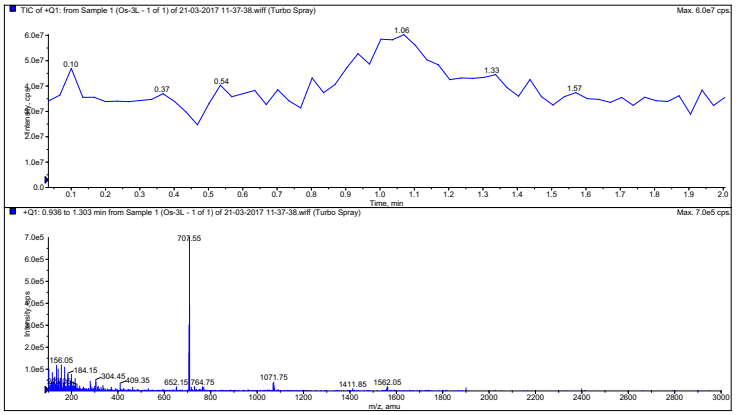

Table S1. Compositions of the membranes used in the present work. The amounts are relative to a total mass of 100 mg dissolved in 1 mL of THF.

	component				
Membrane	NaTFPB[a]	$TDMANO_3$	$Os(II)(dnbpy)_3)\cdot(PF_6)_2$[a]	PVC[b]	DOS[b]
M1	10	-	100	27	55
M2	-	-	100	28	55
M3	200	-	75	23	46
M4	150	-	75	25	49
M5	50	-	75	28	55
M6	-	-	75	29	58
M7	40	-	-	33	63
M8	100	-	37.5	28	57
M9	150	-	56.2	26	51
M10	-	-	75	29	58
M11	-	-	50	30	61
M12	-	-	25	32	64
M13	-	-	10	33	66
M14	-	25	50	30	60

[a]mmol kg^{-1}, [b]mass percentage

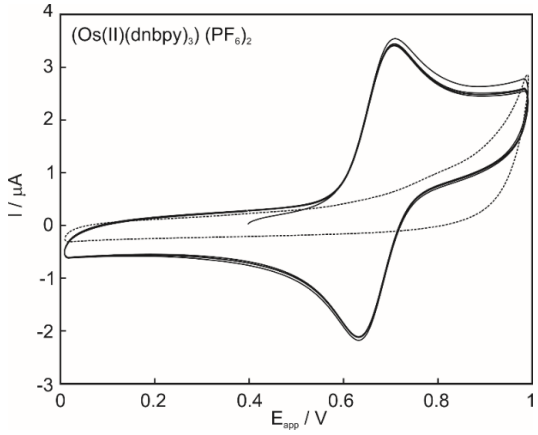

Figure S1. Consecutive cyclic voltammograms in 0.2 mM Os(II)(dnbpy)3.(PF6)2 and 0.1 M tetrabutylammonium perchlorate (TBAClO4) in acetonitrile. WE: Glassy carbon electrode, RE: Ag wire and CE: Pt electrode. Scan rate: 100 mV s-1.

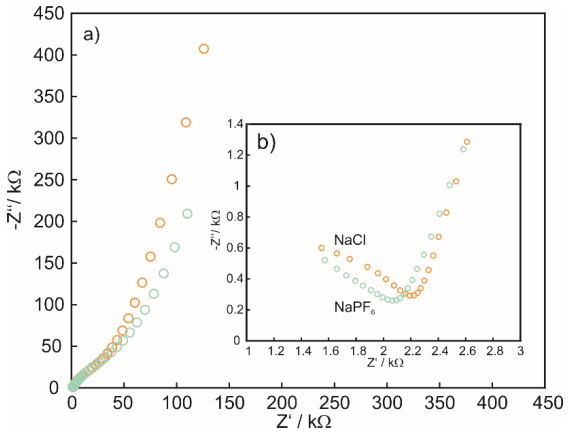

Figure S2. (a) Complex impedance plots observed for membrane M1 in 10 mM NaCl and $NaPF_6$ solutions. (b) Zoom of the semicircles. Parameters: first frequency=100000 Hz, last frequency=0.1 Hz, number of frequencies=50, amplitude=0.01 V, integration time=0.125s, Edc=100 mV+OCP (0.4 and 0.2 V respectively).

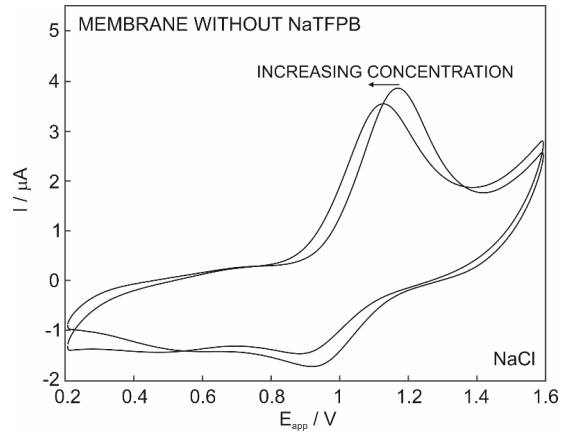

Figure S3. Cyclic voltammograms obtained for 10 and 100 mM NaCl using membrane M1 (10 mmol kg^{-1} of NaTFPB and 100 mmol kg^{-1} of $(Os(II)(dnbpy)_3)\cdot(PF_6)_2$). Scan rate: 100 mV s^{-1}.

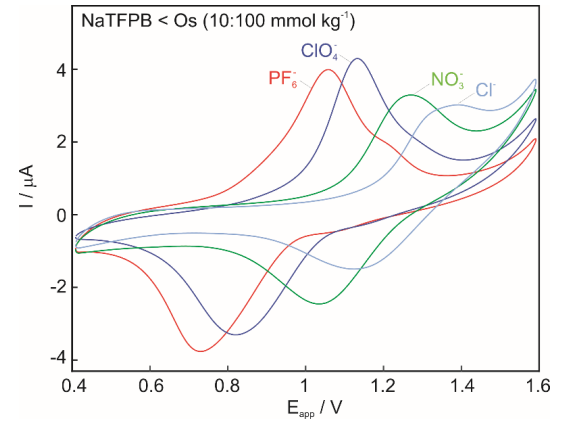

Figure S4. Cyclic voltammograms in 10 mM of sodium salts of different anions using membrane M1. Scan rate: 100 mV s^{-1}.

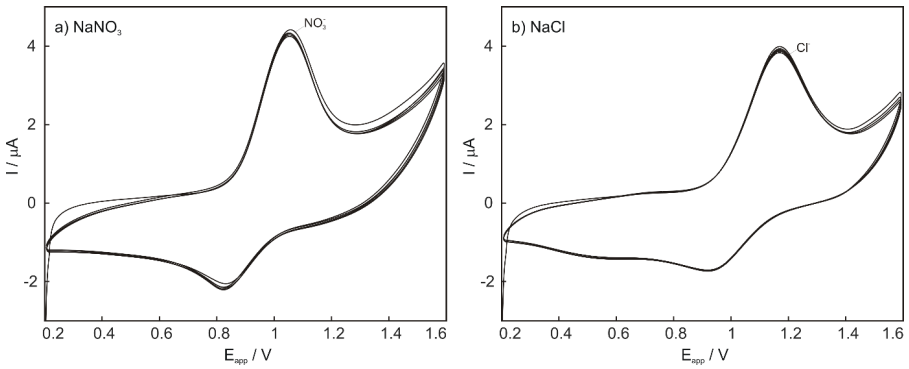

Figure S5. 10 consecutive voltammograms using membrane M2 containing 100 mmol kg^{-1} of $(Os(II)(dnbpy)_3)\cdot(PF_6)$ observed for (a) 10 mM $NaNO_3$ and (b) 10 mM NaCl. Scan rate: 100 mV s^{-1}.

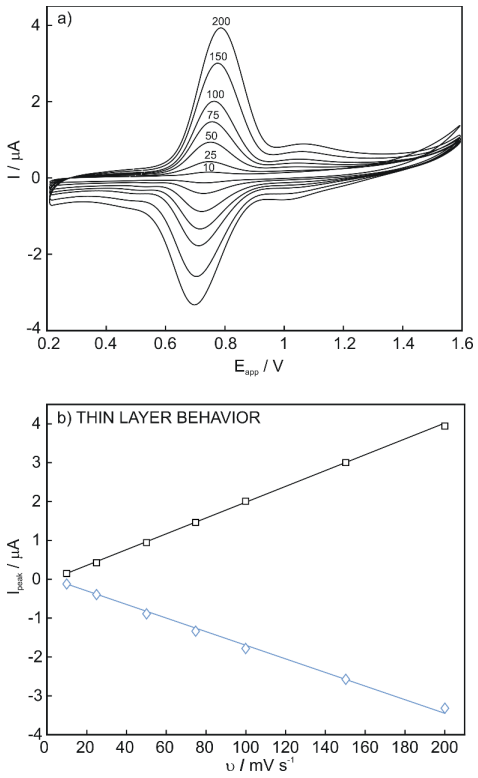

Figure S6. (a) Cyclic voltammograms in 10 mM NaCl using membrane M3 (200 mmol kg^{-1} of NaTFPB and 75 mmol kg^{-1} of $(Os(II)(dnbpy)_3)\cdot(PF_6)_2$ at different scan rates. b) Thin layer behavior for cathodic and anodic waves as confirmed by linear dependence of peak current on scan rate.

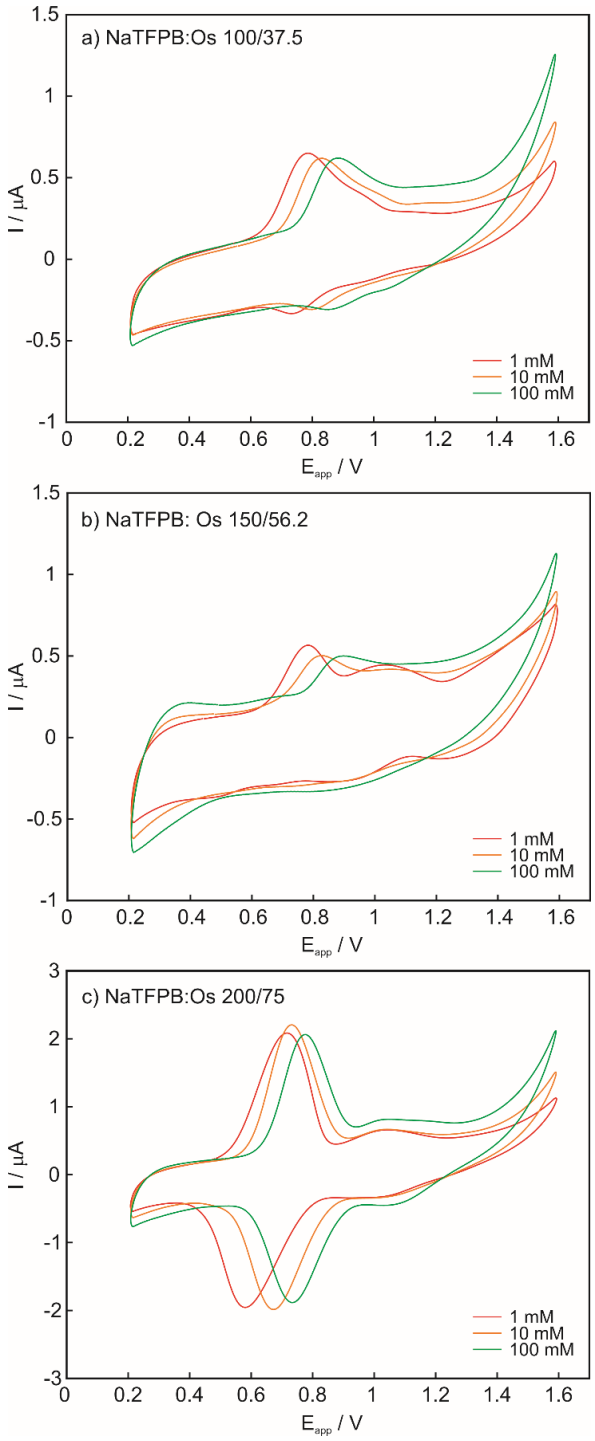

Figure S7. Cyclic voltammograms obtained using membranes containing a fixed NaTFPB:Os ratio of 2.7 and reducing their loading in the membrane: a) 100/37.5 (M8), b) 150/56.2 (M9) and c) 200/75 (M3). Scan rate: 100 mV s^{-1}.

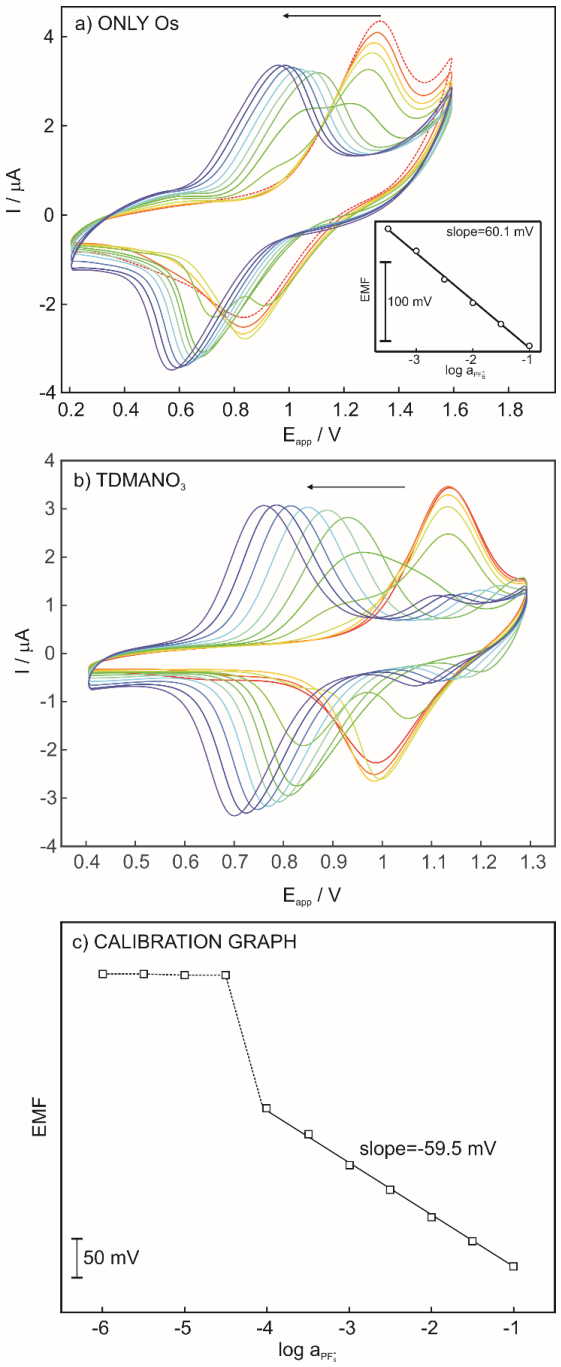

Figure S8. Cyclic voltammograms for increasing concentrations of $NaPF_6$ (from 10^{-6} to 10^{-1} M in 1 mM $MgCl_2$ background electrolyte): a) with membrane M2 containing 100 mmol kg^{-1} of $(Os(II)(dnbpy)_3)\cdot(PF_6)_2$. Inset: peak current vs. potential; b) with membrane M14 containing 25 mmol kg^{-1} of $TDMANO_3$ and 50 mmol kg^{-1} of $(Os(II)(dnbpy)_3)\cdot(PF_6)$. c) Observed calibration graph for PF_6^- using membrane M14. Scan rate: 100 mV s^{-1}.

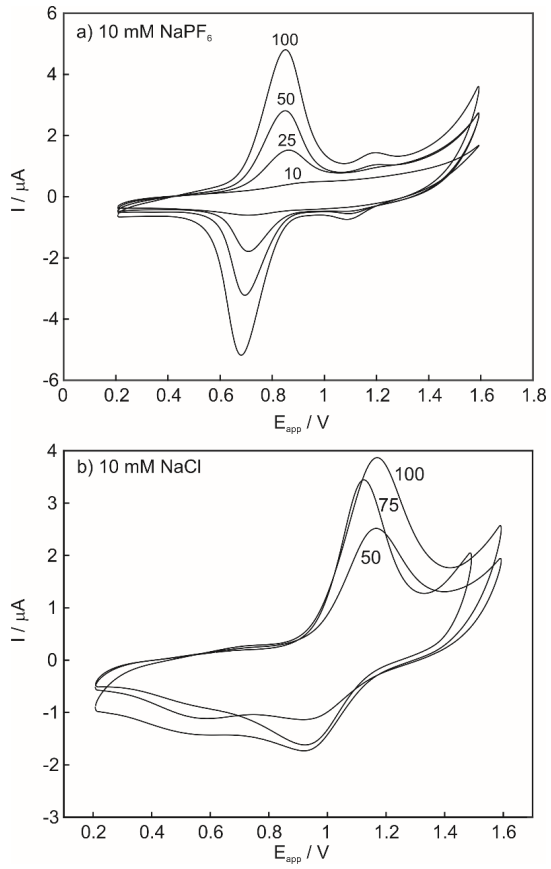

Figure S9. Cyclic voltammograms observed using membranes with increasing amount of $(Os(II)(dnbpy)_3)\cdot(PF_6)_2$ and without any ion exchanger. a) Membranes M2, M11-13 containing 100, 50, 25 or 10 mmol kg^{-1} of $(Os(II)(dnbpy)_3)\cdot(PF_6)_2$ in 10 mM $NaPF_6$. b) Membranes M2, M10-11 containing 100, 75 or 50 mmol kg^{-1} of $(Os(II)(dnbpy)_3)\cdot(PF_6)_2$ in 10 mM NaCl. Scan rate: 100 mV s^{-1}.

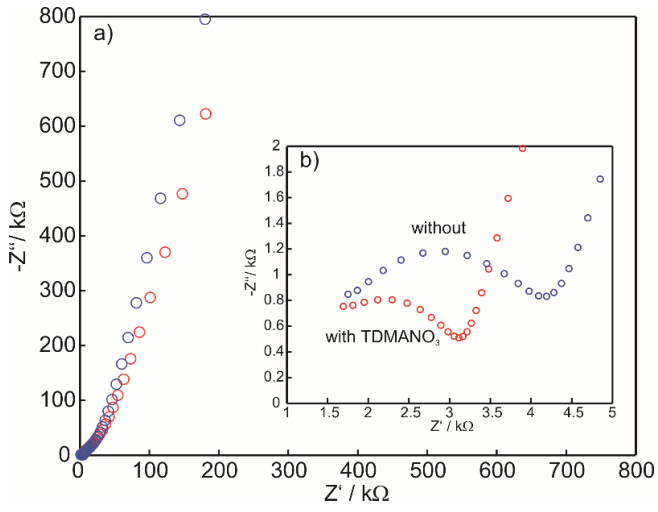

Figure S10. (a) Complex impedance plots observed for membranes M14 and M11 with and withouth $TDMANO_3$ in 10 mM NaCl solution. (b) Zoom of the semicircles. Parameters: first frequency=100000 Hz, last frequency=0.1 Hz, number of frequencies=50, amplitude=0.01 V, integration time=0.125s, Edc=100 mV+OCP (0.4 and 0.3 V respectively).

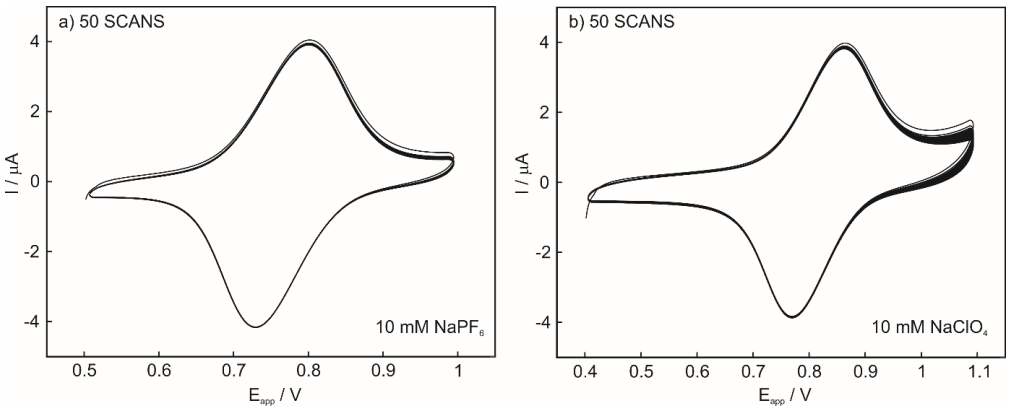

Figure S11. Consecutive voltammograms using membrane M14 containing 25 mmol kg^{-1} of $TDMANO_3$ and 50 mmol kg^{-1} of $(Os(II)(dnbpy)_3)\cdot(PF_6)_2$, demonstrating electrochemical stability. a) 10 mM $NaPF_6$. b) 10 mM $NaClO_4$. Scan rate: 100 mV s^{-1}.

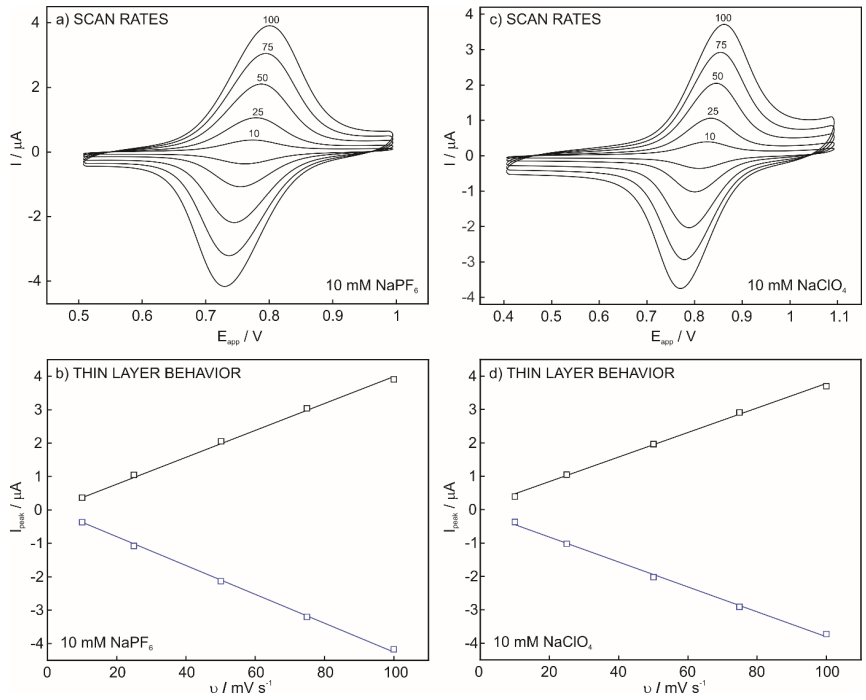

Figure S12. Cyclic voltammograms observed using membrane M14 (25 mmol kg^{-1} of $TDMANO_3$ and 50 mmol kg^{-1} of $(Os(II)(dnbpy)_3)\cdot(PF_6)_2$ at different scan rates in: a) 10 mM $NaPF_6$ and b) 10 mM $NaClO_4$. Graphs c) and d) confirm the corresponding thin layer behaviour, as evidenced by the linear dependence of peak current on scan rate.

2.7 References

1. Cadogan, Z. Q. Gao, A. Lewestam, A. Ivaska and D. diamond, Anal. Chem., 1992, 64, 2496-2501; J. Bobacka, A. Ivaska and A. Lewenstam, Chem. Rev., 2008, 108, 329-351.
2. Y. Kim and S. Amemiya, Anal. Chem. 2008, 80, 6056-6065; B. Kabagambe, M. B. Garada, R. Ishimatsu and S. Amemiya, Anal. Chem., 2014, 86, 7939-7946.
3. Y. Yoshida, S. Yamaguchi and K. Maeda, Anal. Sci., 2010, 26, 137-139.
4. G. Crespo, M. Cuartero and E. Bakker, Anal. Chem., 2015, 87, 7729-7737; M. Cuartero, G. Crespo and E. Bakker, Anal. Chem., 2016, 88, 5649-5654.
5. M. Cuartero, G. Crespo and E. Bakker, Anal. Chem., 2016, 88, 1654-1660; M. Cuartero, J. Bishop, R. Walker, R. G. Acres, E. Bakker, R. de Marco and G. Crespo, Anal. Chem., 2016, 88, 6939-6946.
6. A. Izadyar, Y. Kim, M. M. Ward and S. Amemiya, J. Chem. Educ., 2012, 89, 1323-1326.
7. Z. Mousavi, J. Bobacka, A. Lewenstam and A. Ivaska, J. Electroanal. Chem., 2009, 633, 246-252.
8. M. Cuartero, R. G. Acres, J. Bradley, Z. Jarolimova, L. Wang, E. Bakker, G. Crespo and R. de Marco, Electrochim. Acta, 2017, 238, 357-367.
9. X. U. Zou, J. H. Cheong, B. J. Taitt and P. Buhlmann, Anal. Chem., 2013, 85, 9350-9355.
10. E. Jaworska, M. L. Naitana, E. Stelmach, G. Pomarico, M. Wojciechowski, A. Bulska, K- Maksymiuk, R. Paolesse and A. Michalska, Anal. Chem. 2017, 89, 7107-7114.
11. R. J. Forster, D. A. Walsh, N. Mano, F. Mao and A. Heller, Langmuir, 2004, 20, 862-868.
12. P. Pinyou, A. Ruff, S. Poller, S. Ma, R. Ludwig and W. Schuhmann, C. Kranz, J. Huber and H. Wohlschlager, Chem. Eur. J., 2016, 22, 5319-5326.
13. H. Jaegfeldt, A. Torstensson, L. Gorton and G. Johansson, Anal. Chem., 1981, 53, 1979-1982.
14. D. Yuan, M. Cuartero, G. Crespo and E. Bakker, Anal. Chem., 2017, 89, 586-594.
15. S. Peper, A. Ceresa, E. Bakker, E. Pretsch, Anal. Chem. 2001, 73, 3768-3775.

Chapter 3: Colorimetric Readout for Potentiometric sensors with Closed Bipolar Electrodes

This work has been published in: Jansod, S.; Cuartero, M.; Cherubini, T.; Bakker, E. *Anal. Chem*. **2018**, *90*, 6376-6379.

3.1 Abstract

We present here a general strategy to translate potential change at a potentiometric probe into a tunable color readout. It is achieved with a closed bipolar electrode where the ion-selective component is confined to one end of the electrode while color is generated at the opposite pole, allowing one to physically separate the detection compartment from the sample. An electrical potential is imposed across the bipolar electrode by solution contact such that the potentiometric signal change at the sample side modulates the potential at the detection side. This triggers the turnover of a redox indicator in the thin detection layer until a new equilibrium state is established. The approach is demonstrated in separate experiments with a chloride responsive Ag/AgCl element and a liquid membrane based calcium-selective membrane electrode, using the redox indicator ferroin in the detection compartment. The principle can be readily extended to other ion detection materials and optical readout principles.

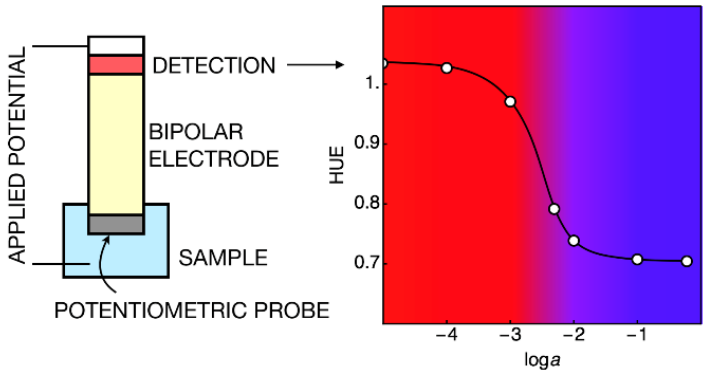

3.2 Introduction

It is shown here for the first time that a potentiometric probe signal can be converted to a colorimetric output with closed bipolar electrodes. The principle is scalable to large arrays of electrodes with little increase in complexity, paving the way for the realization of powerful and fundamentally convincing chemical imaging tools. The color is generated in a compartment separate from the sample, resulting in an optical readout that is not affected by turbid or colloidal samples. The measuring range of the colorimetric signal change is controlled electrochemically.

The visualization of chemical changes is important in view of low cost and field based instrumentation[1,2] and equally forms the basis for massively parallel arrays[3] and chemical imaging tools.[4] Only a limited number of ionic species may be selectively recognized with chromogenic and photoacoustic reagents.[5] Ion optodes containing lipophilic ionophores as selective receptors open up a wider palette of detectable species.[6] Traditional ion optodes require the additional presence of a lipophilic pH indicator, resulting in an undesired pH cross-response, while more recent approaches use ionic solvatochromic dyes to overcome this limitation.[7,8] With the latter approach, the ion of interest partitions into the sensing phase and expels only the ionized chromogenic part of the dye molecule into the aqueous side of the interface to generate the signal, retaining it to the sensor surface. As the ion-exchange equilibrium is also influenced by the surface potential and background electrolyte, such ion optodes are fundamentally less robust than established ion-selective electrodes.[9]

This work aims to translate a potential change at a potentiometric sensing probes into color change. Earlier, our group showed that the working potential at an electrode used to generate electrochemiluminescence can be modulated by a potentiometric probe placed in a separate sample compartment.[10] The probe took the place of the reference electrode in the electrochemical cell, so that a potential change at the probe electrode altered the resulting working electrode potential, giving a change in light output. Gooding's group demonstrated a conceptually similar modulation to induce electrochromicity of a conducting polymer as readout.[11] As an electrochemical circuit is required for each probe, however, large arrays of electrodes cannot be made for imaging applications without unduly complicating the associated control and readout electronics.

3.3 Experimental Details

Materials, reagents, and instrumentation

Potassium chloride, potassium nitrate, hydrochloric acid solution (HCl, 1.0 M), tris(1,10-phenanthroline iron (II) sulfate, calcium chloride, magnesium chloride hexahydrate, sodium tetrakis-[3,5-bis(trifluoromethyl)phenyl]borate (NaTFPB), tetrakis(4-chlorophenyl)borate tetradodecylammonium salt (ETH 500), calcium ionophore IV, 2-nitro-phenyloctylether (*o*-NPOE), 2-amino-2-hydroxymethyl-propane-1,3-diolhydrochloride (Tris-HCl), tetrahydrofuran (THF), indium tin oxide (ITO, surface resistivity 1.28-1.92 $\Omega \cdot cm^{-2}$) were purchased from Sigma-Aldrich. The porous polypropylene (PP) membrane (Celgard 0.237 cm^2 surface area and 25 μm thickness) was provided by Membrana, Wuppertal, Germany. Silver foil, of 99.97% purity, thickness 0.025 mm was purchased Advent Research Materials (Oxford, UK).

An insulating transparent Scotch 3M tape (80 μm thickness) was used. Ag electrode tips with a diameter of 3.00±0.05 mm (6.1204.330) were sourced from Metrohm (Switzerland). IPC ISMATEC peristaltic pump (Model ISM935C, Clattbrug, Switzerland), TYGON tubing (inner diameter 1.42 mm, wall 0.86 mm) and PTFE tubing (L × OD × ID = 300 mm × 1/16 × 100 μm, Supelco) were used in the flow system. The electrochemical measurements of cyclic voltammetry and chronoamperometry were performed in a faraday cage with a potentiostat/galvanostat PGSTAT 204 (Metrohm Autolab, Utrecht, The Netherlands) that was controlled by Nova 2.1 software. A computer tethered digital camera (Canon EOS 5D Mark II equipped with a MP-E 60mm macro lens and matching ring flash) was used to capture the images of the detection cell. Aqueous solutions were prepared in MilliQ water.

Procedure for coating the Ag elements with AgCl

Ag foil used in detection compartment was cut into a 25 × 8 mm piece. The foil and the silver electrode to make the chloride probe were cleaned with abundant MilliQ water. A layer of AgCl was electrochemically deposited on both electrodes by oxidizing the Ag in a solution of 1 M HCl for 30 min at a constant anodic current density of approximately 1.25 mA cm^{-2}.

Membrane preparation

A calcium porous polypropylene membrane, used as supporting material for calcium-ion selective electrode was prepared. A cocktail solution of 180 mm kg^{-1} of calcium ionophore IV, 5 mm kg^{-1} of NaTFPB, 90 mm kg^{-1} of ETH 500 and 75 mg of *o*-NPOE was completely dissolved in 1 mL THF. The membrane was washed with THF for 10 min to minimize any possible contaminants. When the membrane was found to be completely dry, 3 μL of the prepared cocktail solution was deposited on it. The membrane was kept in the Petri Dish for ca. 10 min to ensure a homogenous and reproducible impregnation of the pores. Afterwards, the membrane was conditioned in 10 mM $CaCl_2$ for 40 min. Finally the membrane was mounted in the Ostec electrode body. The inner compartment was filled with 10 mM $CaCl_2$.

Sample compartment

The potentiometric measurement of Ag/AgCl on Ag electrode (reference/counter electrode) and calcium porous polypropylene membrane electrode were carried out against a commercial reference electrode (6.0729.100, Metrohm) with double junction reference electrode (Ag | AgCl | KCl, 3 M | LiOAc, 1 M) in a faraday cage using a 16-channel EMF interface (Lawson Laboratories, Inc., Malvern, Pa). A Ag counter electrode was placed opposite the potentiometric chloride electrode, separated by a narrow solution gap into which the samples were delivered to the cell by peristaltic pumping. The reference electrode was placed in the outside beaker containing 3M KCl and connected to the sample cell through the fluid outlet (1mm dia.). A 10 mM KNO_3 was maintained as a background for chloride detection. Whereas a 10 mM Tris-HCl buffer pH 7.4 in 10 mM KCl was maintained as a background for calcium detection in the sample compartment.

Detection compartment

A circular opening of 2.9 mm diameter was punched into transparent adhesive insulating tape. This tape was then fixed onto a planar Ag/AgCl foil, and a 2 μL drop of 10 mM of ferroin in 0.1 M KCl was placed into the recess.

The transparent ITO working electrode was placed on top and made to contact the ferroin solution. Optical images were captured with a digital camera. Hue values from all pixel of the image was characterized using the Mathematica software 11.1 (Wolfram Research). The circular opening of 1.2 mm diameter was used for determination of calcium ion with a 0.3 µL drop of the ferroin mentioned above.

3.4 Results and Discussion

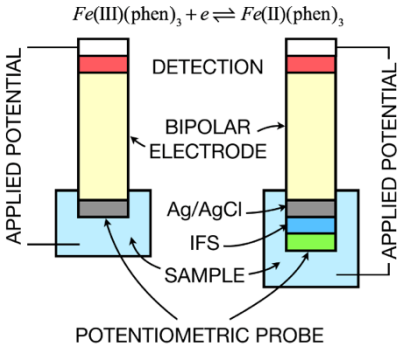

Figure 1. Color visualization of a potentiometric sensing probe by means of a closed bipolar electrode (CBE). A voltage is imposed at a transparent working electrode in contact with a thin layer detection compartment, relative to reference and counter electrodes placed in the sample solution. The CBE separates the two compartments, giving a color change on the basis of a concentration change in the sample on the basis of the indicated reactions. In the top half reaction, phen stands for 1,10-phenanthroline.

Figure 1 shows the basic principle of the approach introduced here. It involves one or more closed bipolar electrodes (CBE) that separate the sample from a detection compartment. An electrical potential difference is imposed between the two compartments, resulting in a predetermined voltage drop across the bipolar electrode. Unlike related amperometric sensing approaches,[12,13] the electrode side in contact with the sample is a potentiometric sensing probe. The opposite side of the bipolar electrode contacts a thin solution layer containing a redox indicator. The applied potential at that side imposes a given ratio of reduced and oxidized form as dictated by the Nernst equation. A change in the sample concentration will result in a defined potential change at the potentiometric probe side of the bipolar electrode. As the imposed cell potential remains indifferent, the change at the sample side must be compensated for at the detection side of the CBE. This results in a new equilibrium ratio of redox probe and therefore a detectable change in color.

The concept is illustrated with the colorimetric redox indicator ferroin, a water soluble tris(1,10-phenanthroline) Fe(II) complex that changes color from red to blue upon electrochemical oxidation to Fe(III). A 10 mM ferroin solution in 100 mM KCl was dropped into a 2.9–mm dia. punched recess in a 80-µm thick adhesive insulating tape placed on a planar Ag/AgCl element. This detection compartment was covered with a transparent electrode (indium tin oxide) and fitted into a detection cell, see Supporting Information for details. Thin layer dimensions were used to reduce mass transport rates and achieve acceptable redox equilibration times. The detection cell was characterized separately by imposing a potential between the transparent electrode and the Ag/AgCl electrode. Figure 2 shows the current and color response (visualized hue value) that result from an oxidative linear potential scan at 0.2 mV s^{-1}. The observed bell-shaped current peak is characteristic for an exhaustive electrochemical conversion.

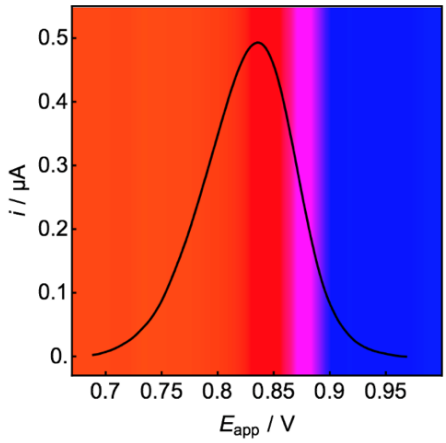

Figure 2. Background subtracted current response of the detection compartment containing ferroin for a linear anodic scan at 0.2 mV s^{-1}. The color background shows the experimentally observed hue value for each applied potential.

The color change in the detection compartment was recorded with a tethered digital camera (Canon EOS 5D Mark II) equipped with a MP-E 60mm macro lens and a ring flash. The recorded jpg images were automatically analyzed for hue value by a custom software routine that involves importing each consecutive image, automatic cropping for the detection compartment area, and computing the mean hue value from all residual pixels. The observed change in hue value qualitatively agrees with the extent of charge conversion, see Figure S1.

The cell containing the closed bipolar electrode was completed by coupling the AgCl element of the detection compartment to an Ag/AgCl electrode as potentiometric chloride probe that was immersed in a sample solution containing variable concentrations of KCl. Ag/AgCl serves as ubiquitous inner element in a wide variety of membrane electrodes[9] and is a good first model system. A liquid junction based reference and Ag counter electrode were placed in contact with the sample. The potentiometric probe in the sample compartment was first characterized potentiometrically against the reference electrode only. It was confirmed to give potential changes in agreement with the Nernst equation, see Figure S2 in Supporting Information.

In the assembled cell containing the bipolar electrode (Figure 1), the potential is applied between the ITO glass electrode in the detection compartment and the reference/counter electrodes in the sample compartment. An anodic linear potential scan gives the same peak-shaped current response as for the detection cell alone, see Figure 3. This indicates that the current is still limited by conversion of the redox probe, assuring maximum change of color and negligible concentration polarization of the potentiometric probe. Unlike the data in Figure 2, the position of the current wave is now found to shift to less positive potentials with increasing chloride concentration in the sample compartment (Figure 3a). The shift is Nernstian, 58.6 mV per 10-fold chloride activity change, and confirms the potential modulation at the detection side by the presence of the potentiometric probe at the sample side of the bipolar electrode. Figure 3b shows the corresponding observed hue values for this experiment that are equally found to shift with chloride concentration.

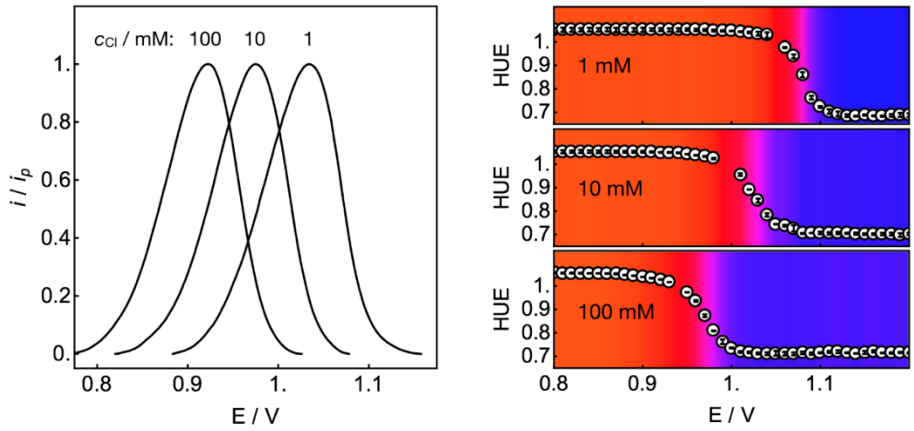

Figure 3. Top: Normalized current responses of the complete cell containing the closed bipolar ion-selective electrode, for the indicated chloride concentrations in the sample compartment. Bottom: Corresponding changes of the hue value in the detection compartment, with the observed hues shown as color background.

The color of the detection compartment also changes sigmoidally for variable chloride concentrations in the sample at a fixed potential, which is how a sensor would be interrogated. Figure 4a shows observed color images for the indicated chloride concentrations at 1.00 V. The color is found to change from red to blue with increasing chloride activity. Higher chloride levels result in a more negative potential at the potentiometric probe, which is compensated at the detection side with a more positive anodic potential, resulting in increased oxidation of redox probe. For such hue based calibrations, trendlines may need to use semi-empirical relationships as hue values are less quantitative than absorbance.

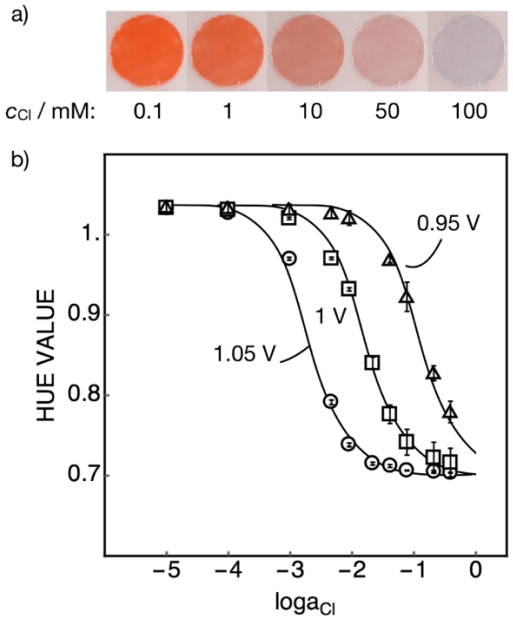

Figure 4. a) Images recorded in the detection compartment for the indicated chloride concentrations in the sample (at 1.00 V). b) Corresponding hue values, giving response curves that can be tuned by the magnitude of the applied potential (circles, 1.05 V; squares, 1.00 V; triangles, 0.95 V). Error bars are standard deviations (n=3). Solid lines are a guide to the eye.

Figure 4b shows the observed hue values as a function of logarithmic ion activity, giving the 2 orders of magnitude typical for optical sensors.[6] A very attractive feature of the concept introduced here is that the applied potential can

be used to tune this measuring range to match the intended application. This characteristic is confirmed in Figure 4b, where chloride calibration curves are shown for three different applied potentials, each separated by 50 mV.

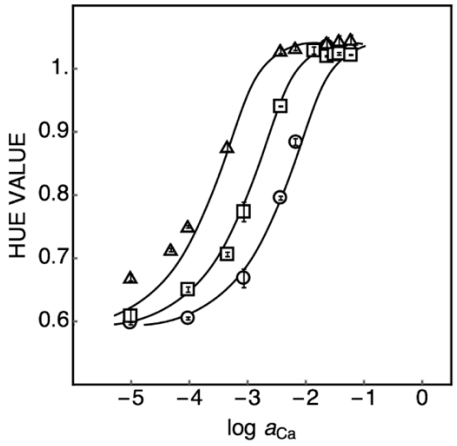

Figure 5. Colorimetric calibration curves of bipolar electrodes coupled to a calcium-selective membrane as potentiometric probe at different applied potentials (circles, 1.000 V; squares, 0.980 V; triangles, 0.960 V). Error bars are standard deviations (n=3); solid lines are to guide the eye. The curves are inverted relative to Figure 4 owing to the different charge sign of calcium relative to chloride, and are closer together owing to the reduced Nernstian slope for a divalent ion.

As the approach introduced here optically records an electrochemical equilibrium state, it is superbly adapted to the interrogation of potentiometric sensing probes. To demonstrate the wider applicability of the concept introduced here, a ionophore-based calcium selective membrane electrode with aqueous inner solution containing an Ag/AgCl element was integrated into the sensing end of the bipolar electrode (see Scheme 1 right for setup). The potentiometric probe was confirmed to exhibit a Nernstian response slope to calcium ion activity, as expected on the basis of the highly selective ionophore incorporated into the membrane (see Figure S3 in SI). In analogy to the results shown above, a bell shaped voltammetric response curve is observed that shifts to more positive potentials with increasing calcium activity, in agreement with the Nernst equation (Figure S4 in SI).

Figure 5 shows the corresponding colorimetric hue output at the detection side of the bipolar electrode, which again agrees with expectations. The observed deviations for low concentrations at 0.960 V will be studied in future work but may originate from the current transients that result in ion fluxes across the membrane. The s-shaped calibration curve for a fixed applied potential is conveniently shifted to lower calcium concentration with decreasing applied potential, allowing one to use the potential amplitude to fine tune the measuring range to the requirements of the intended application.

3.5 Conclusions

To summarize, a colorimetric readout of potentiometric measurement probes can be conveniently realized by coupling the potential change to the turnover of a redox indicator in a thin layer compartment. The approach introduced here appears to be universal, and its principal requirement is that the potentiometric probe should allow for sufficient passage of the transient current without resulting in undesired polarization, as recently demonstrated by means of a coulometric readout of ISEs.[14]

3.6 Acknowledgements

The authors acknowledge the Swiss National Science Foundation for supporting this work. S.J. thanks the Swiss Government Fellowship in support of her doctoral studies.

3.7 Supporting Information

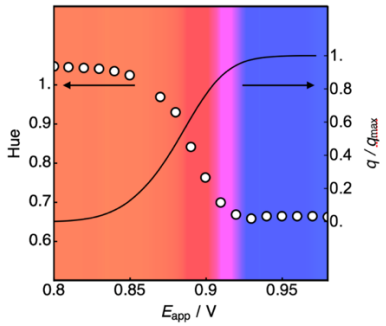

Figure S1. Solid line, right axis: Relative charge conversion as a function of applied potential for the data shown in Figure 2. Data points, left axis: Observed hue value of the detection cell for the same experiment. The background color shows the observed potential dependent hue values. The color change correlates with conversion of redox indicator.

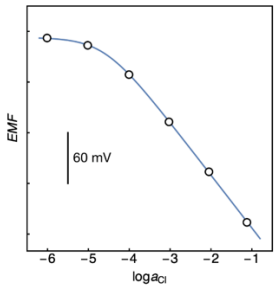

Figure S2. Potentiometric calibration curve for the Ag/AgCl element used as chloride sensing probe in the sample compartment, measured at zero current against a traditional 3M KCl based reference electrode to confirm a Nernstian response slope of a mV decade^{-1}. The line is the expected response curve based on the Nicolsky equation with this slope value.

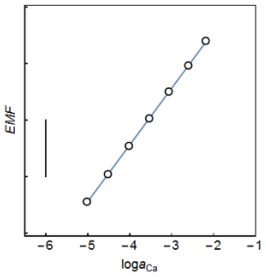

Figure S3. Potentiometric calibration curve for the calcium-selective membrane electrode used as calcium sensing probe in the sample compartment, measure at zero current against a traditional 3M KCl based reference electrode to confirm a Nernstian response slope of 29.12 mV decade^{-1}. The line exhibits a slope of 29 mV.

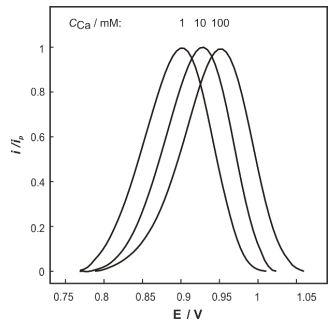

Figure S4. Normalized bell-shaped current responses as a function of applied potential (0.2 mV s^{-1} scan rate) for the bipolar electrode arrangement containing the calcium-selective probe in the sample compartment. The curves shift to higher potentials with increasing calcium concentrations as indicated.

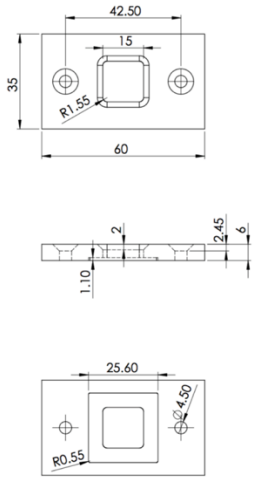

Figure S5. Technical drawing of the top cover of the acrylic detection cell, with units of mm. Top: top view, bottom image: bottom view. The 25.6mm wide ITO glass is placed into the bottom recess. The top cover is then screwed into the lower part (Figure 4S).

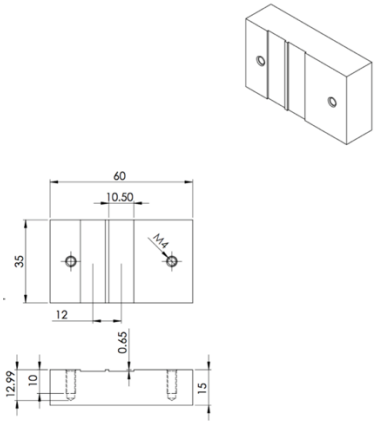

Figure S6. Bottom part of acrylic detection cell. The recessed grooves accept a pair of rubber spacers on top of which the Ag/AgCl foil containing the punched adhesive tape is placed. Screwing top and bottom parts together completes the cell.

3.8 References

1. Cunningham, J. C.; DeGregory, P. R.; Crooks, R. M. *Annu. Rev. Anal. Chem.* **2016**, *9*, 183.
2. Srisa-Art, M.; Boehle, K. E.; Geiss, B. J.; Henry, C. S. *Anal. Chem.* **2018**, *90*, 1035.
3. Chow, K.-F.; Mavré, F.; Crooks, J. A.; Chang, B.-Y.; Crooks, R. M. *J. Am. Chem. Soc.* **2009**, *131*, 8364.
4. Moßhammer, M.; Strobl, M.; Kühl, M.; Klimant, I.; Borisov, S. M.; Koren, K. *ACS Sens.* **2016**, *1*, 681.
5. Roberts, S.; Seeger, M.; Jiang, Y.; Mishra, A.; Sigmund, F.; Stelzl, A.; Lauri, A.; Symvoulidis, P.; Rolbieski, H.; Preller, M.; Deán-Ben, X. L.; Razansky, D.; Orschmann, T.; Desbordes, S. C.; Vetschera, P.; Bach, T.; Ntziachristos, V.; Westmeyer, G. G. *J. Am. Chem. Soc.* **2018**, *140*, 2718.
6. Mistlberger, G.; Crespo, G. A.; Bakker, E. *Annu. Rev. Anal. Chem.* **2014**, *7*, 483.
7. Xie, X.; Szilagyi, I.; Zhai, J.; Wang, L.; Bakker, E. *ACS Sens.* **2016**, *1*, 516.
8. Xie, X.; Zhai, J.; Bakker, E. *J. Am. Chem. Soc.* **2014**, *136*, 16465.
9. Bakker, E.; Buhlmann, P.; Pretsch, E. *Chem. Rev.* **1997**, *97*, 3083.
10. Crespo, G.; Mistlberger, G.; Bakker, E. *J. Am. Chem. Soc.* **2012**, *134*, 205.
11. Chow, E.; Liana, D. D.; Raguse, B.; Gooding, J. J. *Aust. J. Chem.* **2017**, *70*, 979.
12. Crooks, R. M. *ChemElectroChem* **2016**, *3*, 357.
13. Xu, W.; Fu, K.; Bohn, P. W. *ACS Sens.* **2017**, *2*, 1020.
14. Vanamoo, U.; Hupa, E.; Yrjana, V. Bobacka, J. *Anal. Chem.*, **2016**, *88*, 4369–4374.

Chapter 4: Tunable Optical Sensing with PVC-Membrane-Based Ion-Selective Bipolar Electrodes

This work has been published in: Jansod, S.; Bakker, E. *ACS Sens*. **2019**, *4*, 1008-1016.

4.1 Abstract

We show here that the response of ion-selective membrane electrodes (ISEs) based on traditional PVC membranes can be directly translated into a colorimetric readout by a closed bipolar electrode (BPE) arrangement. Because the resulting optical response is based on the turnover of the redox probe, ferroin, dissolved in a thin layer compartment, it directly indicates the potential change at the ISE in combination with a reference electrode. This class of probes measures ion activity, analogous to their ISE counterparts. Unlike other ion optodes, the response if also fully tunable over a wide concentration range by the application of an external potential and occurs in a compartment that is physically separate from the sample. To allow for the electrical charge to pass across the ion-selective electrodes, the membranes are doped with inert lipophilic electrolyte, ETH 500, but are otherwise of established composition. The observed response behavior correlates well to theory. A wide range of ion-selective membranes are confirmed to work with this readout principle, demonstrating the detection of potassium, sodium, calcium and carbonate ions. The corresponding sigmodal calibration curve is used for the quantitative analysis in a range of samples including commercial beverages and river and lake samples. The data are successfully correlated with atomic emission spectroscopy and direct potentiometry.

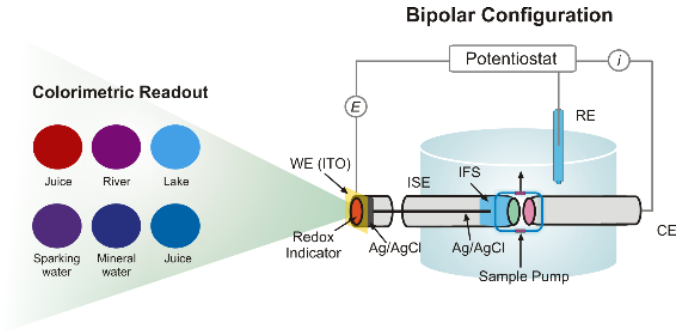

4.2 Introduction

Potentiometric ionophore-based ion selective electrodes (ISEs) are a class of chemical sensors that are well-known tools for routine determination in a broad range of applications such as clinical analysis and environmental monitoring[1-5]. They are simple, robust, require low power, often demonstrate adequate selectivity and sensitivity, and are easily connected to communication devices. To realize alternative readout approaches and achieve complementary speciation information, ISEs have started to be interrogated by chronoamperometry[6-7], chronopotentiometry[8-11], thin layer coulometry[12-14] and cyclic voltammetry[15-18]. In many of these approaches the ISE membrane composition and material requires adequate adaptation to sustain the associated currents.

An optical detection of ion concentration is often quite attractive because it allows for a simpler readout that may be well suited for handheld and zero power devices. Ion optodes can be miniaturized, even down to the nanoscale, and can be used in bioanalytical applications and for the mapping of ion gradients[19-23]. However, there are also disadvantages associated with existing optical sensing approaches. First, ion optodes are more difficult to respond to just a single ion and the required extra-thermodynamic assumptions are different and often more severe than with ISEs[24]. Second, the optical response is generated at the actual sensing location, and turbid or colored samples may cause severe interference[25-27]. Third, the measuring range of ion optodes is much more limited than that of a corresponding potentiometric probe.

Our group reported on an electrochemiluminescence (ECL) detection approach for potentiometric probes[28] that can potentially overcome the three drawbacks mentioned above. The potential change of the ISE, placed in a compartment separate from the detection cell, is treated as the reference electrode in the ECL detection cell. In this manner, a change in ion activity modulates the potential applied to the working electrode and changes the light output. This concept, while promising, is not easily amendable to multiplexed detection of electrode arrays.

Bobacka's group introduced a constant potential coulometric readout based on a redox process for solid-contact ISEs (SC-ISEs) with a conducting polymer inner transducing layer for the determination of analyte[29-31]. The potential change at the SC-ISE is compensated with a corresponding change in the potential of the capacitive transducing layer. The charging of the capacitive layer results in a transient current that can be analytically observed by the electrical current and charge.

In recent work, a potentiometric signal change from an ISE to a fluorimetric readout was introduced by means of a bipolar electrode[32]. The potential change at the ISE induced a potential change at the opposite end of the bipolar electrode, triggering a release of zinc ions that, after appropriate complexation, gave rise to a fluorescence change.

At about the same time, we reported in a *letter* on the concept of a closed bipolar electrode principle to translate ISE potential change into the quantitative turnover of a water-soluble redox probe, ferroin, placed in a physically separated thin detection layer[33]. Conceptually, it is most closely related to Bobacka's capacitive readout mechanism described above. An external applied potential may tune the measuring range of the optical readout. The concept was introduced with a well-established electrode of the second kind, Ag/AgCl, as model ion-selective element for the detection of chloride. It also included a calcium-selective probe on the basis of a doped Celgard membrane of high mobility, chosen to sustain the required current transients.

This bipolar readout concept is here fully established and optimized to work with a range of traditional plasticized PVC membranes for the detection of a variety of ions. The approach is supported by an adequate theoretical model that shows how the applied cell potential can tune the optical response range as a function of analyte ion valency. Measurements in a range of real-world samples are demonstrated.

4.3 Theory of the Bipolar Ion Sensor

A closed bipolar ion selective sensor is considered where a colorimetric redox indicator is confined in a thin layer compartment and connected by an electron conductor to the ion-selective electrodes placed in sample solution. For a cation-selective electrode as an example, detecting analyte ions *i* of charge *z*, the complete electrochemical cell used here is given as:

$$\text{ITO} \mid \text{Ind}_{red}, \text{Ind}_{ox}, \text{KCl} \mid \text{AgCl} \mid \text{Ag (BPE)} \mid \text{AgCl} \mid i\text{Cl}_z\text{(IFS)} \mid \text{Membrane} \mid i\text{Cl}_z\text{ (Sample)} \mid \text{AgCl} \mid \text{Ag}$$

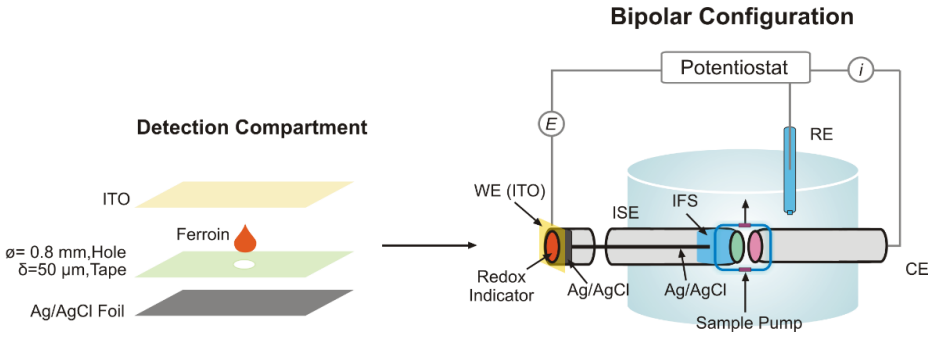

Figure 1. Construction of the closed BPE where the detection (left) and sample compartments are physically separated from each other. In the closed bipolar configuration (right), the Ag/AgCl element in detection compartment is connected to the potentiometric probe in sample compartment. A closed BPE setup composes of the redox indicator in detection compartment and another pole end is potentiometric sensing probe based on the liquid PVC ISE in sample compartment, where WE is the working electrode, RE the reference electrode, CE the counter electrode, IFS the inner filling solution. Sample is delivered to the thin solution layer by a peristaltic pump (see Supporting Information for the realistic experimental setup).

The corresponding experimental setup is shown in Figure 1. The closed BPE setup comprises the potentiometric probe in the sample compartment and, at the opposite pole, the colorimetric redox indicator. This results in a detection compartment that is physically separated from the sample. The potential is imposed between the transparent indium tin oxide (ITO) coated glass slide working electrode and the reference/counter electrodes in the sample as shown.

The reduction potential for the colorimetric redox indicator ferroin, ($Fe^{II}(phen)_3$) in the detection compartment is dictated by the potential at the ITO working electrode and described by the Nernst equation 1:

$$E_{\text{detection}} = E^0_{ferroin} - s \log \frac{[Ind_{red}]}{[Ind_{ox}]} \qquad (1)$$

Where s is the Nernstian slope for n=1 (number of transferred electrons), ideally 59.2 mV at 298 K. Consequently, a more positive applied potential at the ITO working electrode results in an increase of oxidized form of the colorimetric redox indicator ferroin. The color changes from red (Ind_{red}) to blue color (Ind_{ox}). The thin layer cell

geometry aims to reduce mass transport limitations of the reaction, giving a concentration ratio of redox probe that, ideally, always reflects the value of the applied potential.

In the closed bipolar electrode arrangement, the detection cell is connected in series to the potentiometric sensing probe in the sample compartment (see Supporting Information for the derivation of the equations). The concentration ratio of redox probe in the detection cell now becomes a direct function of the ion activity of i in the sample

$$s \log \frac{[Ind_{ox}]}{[Ind_{red}]} = E_{app} - \frac{s}{z_i} \log a_i + E_{const} \qquad (2)$$

Where E_{app} is a constant potential applied across the cell containing the bipolar electrode, a_i the ion activity of ion M with charge z_i.

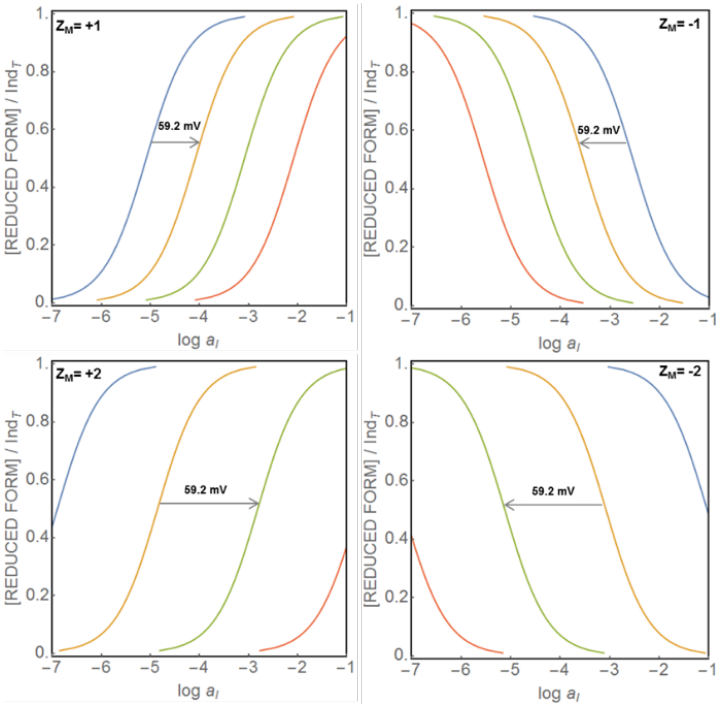

Figure 2. Calculated change in the mole fraction of reduced form of the colorimetric redox indicator ferroin using eq. 2.

Figure 2 shows the calculated mole fraction of reduced redox probe as a function of logarithmic ion activity at different applied potentials and various ion valencies. The sigmoidal response covers about two orders of magnitude concentration range, which is typical for optical sensors. Perhaps unique to this approach, the applied potential directly controls the position of the measuring range and can therefore be used to adjust to any problem at hand without any chemical adjustment. If divalent, rather than monovalent ions are detected, a potential change of 59.2 mV shifts the measuring range by two, rather than one order of magnitude. If anionic species are measured, a decreased, rather than increased concentration of reduced form of indicator is expected for increasing analyte activity.

4.4 Experimental Details

Materials, reagents and instrumentation Potassium chloride, potassium nitrate, sodium chloride, sodium bicarbonate, calcium chloride, hydrochloric acid solution (HCl, 1.0 M), tris(1,10-phenanthroline iron (II) sulfate (ferroin), sodium tetrakis-[3,5-bis(trifluoromethyl)phenyl]borate (NaTFPB), tridodecylmethylammonium chloride (TDMACl), tetrakis(4-chlorophenyl)borate tetradodecylammonium salt (ETH 500), poly(vinyl-chloride) (PVC, high molecular weight), potassium ionophore I, sodium ionophore X, calcium ionophore IV, carbonate ionophore VII, dodecyl 2-nitrophenyl ether (DD-NPE), 2-amino-2-hydroxymethyl-propane-1,3-diolhydrochloride (Tris-HCl), tris(hydroxymethyl)aminomethane hemisulfate salt (Tris-H_2SO_4), tetrahydrofuran (THF), indium tin oxide (ITO, surface resistivity 1.28-1.92 $\Omega \cdot cm^{-2}$) were purchased from Sigma-Aldrich. Silver foil, of 99.97% purity, thickness 0.025 mm was purchased from Advent Research Materials (Oxford, UK). An insulating transparent Scotch 3M tape (50 μm thickness) and a metallic hole punch tool (0.8 mm diameter) were used. Ag electrode tip with a diameter of 3.00±0.05 mm (6.1204.330) was sourced from Metrohm (Switzerland). IPC ISMATEC peristaltic pump (Model ISM935C, Clattbrug, Switzerland), TYGON tubing (inner diameter 1.42 mm, wall 0.86 mm) and PTFE tubing (L × OD × ID = 300 mm × 1/16 × 100 μm, Supelco) were used in the flow system. The electrochemical measurements of cyclic voltammetry and chronoamperometry were performed in a faraday cage with a potentiostat/galvanostat PGSTAT 204 (Metrohm Autolab, Utrecht, The Netherlands) that was controlled by Nova 2.1 software. A computer tethered digital camera (Canon EOS 5D Mark II equipped with a MP-E 60mm macro lens and matching ring flash) was used to capture the images of the detection cell. Aqueous solutions were prepared in MilliQ water. Mineral water, apple juice and sparkling water were purchased from a local supermarket in Switzerland. Samples from the Arve river and Geneva lake were collected in the Jonction area in Geneva. The background electrolyte for all artificial samples was maintained at 10 mM NaCl.

Coating AgCl on Ag foil. Ag foil used in detection compartment was cut into a 25 × 8 mm piece. A layer of AgCl was electrochemically deposited by oxidizing the Ag in a solution of 1 M HCl for 30 min at a constant anodic current density of 1.25 mA cm^{-2}.

Sample compartment. The potentiometric measurement of potentiometric based PVC membrane sensing probes acting as a working electrode were carried out against a commercial reference electrode (6.0729.100, Metrohm) with a double junction reference electrode (Ag | AgCl | KCl, 3 M | LiOAc, 1 M) in a faraday cage using a 16-channel EMF interface (Lawson Laboratories, Inc., Malvern, Pa). An Ag counter electrode was placed opposite the potentiometric electrode, separated by a narrow solution gap into which the samples were delivered to the cell by peristaltic pumping, see in Figure 1. This arrangement reduces equilibration times in the sample compartment and allows one to place the reference electrode in the contacting aqueous electrolyte reservoir containing 3M KCl that was connected to the sample cell through the fluid outlet (1mm dia.). The backgrounds used for determination of potassium, sodium, calcium and carbonate were maintained by using 10 mM NaCl, 10 mM KCl, 10 mM Tris-HCl pH 7.2 + 10 mM KCl and 0.1 M Tris-H_2SO_4 pH 8.0 + 10 mM KCl, respectively.

Detection compartment. A circular opening of 0.8 mm diameter was punched in a 50 μm thick adhesive insulating tape to form a recess and placed on a planar Ag/AgCl foil that acts as a reference/counter electrode, and a 0.3 μL drop of 22.7 mM of ferroin in 100 mM KCl was placed into the recess. The transparent ITO working electrode was

placed on top and made to contact the ferroin solution. The optical signal was recorded with a tethered digital camera (Canon EOS 5D Mark II) equipped with a Canon MP-E 60 mm macro lens and a ring flash. The camera captured the images in JPEG format, which were analyzed for hue value by Mathematica software 11.1 (Wolfram Research) that involves importing each image, automatic cropping for the detection compartment area, and computing the average hue value from all residual pixels.

Preparation of membrane electrodes. A mixture of ionophore, ion exchanger, PVC and plasticizer was used to prepare the cocktail for potentiometric sensing probe. The cocktail solution of 15 mmol kg^{-1} ionophore, 5 mmol kg^{-1} ion exchanger, 90 mmol kg^{-1} of ETH 500 with PVC and plasticizer (1:2 by weight; total mass 200 mg) were dissolved in 2 mL THF and poured into a glass ring (22 mm i.d.) fixed on a glass slide with rubber bands. The composition of the membrane cocktails is shown in Table 1. The solution was evaporated overnight at room temperature. The homogenous master membrane was punched into disks of 8 mm diameter (200-300 µm thickness). The membranes were conditioned in 1 mM of primary ion for a few hours. Afterwards, the membrane was mounted in an Ostec electrode body (Oesch Sensor Technology, Sargans, Switzerland). The inner filling solution (IFS) for potassium, sodium, calcium and carbonate detections were filled with 1 mM KCl, 1mM NaCl, 1 mM $CaCl_2$ in the buffer pH 7.2 and 10 mM $NaHCO_3$ in the buffer pH 8.0 + 10 mM NaCl, respectively.

Table 1. Compositions of the membranes used as the potentiometric sensing probe. The amounts are relative to a total mass of 200 mg dissolved in 2 mL of THF.

	M1	**M2**	**M3**	**M4**
Ionophore[a]	15[c]	15[d]	15[e]	15[f]
NaTFPB[a]	5	5	5	-
TDMACl[a]	-	-	-	5
ETH 500[a]	90	90	90	90
PVC[b]	30	29	29.5	29.5
DD-NPE[b]	60	59	59	59.5

[a]mmol kg-1, [b]mass percentage, [c]potassium ionophore I, [d]sodium ionophore X, [e]calcium ionophore IV and [f]carbonate ionophore VII,

Closed BPE setup. The Ag/AgCl element in the detection compartment coupled to a liquid membrane based ion-selective PVC membrane electrode with aqueous inner solution containing an Ag/AgCl element as a potentiometric sensing probe. This potentiometric probe was immersed in a sample solution containing variable concentrations of the samples. The Ag counter electrode was placed opposite the potentiometric electrode, separated by a thin solution layer, which the samples were transported to the inlet-outlet flow cell by peristaltic pumping. A double junction reference electrode was placed in contact with the sample bulk.

Selectivity coefficient determination. The selectivity coefficients of each potentiometric probes were measured by the separate solutions method (SSM)[34]. The conventional PVC membranes of M1 and M2 were conditioned in 1 mM $MgCl_2$ solution, the membrane M3 and M4 were conditioned in 1 mM KCl and 0.1 M tris-H_2SO_4 + 10 mM

KCl (pH 8.0), respectively. All the membrane were conditioned for 12 h in the same solution used as inner filling solution. The EMF values for different concentrations were recorded in the concentration range from 10^{-6} to 10^{-2} M. For the potentiometric carbonate probe, the EMF values were measured in a background of 0.1 M Tris-H_2SO_4 + 10 mM KCl (pH 8.0). The selectivity coefficients were calculated regarding to eq 3 using the observed EMF values for the highest measured ion activities corresponding to the Nernstian measuring range of the electrode responses[34-35].

$$\log K_{i,j}^{pot} = \frac{(E_j - E_i)Z_i F}{2.303RT} + \log \frac{a_i}{a_j^{z_i/z_j}} \qquad (3)$$

Where i and j are the primary and interfering ion, respectively.

4.5 Results and Discussion

Four different types of ionophore-based ISEs were used as potentiometric sensing probes in this work, see Table 1 for membrane compositions. Figure 3 shows the separate calibration curves for each of these probes, characterized separately in the sample flow cell compartment by zero current potentiometry. They were all confirmed to exhibit near-Nernstian response slopes to the activities of potassium (59.29 mV), sodium (58.40 mV), calcium (29.43 mV) and carbonate (-28.55 mV), respectively, see Figures 3a-d.

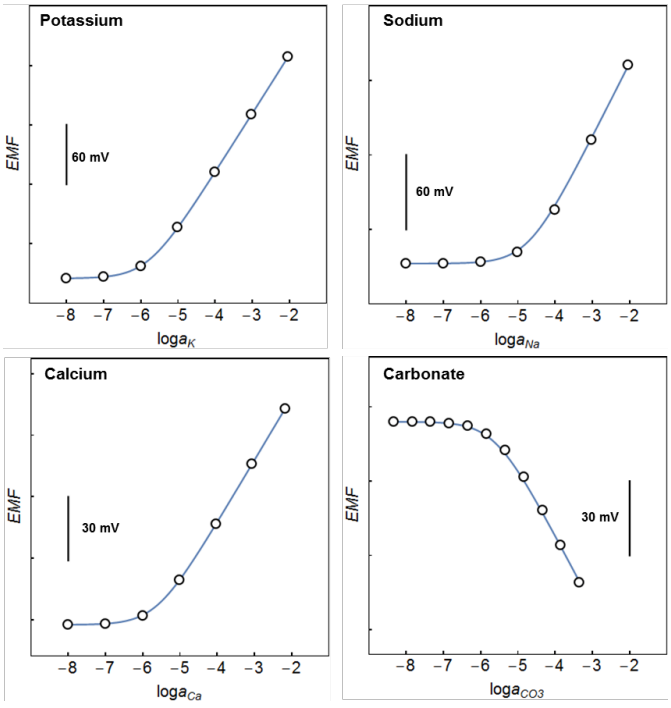

Figure 3. Potentiometric responses of different potentiometric probes based on the liquid PVC membranes electrodes.

Preliminary studies found that plasticized PVC membranes of traditional composition did not properly function in a bipolar electrode arrangement, giving no discernable color change in the detection compartment. To reduce the membrane resistance while maintaining ion selectivity and diffusive characteristics, the membranes were doped

with a high concentration of lipophilic salt, ETH 500. Earlier work used the same modification for the successful realization of chronopotentiometric sensors, where a constant current period must be passed across the ion-selective membrane[36-37]. In our recent work, the resistance of the membranes with (M1) and without ETH 500 was found at 96 kΩ and 265 kΩ, respectively, see Figure S1 in Supporting Information. The ohmic potential drop is quite small, calculated as up to 8.6 mV (i=90 nA). Resistance changes are found not to affect the final optical signal, because each equilibrium state is at zero current. To verify, a 51 kΩ resistor was placed between the ISE and detection compartment in the bipolar configuration. The observed final hue values with and without the resistor were indeed the same, only giving a slower response time for the one with added resistor, see Figure S2. All ion-selective membrane modified in this manner were thus successfully applied for the purpose of colorimetric readout.

The modified membranes are characterized in terms of selectivity coefficients, see Table S1 in Supporting Information. Membrane M1, M2 and M3 exhibit a high selectivity of their primary ions over the interfering ones. We note, however, that for the carbonate-selective membrane M4, doping with ETH 500 results in a somewhat deteriorated selectivity over perchlorate and thiocyanate ions. This membrane may benefit from further optimization in the future.

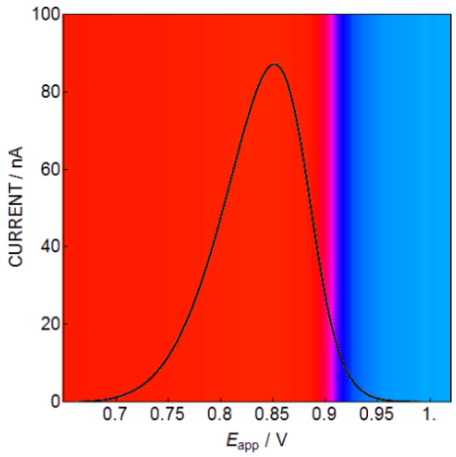

Figure 4. Background subtracted current response of detection compartment by applying an oxidative linear potential scan at 0.2 mV s-1. It contains 22.7 mM ferroin in 100 mM KCl dropped on the tape with an opened circle diameter of 0.8 mm. The background density plot is computed from the experimentally observed hue values for each applied potential.

With a constant imposed applied potential across the bipolar electrode cell, the potential change at the ion-selective electrode that results from a variation in sample ion activity must be compensated for by a corresponding concentration change of colorimetric redox indicator in the detection compartment. This can be observed visually, and the resulting hue values may be analyzed by image analysis software. The turnover of colorimetric redox indicator necessitates an electrical charge to pass through the BPE. This same charge will also pass through the potentiometric sensing probe, which might result in undesired signal drifts. To be able to utilize conventional PVC membranes, the magnitude of the current transient was limited by minimizing the area of the detection zone by cutting a smaller hole of 0.8-mm dia. in the insulating tape (50 µm thickness) attached on the ITO electrode. This opening defined the detection compartment volume at about 25 nL into which the 22.7 mM ferroin solution was dropped. The chloride concentrations in the detection compartment and inner solution of the ISE were sufficiently large to avoid concentration changes upon temporal charge transfer during measurement.

Figure 4 shows the typical bell-shaped current peak observed upon direct electrochemical oxidation of the probe in the detection compartment, in the absence of any bipolar electrode. The shape of the curve suggests exhaustive turnover, as desired, while the background color shows the simultaneously recorded hue values during the same experiment. The indicator color transitions from red to blue to reflect the oxidation state of the probe. With the selected experimental conditions the current peaks at about 90 nA, with a charge of 44.2 µC. On the other hand, the visible color change of the indicator occurs from 0.87 to 1.0 V. This range requires just 10 µC, or 23% of the total charge. This charge was imposed on the potentiometric probe only, resulting in a potential change of around 4 mV until the new equilibrium state was reached, see Figure S3. The sigmoidal response normally exhibits a two orders of magnitude concentration range. The colorimetric signal change for the bipolar electrode for a concentration change from 10^{-5} to 10^{-3} M KCl (and back) in the sample compartment was therefore measured, resulting in a transfer of charge of 3.7 µC (and 3.8 µC), see in Figure S4. This charge results in a transient potential change up to about 3 mV, which may be acceptable because the hue value is observed after stabilization at which time the transient current should again be near zero.

Translation of potentiometric signal into colorimetric readout in the closed BPE. In the complete cell of the BPE, the potentiometric probe immersed in the sample compartment translates that potential into the colorimetric indicator in the detection compartment. Figure 5 (top) shows the voltammograms from an anodic potential scan at 0.2 mV s^{-1} for the different potentiometric probes in the closed BPE configuration. The potentiometric sensing probes for potassium, sodium and calcium result in a more positive potential with an increase in sample concentration. The shift agreed with the Nernst equation, 59.09 mV per 10-fold potassium activity change in the sample compartment (Figure 5a). In analogy, the shift of the potentiometric probes for sodium and calcium gave a Nernstian shift of 61.40 mV $decade^{-1}$ (Figure 5b) and 30.03 mV $decade^{-1}$ (Figure 5c), respectively. The peak shifts to more anodic potentials, confirming the Nernstian response to cations.

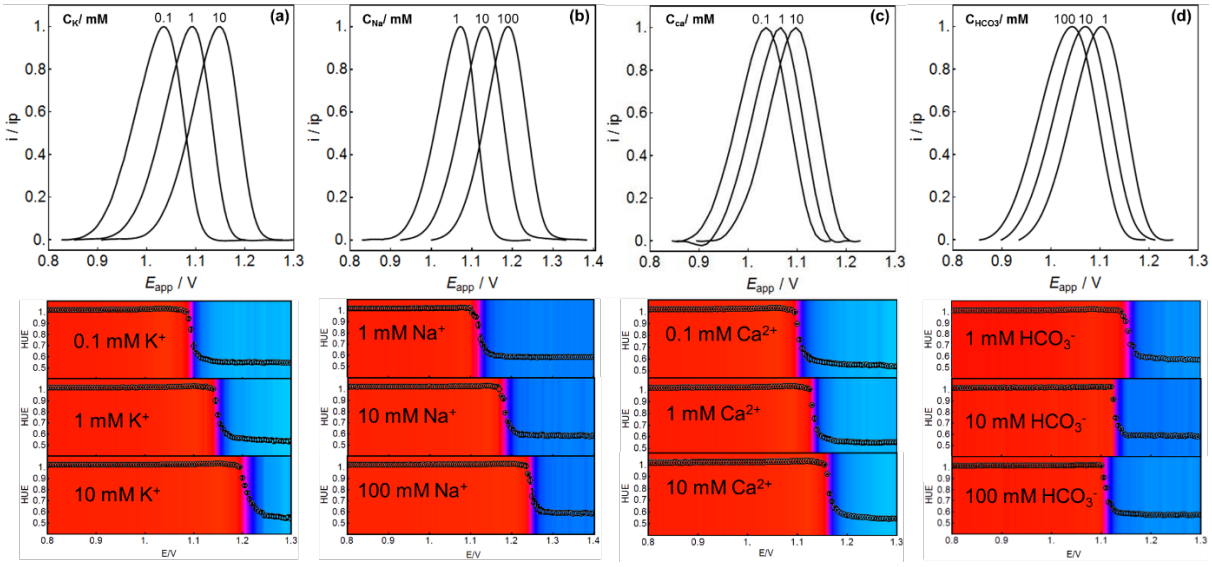

Figure 5. Top: Normalized current responses of the complete cell of the BPE composes of the colorimetric redox indicator ferroin in detection compartment coupled to the potentiometric sensing probe in sample compartment; (a) Potassium-ISE, (b) Sodium-ISE, (c) Calcium-ISE and (d) Carbonate-ISE. Bottom: Corresponding color changes in the detection compartment with the observed hue values shown as calculated density plot background. Error bars are standard deviations (n= 3).

As expected, the peak potential for the potentiometric carbonate probe changes to more negative potentials with increasing carbonate concentration, indicating that the probe responds to anions in agreement with theory. The shift amounts to -30.63 mV per 10-fold carbonate activity increase (Figure 5d). Figure 5 (Bottom) shows the corresponding observed hue values for each applied potential that are found to shift with an increase of sample concentrations. Theoretically from eq 2, increasing primary cation concentrations result in a higher concentration ratio of reduced form of ferroin (Fe^{II}, red), as demonstrated in stronger red coloration (Figure 5a-c, Bottom). Conversely, increasing concentrations of primary anion give a higher mole fraction of oxidized ferroin (Fe^{III}, blue), see Figure 5d, Bottom. In all cases, the measuring range of the colorimetric response can be tuned electrochemically.

Colorimetric calibrations with the Ion-Selective BPEs. The traditional potentiometric probes coupled to the colorimetric redox indicator ferroin in the BPE have been used to determine ions of interest at a suitably fixed potential value. Figure 6 shows the corresponding changes of hue value for calibrations at three different applied potentials with increasing concentration of the analyte ions potassium, sodium, calcium, and carbonate. The reversal of the colorimetric calibration curves for cations and anions reflect the different charge signs, see eq 2. The corresponding hue values for the divalent ions move closer compared to monovalent ions, similar to Figure 5c-d, which is caused by the reduced Nernstian slopes for ions of higher valency. A clear advantage of the optical sensing concept used here is that the applied potential across the BPE can be tuned to agree with the concentration range of interest. For the purpose of curve fitting, the Boltzmann equation[38] was used to describe the sigmoidal response curves as described in the Supporting Information. The R-squares for each applied potential of the different probes are shown in Table S2.

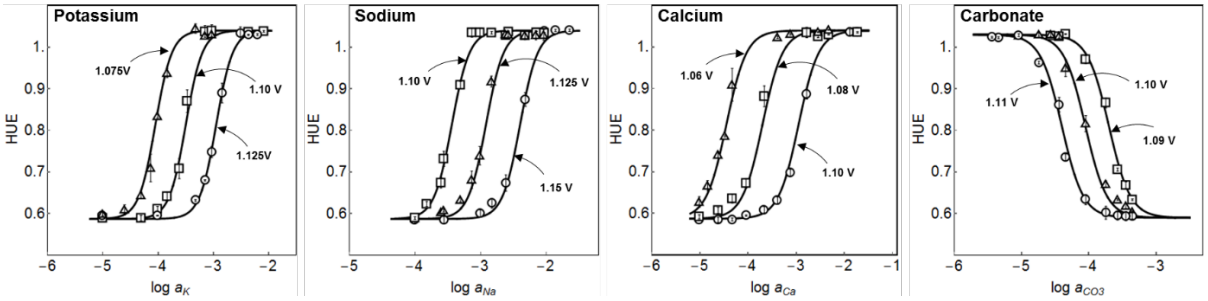

Figure 6. Colorimetric calibration curves of the BPE at three different applied potentials. The colorimetric redox probe is coupled to the potentiometric ISE probe. All the data points are fitted by the sigmodal lines calculated by the Boltzmann equation.

Quantitative analysis with the closed BPE. The potentiometric probe based on the ion-selective PVC membrane electrode for determining potassium ions by BPE was chosen for further experiments. The observed hue values at three fixed applied potentials with different activities of potassium were recorded. The quantitative analysis for potassium contents in environmental samples from a river and lake as well as commercial beverages were investigated. Figure 7a shows the observed color change from blue (Fe^{III}) to red (Fe^{II}) with increasing potassium activity. Higher activity of potassium results in an increased reduced form of the colorimetric indicator. In case of apple juice, which contains more potassium, the ratio of reduced form was found to be higher, giving a more intense red color. With the same applied potential of 1.10 V one cannot distinguish the hue signals from lake and river samples, as both gave a blue color outside the dynamic response range. As the applied potential can be used to

electrochemically tune the measuring range, a lower potential of 1.0625 V was imposed to determine the hue values for potassium in the lake and river samples, see Figure 7b. These hue signals are now located on an appropriate curve and give concentration values that correlate well to atomic emission spectroscopy (AES) and direct potentiometry, as shown in Table 2.

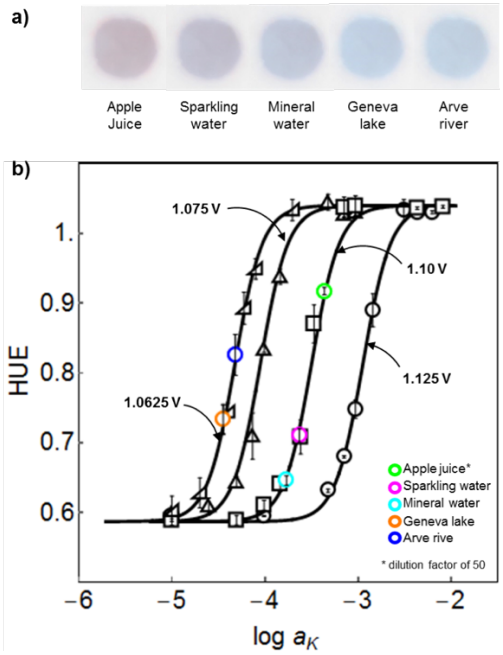

Figure 7. (a) Images captured in the detection compartment for different samples at which the potential at 1.10 V is applied. (b) Observed hue values of the samples plotted on the colorimetric potassium calibration curves for different applied potentials, tuned to the concentration range that give the highest sensitivity.

For the sample analysis, the sigmodal calibration curves were fitted to the Boltzmann equation. Figure 7b shows the observed hue values as a function of potassium ion activity for the complex samples at different applied potentials. The potassium concentrations were then computed from the hue values and shown in Table 2.

Table 2. Determination of potassium content (mM) in various samples (SD, n=3).

Samples	**AES**	**Potentiometry**	**Bipolar electrode**
Apple juice	26.4 ±0.3	25.5 ±0.5	24.7 ±0.4
Sparkling water	0.268 ±0.002	0.258 ±0.001	0.249 ±0.008
Mineral water	0.186 ±0.001	0.189 ±0.001	0.182 ±0.007
Geneva lake	0.0411 ±0.0002	0.0394 ±0.0003	0.0407 ±0.0002
Arve river	0.0540 ±0.0001	0.0528 ±0.0003	0.0546 ±0.0004

Table 2 shows the observed potassium concentrations in the complex samples from the environment and commercial drinks using direct potentiometry and the proposed BPE optode. The results agree with those from AES and direct potentiometry, used here as reference methods. Since the detection compartment was physically

isolated from the sample compartment, other impurities such as dust, soil, colorants and colloids from the samples may not interfere with the optical output of the colorimetric redox indicator in the detection compartment.

Stability and reversibility properties of potentiometric probe and colorimetric redox indicator. The reversibility and stability are crucial characteristics in every type of sensor. The reversibility of the colorimetric redox indicator ferroin in the BPE optode is characterized separately for the detection compartment. Figure 8a demonstrates the reversible hue values of the colorimetric indicator for alternating constant applied potentials of 0.932 V and 0.910 V (each separated by 22 mV). These potentials are imposed between the transparent ITO working electrode and the Ag/AgCl foil counter/reference electrode. For each equilibrium state, the corresponding hue values between 0.6 and 0.7 were observed in a reversible manner. Reversibility was also studied for the complete BPE optode cell. Figure 8b shows the hue values, set to reversibly alternate between 0.6 and 0.7 in the equilibrium states. These color changes are now triggered by the potassium concentration changes between 0.1 mM and 0.25 mM in the sample compartment.

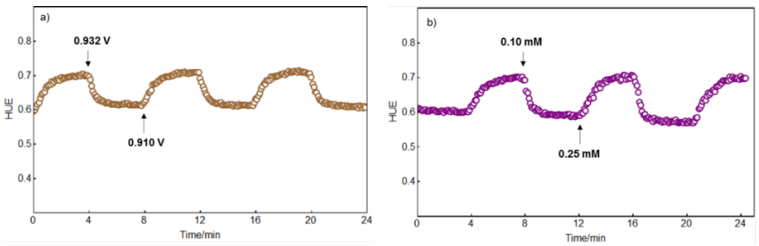

Figure 8. Corresponding changes of hue values; (a) Different applied potentials at 0.932 V and 0.910 V are imposed separately in only detection compartment. (b) Different potassium concentrations of 0.10 mM and 0.25 mM are demonstrated in the BPE, at which the constant potential at 1.10 V is imposed in BPE.

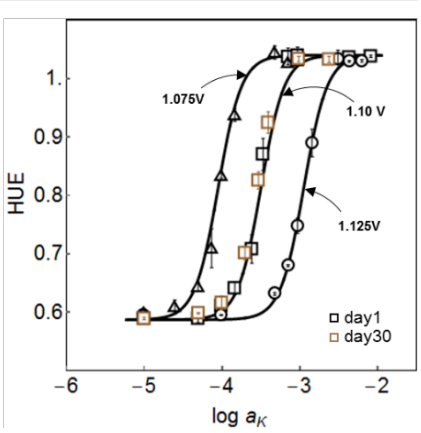

Figure 9. Colorimetric calibrations curves of bipolar electrodes couple to a potassium-selective membrane as potentiometric probe at different applied potentials. Black circles, squares and triangles are investigated on day 1. Brown squares are measured on day 30, at which a potential of 1.10 V is applied. The redox indicator in the detection compartment is refreshed every day.

The high potential stability of just the potentiometric potassium probe from day 1 to day 30 is confirmed in Figure S5. The stability of the colorimetric calibration curves for determination of potassium concentration for the same time interval is shown in Figure 9. The potentiometric probe is well-behaved as the potentials on day 30 are not significantly different. The potentiometric potassium probe in the BPE optode shows that the observed hue values

on day 30 still agree with the sigmoidal calibration curve and suggest that this BPE optode approach may be used for at least 30 days.

4.6 Conclusions

We explored the main theoretical response mechanism of bipolar ion selective optical sensors. The potentiometric response from ionophore-based plasticized PVC membrane electrodes were successfully translated into a colorimetric readout with a closed bipolar electrode configuration. The membrane composition was adapted by the addition of inert lipophilic salt to allow for the required current transient through the electrode without undue polarization of the potentiometric probe. The readout compartment was successfully miniaturized by reducing the surface area, where the colorimetric redox indicator was placed in contact with a Ag/AgCl element. The approach was demonstrated to be useful for the quantitative analysis in real world samples and showed adequate reproducibility and stability. The main attraction of the approach relative to traditional optodes is physical separation of sample and detection compartments and the tunability of the response range by the magnitude of the applied potential. We anticipate that this platform will become especially useful for the fabrication of large sensor arrays where a single potentiostat may control a wide range of bipolar electrodes that can all be simultaneously interrogated by an imaging device.

4.7 Acknowledgements

The authors thank the Swiss National Science Foundation (SNSF grant no. 200021_175622) and the Swiss Government Excellence Fellowship for financial support.

4.8 Supporting Information

Photographs of Experimental Setup[33].

Note: the potentiometric probe in the sample compartment in this work is changed to a polymer membrane electrode, using an Ostec electrode body.

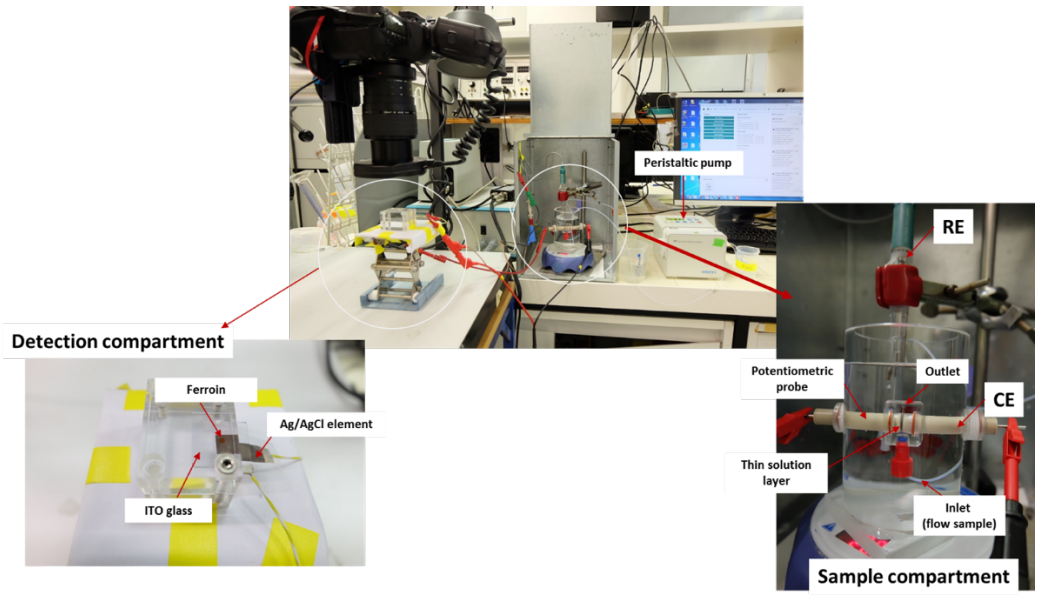

Schematic illustration

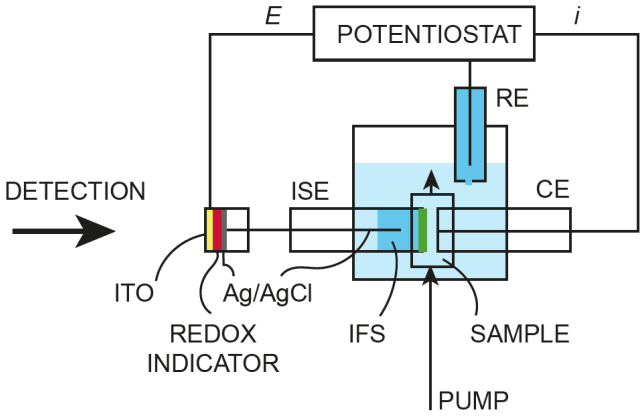

Detailed theoretical closed BPE approach

To potential at each element (number labeled in red) in our closed BPE approach is described as shown below.

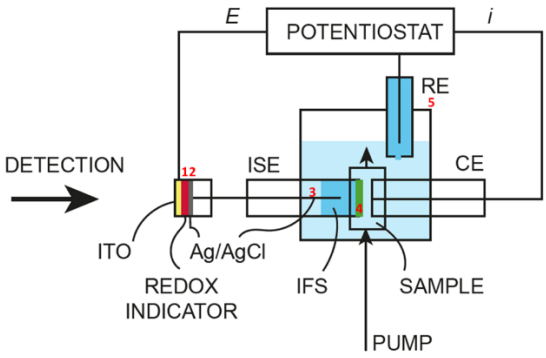

(1) $E_{\det ection} = E^{0}_{ferroin} + s\log\frac{[Ind]_{ox}}{[Ind]_{red}}$

(2) $E^{'}_{AgCl/Cl} = E^{0'}_{AgCl/Ag} - s\log a^{'}_{Cl}$

(3) $E^{"}_{AgCl/Cl} = E^{0"}_{AgCl/Ag} - s\log a^{"}_{Cl}$

(4) $E_{M} = \frac{s}{z_i}\log\frac{a_i^{aq}}{a_i^{IFS}}$

(5) $E^{'''}_{AgCl/Cl} = E^{0'''}_{AgCl/Ag} - s\log a^{'''}_{Cl} + E_{junction}$

When a constant potential is applied in the BPE approach via the ITO working electrode, all the equations above are combined as follows:

$$E_{applied} = (1) + (2) + (3) + (4) + (5)$$

$$E_{applied} = E^{0}_{ferroin} + s\log\frac{[Ind]_{ox}}{[Ind]_{red}} + E^{0'}_{AgCl/Ag} - s\log a^{'}_{Cl} + E^{0"}_{AgCl/Ag} - s\log a^{"}_{Cl} + \frac{s}{z_i}\log\frac{a_i^{aq}}{a_i^{IFS}} + E^{0'''}_{AgCl/Ag} - s\log a^{'''}_{Cl} + E_{junction}$$

$$s\log\frac{[Ind]_{ox}}{[Ind]_{red}} = E_{applied} - E^{0}_{ferroin} - E^{0'}_{AgCl/Ag} + s\log a^{'}_{Cl} - E^{0"}_{AgCl/Ag} + s\log a^{"}_{Cl} - \frac{s}{z_i}\log\frac{a_i^{aq}}{a_i^{IFS}} - E^{0'''}_{AgCl/Ag} + s\log a^{'''}_{Cl} - E_{junction}$$

$$s\log\frac{[Ind]_{ox}}{[Ind]_{red}} = (E_{applied} - E^{0}_{ferroin} - s\log a^{'}_{Cl} + s\log a^{"}_{Cl} - \frac{s}{z_i}\log\frac{1}{a_i^{IFS}} - E^{0'''}_{AgCl/Ag} + s\log a^{'''}_{Cl} - E_{junction}) - \frac{s}{z_i}\log a_i^{aq}$$

$$s\log\frac{[Ind]_{ox}}{[Ind]_{red}} = E_{applied} - \frac{s}{z_i}\log a_i^{aq} + E_{const}$$

Boltzmann equation used to describe the sigmoidal colorimetric response.

$$HUE = \frac{A_1 - A_2}{1 + e^{\log a_i - x_0/dx}} + A_2$$

Where A_1 is an initial hue, A_2 is a final hue, X_0 is a center of the curve, dx is an ion activity constant

Table S1. Observed logarithmic selectivity coefficients for the modified membranes used as potentiometric probes.

Membrane	Ion i, j	log $K_{i,j}^{pot}$ (n=3)
M1	K^+,Mg^{2+}	-5.09 ±0.17
	K^+,Ca^{2+}	-5.15 ±0.12
	K^+,Li^+	-5.18 ±0.06
	K^+,Na^+	-4.31 ±0.05
M2	Na^+,Mg^{2+}	-4.36 ±0.03
	Na^+,Ca^{2+}	-4.58 ±0.02
	Na^+,Li^+	-3.51 ±0.01
	Na^+,K^+	-2.61 ±0.02
M3	Ca^{2+},K^+	-2.24 ±0.10
	Ca^{2+},Na^+	-2.16 ±0.002
	Ca^{2+},Li^+	-2.18 ±0.002
	Ca^{2+}, Mg^{2+}	-2.74 ±0.02
M4	CO_3^{2-}, Cl^-	-2.56 ±0.09
	CO_3^{2-}, Br^-	-2.33 ±0.10
	CO_3^{2-}, NO_3^-	-1.64 ±0.12
	CO_3^{2-}, SCN^-	0.18 ±0.16
	CO_3^{2-}, ClO_4^-	2.44 ±0.19

Table S2. R-square between the fitted line using Boltzmann equation and all the data points of each applied potential on the closed BPE.

E_{app}/ V	log a_K	log a_{Na}	log a_{Ca}	log a_{CO3}
1.0625	0.9975			
1.075	0.9892			
1.100	0.9846			
1.125	0.9972			
1.100		0.9951		
1.125		0.9957		
1.150		0.9933		
1.060			0.9970	
1.080			0.9964	
1.100			0.9870	
1.109				0.9935
1.100				0.9945
1.110				0.9926

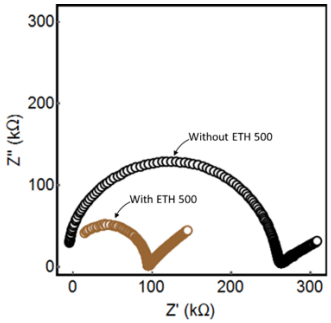

Figure S1. Impedance spectra of potassium-selective membrane electrodes for membrane M1 with ETH 500 (brown circles) and the membrane without ETH 500 (black circles) exhibited the resistance of the membrane at 96 kΩ and 265 kΩ, respectively. These electrodes were measured in electrolyte containing 10 mM NaCl. Parameters: first frequency= 100000 Hz, last frequency= 0.1 Hz, number of frequencies= 50, amplitude= 0.01 V, wave type= sine, frequency step type= points per decade.

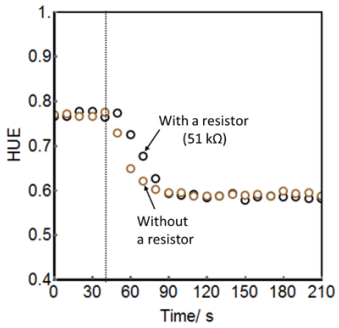

Figure S2. Comparison of corresponding change of hue value with time, at which a resistor is placed (black circles) between the potassium-ISE (M1) and detection compartment in the closed BPE and another one without the resistor (brown circles). An applied potential of 1.1 V is firstly imposed for 40 seconds. Afterwards, a potential of 1.2 V is immediately applied. Sample compartment contains 0.4 mM KCl in 10 mM NaCl (as the background electrolyte).

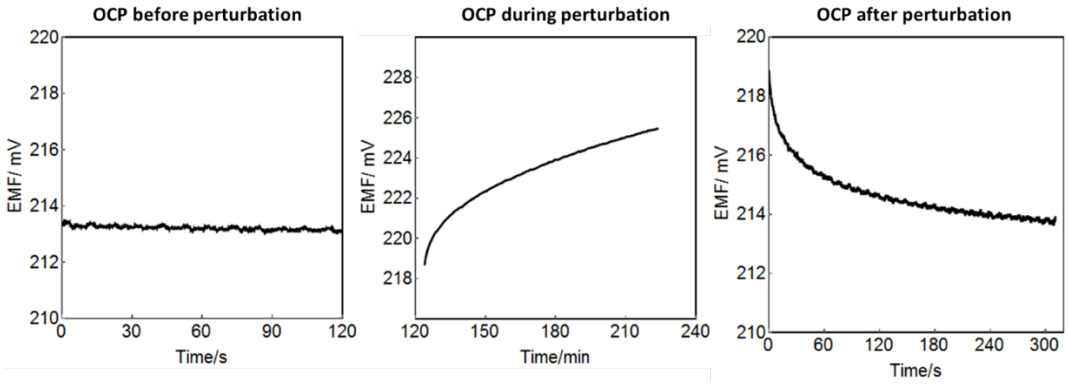

Figure S3. Electrochemical perturbations only at the potassium-ISE probe containing 1 mM KCl in sample compartment. A current amplitudes of 45 nA for a period of 225-s or 10 µC is imposed.

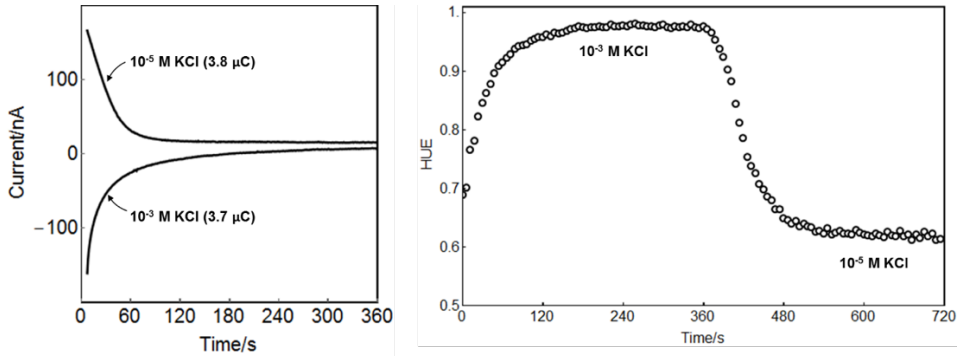

Figure S4. Current pass though the bipolar electrode coupled to the potassium-ISE probe while applying a constant potential of 1.10 V from 10^{-5} to 10^{-3} M KCl and back (left). Corresponding hue values for an applied constant potential of 1.10 V (right).

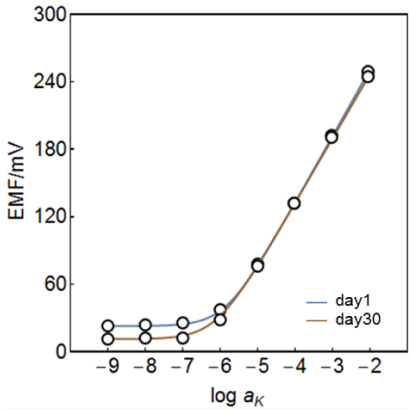

Figure S5. Long-term stability of potassium ISE probe on day-1 and day-30.

4.9 References

1. Bakker, E.; Bhakthavatsalam, V.; Gemene, K. L., Beyond potentiometry: Robust electrochemical ion sensor concepts in view of remote chemical sensing. *Talanta* **2008,** *75* (3), 629-635.
2. Bakker, E.; Pretsch, E., Modern Potentiometry. *Angew. Chem., Int. Ed.*. **2007,** *46* (30), 5660-5668.
3. Bobacka, J.; Ivaska, A.; Lewenstam, A., Potentiometric Ion Sensors. *Chem. Rev.* **2008,** *108* (2), 329-351.
4. De Marco, R.; Clarke, G.; Pejcic, B., Ion-Selective Electrode Potentiometry in Environmental Analysis. *Electroanalysis* **2007,** *19* (19-20), 1987-2001.
5. Zdrachek, E.; Bakker, E., Potentiometric Sensing. *Anal. Chem.* **2019,** *91* (1), 2-26.
6. Jansod, S.; Ghahraman Afshar, M.; Crespo, G. A.; Bakker, E., Alkalinization of Thin Layer Samples with a Selective Proton Sink Membrane Electrode for Detecting Carbonate by Carbonate-Selective Electrodes. *Anal. Chem.* **2016,** *88* (7), 3444-3448.
7. Pendley, B. D.; Lindner, E., A Chronoamperometric Method To Estimate Ionophore Loss from Ion-Selective Electrode Membranes. *Anal. Chem.* **1999,** *71* (17), 3673-3676.
8. Jansod, S.; Afshar, M. G.; Crespo, G. A.; Bakker, E., Phenytoin speciation with potentiometric and chronopotentiometric ion-selective membrane electrodes. *Biosens. Bioelectron.* **2016,** *79*, 114-120.
9. Jarolímová, Z.; Crespo, G. A.; Xie, X.; Ghahraman Afshar, M.; Pawlak, M.; Bakker, E., Chronopotentiometric Carbonate Detection with All-Solid-State Ionophore-Based Electrodes. *Anal. Chem.* **2014,** *86* (13), 6307-6314.
10. Jarolímová, Z.; Crespo, G. A.; Afshar, M. G.; Pawlak, M.; Bakker, E., All solid state chronopotentiometric ion-selective electrodes based on ferrocene functionalized PVC. *J. Electroanal. Chem.* **2013,** *709*, 118-125.
11. Zdrachek, E.; Bakker, E., Electrochemically Switchable Polymeric Membrane Ion-Selective Electrodes. *Anal. chem.* **2018,** *90* (12), 7591-7599.
12. Grygolowicz-Pawlak, E.; Bakker, E., Thin Layer Coulometry with Ionophore Based Ion-Selective Membranes. *Anal. Chem.* **2010,** *82* (11), 4537-4542.
13. Bakker, E., Membrane Response Model for Ion-Selective Electrodes Operated by Controlled-Potential Thin-Layer Coulometry. *Anal. Chem.* **2011,** *83* (2), 486-493.
14. Ghahraman Afshar, M.; Crespo, G. A.; Bakker, E., Coulometric Calcium Pump for Thin Layer Sample Titrations. *Anal. Chem.* **2015,** *87* (19), 10125-10130.
15. Zhang, J.; Harris, A. R.; Cattrall, R. W.; Bond, A. M., Voltammetric Ion-Selective Electrodes for the Selective Determination of Cations and Anions. *Anal. Chem.* **2010,** *82* (5), 1624-1633.
16. Jansod, S.; Wang, L.; Cuartero, M.; Bakker, E., Electrochemical ion transfer mediated by a lipophilic Os(ii)/Os(iii) dinonyl bipyridyl probe incorporated in thin film membranes. *Chem. Commun.* **2017,** *53* (78), 10757-10760.
17. Crespo, G. A.; Cuartero, M.; Bakker, E., Thin Layer Ionophore-Based Membrane for Multianalyte Ion Activity Detection. *Anal. Chem.* **2015,** *87* (15), 7729-7737.
18. Kim, Y.; Amemiya, S., Stripping Analysis of Nanomolar Perchlorate in Drinking Water with a Voltammetric Ion-Selective Electrode Based on Thin-Layer Liquid Membrane. *Anal. Chem.* **2008,** *80* (15), 6056-6065.
19. Xie, X.; Szilagyi, I.; Zhai, J.; Wang, L.; Bakker, E., Ion-Selective Optical Nanosensors Based on Solvatochromic Dyes of Different Lipophilicity: From Bulk Partitioning to Interfacial Accumulation. *ACS Sens.* **2016,** *1* (5), 516-520.
20. Xie, X.; Bakker, E., Ion selective optodes: from the bulk to the nanoscale. *Anal. Bioanal. Chem.* **2015,** *407* (14), 3899-3910.
21. Du, X.; Yang, L.; Hu, W.; Wang, R.; Zhai, J.; Xie, X., A Plasticizer-Free Miniaturized Optical Ion Sensing Platform with Ionophores and Silicon-Based Particles. *Anal. Chem.* **2018,** *90* (9), 5818-5824.
22. Xie, X.; Zhai, J.; Bakker, E., pH Independent Nano-Optode Sensors Based on Exhaustive Ion-Selective Nanospheres. *Anal. Chem.* **2014,** *86* (6), 2853-2856.
23. El-Safty, S. A.; Ismail, A. A.; Matsunaga, H.; Hanaoka, T.; Mizukami, F., Optical Nanoscale Pool-on-Surface Design for Control Sensing Recognition of Multiple Cations. *Adv. Funct. Mater.* **2008,** *18* (10), 1485-1500.
24. Stashkova, A. E.; Peshkova, M. A.; Mikhelson, K. N., Single-ion activity: Optical sensing vs. electrochemical sensing. *Sens. Actuator B-Chem.* **2015,** *207*, 346-350.
25. Chan, W. H.; Lee, A. W. M.; Kwong, D. W. J.; Tam, W. L.; Wang, K.-M., Potassium ion-selective optodes based on the calix[6]arene hexaester and application in human serum assay. *Analyst* **1996,** *121* (4), 531-534.
26. Xie, L.; Qin, Y.; Chen, H.-Y., Direct Fluorescent Measurement of Blood Potassium with Polymeric Optical Sensors Based on Upconverting Nanomaterials. *Anal. Chem.* **2013,** *85* (5), 2617-2622.
27. Pellerin, B. A.; Bergamaschi, B. A., Optical sensors for water quality. *Lakeline* **2014,** (Spring), 13-17.
28. Crespo, G. A.; Mistlberger, G.; Bakker, E., Electrogenerated Chemiluminescence for Potentiometric Sensors. *J. Am. Chem. Soc.* **2012,** *134* (1), 205-207.
29. Hupa, E.; Vanamo, U.; Bobacka, J., Novel Ion-to-Electron Transduction Principle for Solid-Contact ISEs. *Electroanalysis* **2015,** *27* (3), 591-594.
30. Vanamo, U.; Hupa, E.; Yrjänä, V.; Bobacka, J., New Signal Readout Principle for Solid-Contact Ion-Selective Electrodes. *Anal. Chem.* **2016,** *88* (8), 4369-4374.
31. Jarolímová, Z.; Han, T.; Mattinen, U.; Bobacka, J.; Bakker, E., Capacitive Model for Coulometric Readout of Ion-Selective Electrodes. *Anal. Chem.* **2018,** *90* (14), 8700-8707.
32. Jaworska, E.; Michalska, A.; Maksymiuk, K., Fluorimetric readout of ion-selective electrode potential changes. *Electrochim. Acta* **2018,** *284*, 321-327.
33. Jansod, S.; Cuartero, M.; Cherubini, T.; Bakker, E., Colorimetric Readout for Potentiometric Sensors with Closed Bipolar Electrodes. *Anal. Chem.* **2018,** *90* (11), 6376-6379.
34. Bakker, E.; Pretsch, E.; Bühlmann, P., Selectivity of Potentiometric Ion Sensors. *Anal. Chem.* **2000,** *72* (6), 1127-1133.
35. RECOMMENDATIONS FOR NOMENCLATURE OF ION-SELECTIVE ELECTRODES: (Recommendations 1975). In *Recommendations for Nomenclature of Ion-Selective Electrodes*, Pergamon: 1976; pp 129-132.
36. Zook, J. M.; Langmaier, J.; Lindner, E., Current-polarized ion-selective membranes: The influence of plasticizer and lipophilic background electrolyte on concentration profiles, resistance, and voltage transients. *Sens. Actuator B-Chem.* **2009,** *136* (2), 410-418.
37. Ghahraman Afshar, M.; Crespo, G. A.; Bakker, E., Direct Ion Speciation Analysis with Ion-Selective Membranes Operated in a Sequential Potentiometric/Time Resolved Chronopotentiometric Sensing Mode. *Anal. Chem.* **2012,** *84* (20), 8813-8821.
38. Erenas, M. M.; de Orbe-Payá, I.; Capitan-Vallvey, L. F., Surface Modified Thread-Based Microfluidic Analytical Device for Selective Potassium Analysis. *Anal. Chem.* **2016,** *88* (10), 5331-5337.

Chapter 5: Optical Sensing with a Potentiometric Sensing Array by Prussian Blue Film Integrated Closed Bipolar Electrodes

This work has been published in: Jansod, S.; Cherubini, T.; Soda, Y.; Bakker, E. *Anal. Chem.* **2020**. *92*, 9138-9145.

5.1 Abstract

The simultaneous optical readout of a potentiometric sensor array of ion-selective electrodes (ISEs) based on PVC membranes is described here for the first time. The optical array consists of electrochromic Prussian Blue (PB) films in multiple closed ion-selective bipolar electrodes (BPEs), which gives a physical separation between the optical detection and sample compartments. The potential-dependent turnover of PB generates Prussian White (PW). A near-Nernstian response of the PB film is confirmed by colorimetric absorbance experiments as a function of applied potential. In the combined bipolar electrode cell, the overall potential is kept constant with a single potentiostat over the entire array where each PB spot indicates the potential change of an individual connected potentiometric probe. For cation-selective electrodes, the absorbance or blue intensity of the connected PB film is enhanced with increasing target cation activity. The colorimetric absorbance changes are simultaneously followed by a digital camera and analyzed by Mathematica software. A multiple cation-BPE array allows one to achieve simultaneous quantitative analysis of potassium, sodium, and calcium ions, demonstrated here in highly colored fruit juices. Mass transport at the PB thin film is shown not to be rate-limiting. The measuring ranges can be tuned in a wide range by potential control. The PB film exhibits greatly improved reproducibility and stability as compared to previous work with a ferroin redox probe confined in a thin solution layer.

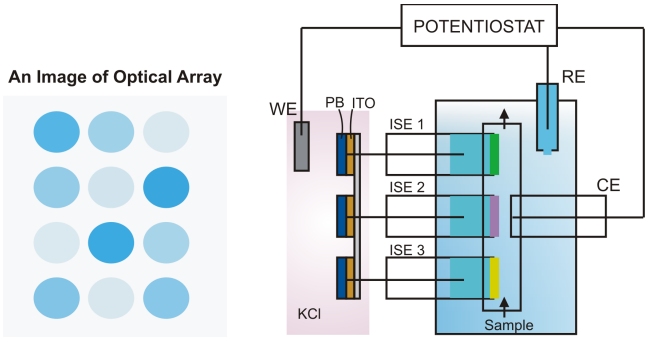

5.2 Introduction

Sensor arrays are used to simultaneously identify multiple target ions in complex mixtures.[1-3] They are particularly useful in clinical and environmental analysis, either for imaging or mapping one or more chemical species[4] or assessing multiple analytes.[5, 6]

Potentiometric sensors based on liquid or polymer membrane material such as ion-selective electrodes (ISEs) combine advantages of adequate selectivity, sensitivity, reproducibility and response time.[7-11] The selective membrane of ISEs is the key component that allows for the recognition of the target ion. Potentiometric sensor arrays have been used for multivariate analysis[12, 13] and are becoming important for the realization of *in situ* sensing tools.[14-16] Moreover, ISE arrays may be miniaturized for flow applications[17, 18] that may give a high sample throughput and allow for small sample volumes, for example in bioanalysis. In environmental analysis, potentiometric sensor arrays have been used in the quantitative analysis of pH, potassium, sodium, calcium, nitrate, carbonate, and ammonium. [15, 19, 20]

Array sensing platforms based on optical sensors have become important for the determination of multiple analytes, to assess near-complete chemical information for a given sample, and to achieve real-time chemical imaging.[21-24] However, traditional optical sensors may be negatively affected by turbid or colored samples, the working ranges are comparatively narrow and the detection of ions require extra-thermodynamic assumptions that are not always well understood or accepted. Such drawbacks may be overcome by coupling their output to a potentiometric probe using closed bipolar electrodes (BPEs) where the sample solution is physically separated from the site of the optical signal change.[25-27]

In this manner, potentiometric signals have been transduced to a series of different optical readouts. Such as electrochemiluminescence (ECL).[28] The potential change at the ISE is acted as the reference electrode in sample compartment. The working electrode activated the ECL output in detection solutions, when the constant potential was applied across the cell. In other work, the light output of multicolor light-emitting diodes (LEDs)[29] was coupled to the potentiometric responses of ISEs by chronoamperometry control. A fluorescence signal was also obtained from a solid-contact ISE containing polypyrrole as ion-to-electron transducing material and connected to a zinc element in the sample compartment.[30] An increasing ion activity triggered the reduction of the polypyrrole and resulted in the oxidation of zinc in another pole. This increased the emission intensity where the charge served as an analytical signal. Unfortunately, the emission obtained by the ECL, LEDs and florescence have some drawbacks such as (i) the detection must be controlled in the dark, (ii) specific instruments, reagents and materials tend to be costly, and (iii) they are not yet applicable for optical sensor array.

Alternatively, the water-soluble redox indicator ferroin was proposed to translate the potential change at the ISEs in the closed-BPEs.[31, 32] This general approach is promising for fabrication of large sensor array. The optical signal was captured by just a digital camera in ambitious light, where the ECL, LEDs and florescence were limited to the dark environment. However, the ferroin indicator requires a dedicated thin layer cell to reduce evaporation losses and allow for an exhaustive turnover in a reasonable amount of time. To overcome these drawbacks, an electrochromic thin film deposited on a conductive electrode surface may be instead used as the optical indicator.

Examples include tungsten oxide (WO_3),[33] polymeric viologen,[34, 35] conjugated conducting polymers such as PEDOT[36] and Prussian blue (PB).[37-40] These electrochromic materials may change their optical properties by a redox process and/or a suitable electrochemical potential.

PB (anodic form) is known as an important functional transition metal hexacyanoferrate with stable electrochemical redox behavior and excellent electrochromic properties, which make it a prominent candidate as electrochromic indicator.[41] The intense blue color of PB, iron(III) hexacyanoferrate(II) chromophore increases from intervalence charge transfer between the mixed-valence iron oxidation by the redox process.[42] The electrochemical reduction of PB produces Prussian White (PW) or iron(II) hexacyanoferrate(II), which becomes transparent as a thin film. The electrochemical deposition of PB films in aqueous solution onto conducting substrates was first described by Neff.[43] The films were prepared in a mixed solution of $FeCl_3$ and $K_3Fe(CN)_6$ in excess of KCl. High concentration of KCl accelerates the PB conversion process.[44]

In 2001, Lin's group used PB film deposited onto tin oxide electrode for directly measuring potassium ion using cyclic voltammetry. This PB film served as a mediator for potassium ion transfer. The voltammograms shifted with increasing potassium concentration, which resulted in a sub-Nernstian response slope.[45] In 2009, Toh's group used a PB nanotube sensor for potassium detection by using cyclic voltammetry. The peaks shifted with a near-Nernstian slope to anodic potentials with increasing potassium concentration.[46] More recently, Rieger's group used PB nanoparticles on a screen-printed carbon electrode covered by a sodium ion-selective membrane for sodium detection. However, this approach exhibited sub-Nernstian response with a limited working range.[47] No reports have used PB thin film as a redox indicator by coupling to potentiometric sensing probes in a bipolar electrode arrangement.

We describe here a closed multiple ion-selective BPE sensor array for the simultaneous detection of multiple analytes with working ranges that can be tuned by the applied potential. This approach demonstrates the translation of potentiometric responses based on ISEs into optical PB thin films. The multiple ion-selective BPEs array allows one to access all quantitative information from each individual BPE. The slopes obtained by the ISEs are near-Nernstian. The conversion of PB/PW is correlated in a Nernstian manner to the BPE response. In this way, colorimetric absorbance can be used to directly detect the concentration (activity) of the target ions.

5.3 Principle of operation

As demonstrated in Scheme 1, each ISE is individually coupled to one PB film in a bipolar arrangement. The cell potential is kept constant by a potentiostat. As the cation activity in the sample increases, it generates a more positive potentiometric signal at the ISE. This potential change must be compensated by an opposite change at the PB film, resulting in the partial oxidation of PW to PB to satisfy the Nernst equation. This results in an absorbance change of the PB film, which serves as analytical signal. Any number of parallel bipolar ISE-PB pairs may be inserted into the cell to give a convenient optical readout of sensing arrays.

The response to sample activity change is transient and ceases upon reaching each new electrochemical equilibrium state. During the transient and for an increasing sample activity change, the cation of interest is extracted and

transported across the ion-selective membrane (ISM in Scheme 1), thereby triggering the partial reduction of the Ag/AgCl element, which releases chloride into the inner solution to maintain charge balance. The electrons required for this reduction process originate from oxidation at the other end of the bipolar electrode, where PW partially converts to PB. To compensate, this releases potassium ions into the contacting solution. The Ag/AgCl elements placed in solution complete the circuit.

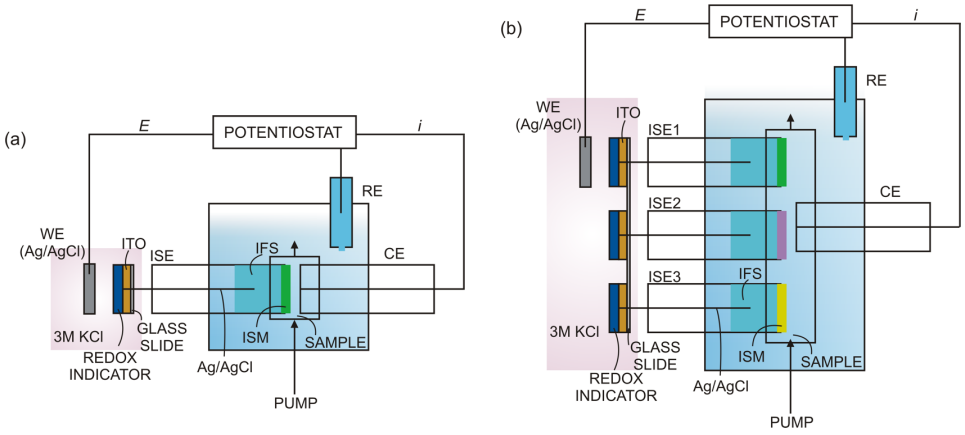

Scheme 1. Construction of ion-selective BPE(s), where the optical detection compartment is physically separated from the sample compartment. (a) Classical ion-selective BPE contains a single ISE, which couples to a PB film. (b) Multiple ion-selective BPEs sensor array contains multiple ISEs, which couple to multiple PB films. Each BPE is disconnected to each other. The potential is applied across a working electrode (WE) in detention compartment and counter (CE), a double junction reference electrodes (RE) in sample compartment.

Each closed bipolar electrode in the array is an ISE in contact with the sample and connected to a transparent electrode coated with an electrochromic Prussian Blue film in a separate detection cell. Scheme 1 (a) shows one such BPE where a single potentiometric probe is coupled to the PB thin film. Scheme 1 (b) then illustrates how multiple ion-selective BPEs sensor array can be likewise coupled to an array of PB thin films.

The electrochemical cell used for the detection of analyte ion *i* of valency z is of the type:

Ag | AgCl | 3M KCl | PB Film | ITO | Ag | AgCl | $i\mathrm{Cl}_z$(IFS) | ISE Membrane | $i\mathrm{Cl}_z$ (Sample) || 1M LiOAc | 3M KCl (aq) | AgCl | Ag

where PB functions as colorimetric redox probe; ITO is a indium tin oxide-based transparent electrode; IFS is the inner filling solution of the membrane electrode; ISE Membrane is the ion-selective membrane; and $i\mathrm{Cl}_z$ is the chloride salt of the analyte cation. In the absence of interference, the potential across the ion-selective membrane, E_M, is described as established by eq. 1.

$$E_M = \frac{s}{z_i} \log \frac{a_i^{sample}}{a_i^{ifs}} \qquad (1)$$

where s is the Nernstian slope for a monovalent cation, ideally 59.2 mV for 25 °C, and a_i is the activity of i in the sample or inner filling solution (IFS) on either side of the membrane, as indicated.

The detection compartment contains a PB film used as optical redox indicator, which changes its color from colorless (PW, reduced form) to blue (PB, oxidized form). The standard reduction potential of PB has been reported as 0.238 V vs. Ag/AgCl at 25 °C.[48] The corresponding half-reaction for PB may be given as:[49]

$$KFe^{III}[Fe^{II}(CN)_6]_{(film)} + K^+_{(aq)} + e^- \rightleftharpoons K_2Fe^{II}[Fe^{II}(CN)_6]_{(film)} \qquad (2)$$

(PB) (PW)

The reduction of PB is accompanied by the incorporation of potassium ion, making this system an ion to electron transducing material. While PB is a polymeric material, we may attempt to describe the potential of a mixed PW/PB film in contact with solution of constant potassium concentration in a Nernstian manner,[45] as shown in eq. 3.

$$E_{\text{detection}} = E^0_{PW/PB} - s \log \frac{c_{PW}}{c_{PB}} + s \log a_K^{aq} \qquad (3)$$

where C_{PW} and C_{PB} are the apparent film concentrations of PW and PB, respectively. If so, these concentrations may be expressed as a function of colorimetric absorbance based on Beer's law as shown in eq. 4. A_{max} and A_{PB} are the absorbances at maximum and at a given PB equilibrium state, respectively, see Supporting Information for the derivation of the equations.

$$E_{\text{detection}} = E^0_{PW/PB} - s \log \frac{A_{\max} - A_{PB}}{A_{PB}} + s \log a_K^{aq} \qquad (4)$$

In a closed-bipolar platform the redox indicating PB film is connected in series to the ISE. The overall potential of the cell (E_{cell}) is described by eq. 5 as:

$$E_{cell} = s \log \frac{A_{\max} - A_{PB}}{A_{PB}} + \frac{s}{z_i} \log a_i^{sample} + E_{const} \qquad (5)$$

Here, E_{cell} is imposed by the potentiostat and the absorbance ratio of PW/PB is a function of the sample activity a_i as shown. Consequently, the potential imposed as E_{cell} can be used to adapt the optical signal to the desired measuring range (see Supporting Information). The PB absorbance is then expressed as:

$$A_{PB} = A_{\max} \left(\frac{\psi}{a_i^{1/z_i}} + 1 \right)^{-1} \qquad (6)$$

with $$\psi = 10^{(E_{cell} - E_{const})/s} \qquad (7)$$

For a constant applied potential, E_{cell}, and a cation-selective electrode, an increasing cation activity in the sample results in a higher PB absorbance.

The absorbance may also be obtained by a digital camera, where the recorded images are analyzed in analogy to spectrophotometry.[50] Here, the PB absorbance is calculated by the acquired red channel image, see eq. 8 in the experimental section.

5.4 Experimental Section

Materials, reagents and instrumentation Potassium chloride (KCl), sodium chloride (NaCl), calcium chloride ($CaCl_2$), magnesium chloride ($MgCl_2$), hydrochloric acid (HCl), sodium hydroxide (NaOH, 1.0 N), potassium ionophore I, sodium ionophore X, calcium ionophore IV, poly(vinyl-chloride) (PVC, high molecular weight), dodecyl 2-nitrophenyl ether (DD-NPE), sodium tetrakis-[3,5-bis(trifluoromethyl)phenyl]borate (NaTFPB), tetradodecylammonium tetrakis(4-chlorophenyl)borate salt (ETH 500), tetrahydrofuran (THF), indium tin oxide (ITO glass slide 25mm×25mm×1.1mm, surface resistivity 1.28-1.92 $\Omega \cdot cm^{-2}$), iron(III) chloride hexahydrate ($FeCl_3.6H_2O$), potassium hexacyanoferrate(III) ($K_3[Fe(CN)_6]$), Whatmann qualitative filter paper grade 2 were purchased from Sigma-Aldrich. An insulating transparent Scotch 3M tape (50 μm thickness) and a metallic hole punch tool (0.8 mm diameter) were used. Ag electrode tip with a diameter of 3.00±0.05 mm (6.1204.330) was sourced from Metrohm (Switzerland). IPC ISMATEC peristaltic pump (Model ISM935C, Clattbrug, Switzerland), TYGON tubing (inner diameter 1.42 mm, wall 0.86 mm) and PTFE tubing (L × OD × ID = 300 mm × 1/16 × 100 μm, Supelco) were used in the flow system. The electrochemical measurements of cyclic voltammetry and chronoamperometry were performed in a faraday cage with a potentiostat/galvanostat PGSTAT 204 (Metrohm Autolab, Utrecht, The Netherlands) that was controlled by Nova 2.1.2 software. A tethered digital camera (Canon EOS 5D Mark II equipped with a MP-E 60mm macro lens and matching ring flash was used to capture the images from the detection cell. Real samples were purchased in Swiss local market. All aqueous solutions were prepared in Milli-Q water. The background electrolyte was 10 mM $MgCl_2$. A studio shooting tent box was purchased from PULUZ Technology Limited (Shenzhen, China).

Fabrication of patterned ITO array. A conductive ITO film coated glass electrode (25×25×1.1mm) was etched into 3 films or channels, as an example. To etch the master ITO film, the glass electrode was entirely covered by the tape. A tiny gap was exposed by a cutter. This exposed area was vanished by immersing in concentrated HCl for 10-20 min. The entire tape was removed. The patterned ITO array was rinsed many times by milli-Q water until there was no acid residues left on the electrode. Dry it in room temperature. The etched tiny gap was measured the surface resistivity by a digital ohmmeter. If these channels were disconnected or isolated from each other, the resistance value of this exposed area should not be found. The patterned ITO array contained three channels in the same glass, see a photograph in Supporting Information.

PB film deposition. 3 circular openings of 0.8 mm diameter were punched in a 50 μm thick adhesive insulating tape to form recesses. This tape was placed on the patterned ITO array. In the electrochemical cell, the ITO electrode acted as the working electrode, platinum rod was the counter electrode and Ag/AgCl wire was the reference electrode. The ITO electrode was immersed in the mixed solution of 20 mM $K_3Fe(CN)_6$, 20 mM $FeCl_3 \cdot 6H_20$ and 10 mM HCl. The PB film was deposited for 20-s by passing a cathodic current density of 2.0 A m^{-2} through the ITO electrode. Each channel was individually deposited, see the photograph of 3 PB electrodes in Supporting Information. The PB sensor array was washed by 10 mM HCl before use.

Stabilization of PB film. A PB electrode acted as a working electrode and the Ag/AgCl wire was the counter/reference electrodes. The PB was first stabilized by using cyclic voltammetry. All electrodes were immersed in 3 M KCl (pH 2, adjusted the pH by using HCl). The potential was reversibly applied between 0.4 and 0.2 V vs Ag/AgCl for 15 cycles

with a scan rate of 10 mV s^{-1} before using in the BPE. PB film was characterized by applying cathodic and anodic linear potential scans at a scan rate of 0.5 mV s^{-1}. The PB absorbance and the integrated charge were observed as a function of applied potential. The images were consecutively captured by the camera every 10 s. All images were computed the PB film from all residual pixels into absorbance with eq. 8.

PB film removal. The PB film deposited on the ITO electrode was effectively removed by rinsing with 10 mM NaOH followed with an abundance of milli-Q water. The ITO electrode was dried at room temperature before use.

Preparation of potentiometric sensing electrodes. A mixture of ionophore (15 mmol kg^{-1}), ion exchanger (5 mmol kg^{-1}), ETH 500 (90 mmol kg^{-1}), PVC and DD-NPE plasticizer (1:2 by weight; total mass 200 mg) was prepared for potentiometric sensing probe, as reported in our previous work.[32] The components were dissolved in 2 mL THF and poured into a glass ring (22 mm i.d.) fixed on a glass slide with rubber bands. The solution was evaporated overnight at room temperature. The homogenous master membrane was punched into disks of 8 mm diameter (200-300 µm thickness). The membranes were conditioned in 1 mM of primary ion for at least 3-4 hours. The membrane was mounted in an Ostec electrode body (Oesch Sensor Technology, Sargans, Switzerland). The inner filling solution (IFS) in the ISE for determination of potassium, sodium and calcium were filled with 1 mM KCl, 1mM NaCl and 1 mM $CaCl_2$, respectively.

Sample compartment. The potentiometric measurement of ISEs based PVC membranes were carried out against a commercial reference electrode (6.0729.100, Metrohm) with a double junction reference electrode (Ag | AgCl | KCl, 3 M | LiOAc, 1 M) in a faraday cage using a 16-channel EMF interface (Lawson Laboratories, Inc., Malvern, Pa). The K-ISE, Na-ISE, Ca-ISE and the Ag counter electrode were placed in the flow cell, separated by a narrow solution line, to which the ion is transported to the ISEs by a peristaltic pump through the inlet and waste to bulk solution through the outlet, see photograph of the flow cell in Supporting Information. The reference electrode was placed in the bulk solution in the beaker. All solutions were maintained in 10 mM $MgCl_2$. Real samples were filtered by filter paper before sampling to the sample cell.

Detection compartment. The PB array on the glass electrode was inserted in the detection cell, which contains 3 M KCl (pH 2). The image was captured in the white bright studio shooting tent at ISO 400, f/ 5.0, flash power 1/128. The camera was set in front of the tent. The optical signals were recorded with a tethered digital camera (Canon EOS 5D Mark II) equipped with a Canon MP-E 60 mm macro lens and a ring flash. Only the macro lens with the ring flash were in the tent. The camera captured all images in JPEG format, which were analyzed for absorbance. This involved in importing each image, automatic cropping for the detection compartment area, and computing the absorbance from red channel as shown in eq. 8.

Experimentally, the absorbance of the PB film, which serves as an optical redox indictor can be obtained by computing the color intensity by Mathematica software 11.1 (Wolfram Research). Consecutive images were captured by a digital camera. The colorimetric absorbance (A) for any of the three color channels, *R, G or B*, was determined as described recently.[50] For the red channel,

$$A(R) = -\frac{1}{\gamma} log \frac{I(R)}{I_0(R)} \qquad (8)$$

where $I(R)$ and $I_0(R)$ are the recorded red channel intensities of the PB film and the background, respectively. γ is the gamma correction (γ= 1/2) applied in camera to make the image output more realistic to the human eye. The observed absorbance (A) from the image was obtained after gamma correction as shown in eq 8.

Construction of ion-selective BPE. The optical PB electrode individually coupled to the ISE in the sample cell with the closed BPE configuration, as shown in Scheme 1. The potential is applied between the Ag/AgCl wire (WE) in detection cell and Ag counter electrode (CE), double junction reference electrodes (RE) in sample compartment, see a photograph in Supporting Information.

5.5 Results and Discussion

I) Characterization of PB Films. Figure S1 shows the cyclic voltammogram of the turnover of the PB thin film deposited on the ITO electrode in 3 M KCl (pH 2). The reduction potential of PB in 1 M KCl was found at 0.216 ±0.0006 V vs. Ag/AgCl. For the conditions used here, the charge of the PB film was found as 7.48 ±0.08 µC and 7.53 ±0.15 µC for the anodic and cathodic peaks, respectively. Figure S2 (Left) gives the typical Gaussian shape of the corresponding voltammetric waves at different scan rates upon electrochemical oxidation/reduction of the PB redox indicator. A thin layer behavior of the PB membrane was confirmed, as evidenced by the linear dependence of peak height current with scan rate. This indicates that mass transport is not rate-limiting under these conditions, see Figure S2 (Right). Figure S3a shows the corresponding change of integrated charge with different applied potentials, when anodic and cathodic potentials are applied by cyclic voltammetry to the detection cell only. This applied potential scan allows one to observe the PB absorbance change, as shown in Figure 1 (Left). The absorbance does increase with increasing integrated charge (Figure S3b) although a deviation from linear behavior is observed. The deviation was minimized by applying constant potential increments instead of a linear scan. Figure 1 (Right) demonstrates a near-Nernstian response (slope of 60.7 mV) of the optical redox indicator, in reasonable agreement with eq. 4.

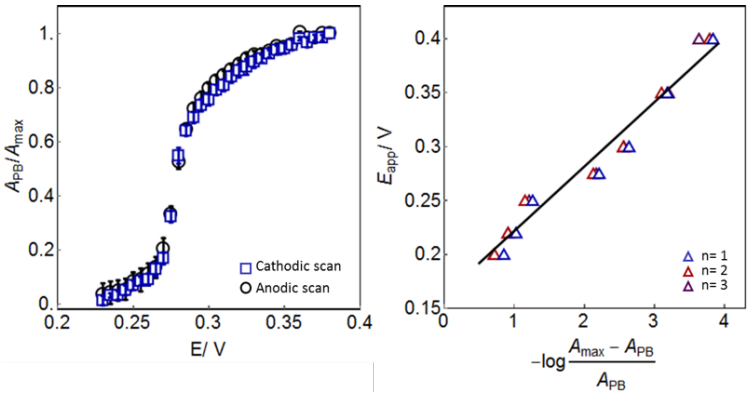

Figure 1. (Left) Absorbance with constant applied potential. The scan rate is 0.5 mV s^{-1}. (Right) Observed linear relationship between the discrete applied potentials and the logarithmic concentration ratio of PB/PW from colorimetric absorbance, demonstrating near-Nernstian behavior in reasonable agreement with eq. 4.

Figure 2 demonstrates the reproducibility and stability of the PB film when subjecting it to alternating potentials of 0.3 and 0.2 V, which resulted in corresponding red channel colorimetric absorbance values of 0.151 ±0.3% (translating into 2% uncertainty in activity determination by eq. 6) and 0.0183 ±0.1% (corresponding to a 5.9%

uncertainty in activity). The images were captured every 6 s. The response time was found as $t_{95\%}$ = 11 s. The absorbance change follows the potential change rapidly, in agreement with the absence of mass transport limitation noted above.

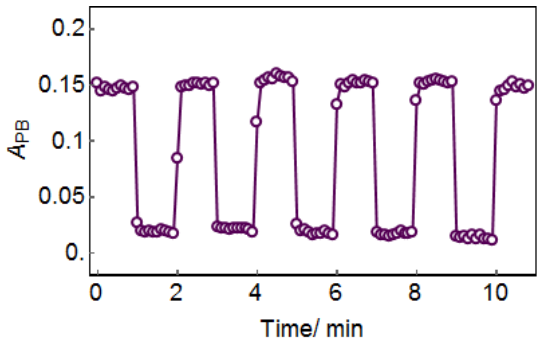

Figure 2. Corresponding PB absorbance changes in detection compartment. The constant potentials of 0.3 V and 0.2 V are imposed on the PB electrode in detection cell only. All electrodes are immersed in 3 M KCl (pH 2).

II) Characterization of the potentiometric sensor array flow cell. An array of three cation-selective electrodes (ISEs) was used in the sample compartment. All were ionophore-doped sensing membranes individually selective towards their target ion. The observed logarithmic selectivity coefficients for the prepared membranes have been reported earlier.[32] The flow cell was designed to accommodate numerous ISEs so that multiple analytes can be simultaneously measured in a selective manner. Figure S4 (Left) shows potentiometric calibration curves of the K-ISE, Na-ISE and Ca-ISE. These potentiometric probes were simultaneously characterized by open circuit potentiometry in mixed solutions containing the chloride salts of potassium, sodium, calcium, using magnesium salt as background electrolyte. The potentiometric probes were confirmed to exhibit near-Nernstian response slopes to the activities of potassium (58.6 ± 0.1 mV), sodium (58.0 ± 0.7 mV) and calcium (29.6 ± 0.6 mV). The corresponding potential-time traces (n=3) are shown in Figure S4 (Right).

The sample flow cell was confirmed to be free of solution carry-over by alternating the solution between 1 and 10 mM of KCl, NaCl and $CaCl_2$, see Figure S5 (Left). The peristaltic pump required about 60-s to replace each solution and to allow for the potentiometric signal to stabilize. Replicate measurements exhibited small deviations (maximum deviation was 0.6 mV, n=3), see Figure S5 (Right).

The conversion of the PB film triggered by the potential change at the corresponding potentiometric probe is accompanied by an electrical charge that passes through the cell. To evaluate its effect on the potentiometric probe, the same charge (7.5 µC) was applied to the potentiometric probe individually by imposing 0.25 µA for 30-s to the Na-ISE. The electrochemical perturbation resulted in a brief potential excursion of 17 mV before returning to the new equilibrium state within 2 min, see Figure S6. This suggests that the optical readout of the PB film accurately reflects the potential change at the ISE after stabilization, once the transient current is again near zero.

III) Characterization of a closed BPE containing a single ISE. For an ion-selective bipolar electrode, the PB spot indicates the potential change of its individual, connected potentiometric probe. A sample activity change at the ISE results in a well-defined potential change (EMF). Here, E_{cell} is maintained to a constant value, and the

potential change at the ISE is compensated by an opposite potential change of equal amplitude at the PB film-coated ITO electrode. At an appropriate applied potential value, this results in an absorbance change of the PB film until the new electrochemical equilibrium state is reached. The colorimetric absorbance was captured by a camera and analyzed with eq. 8.

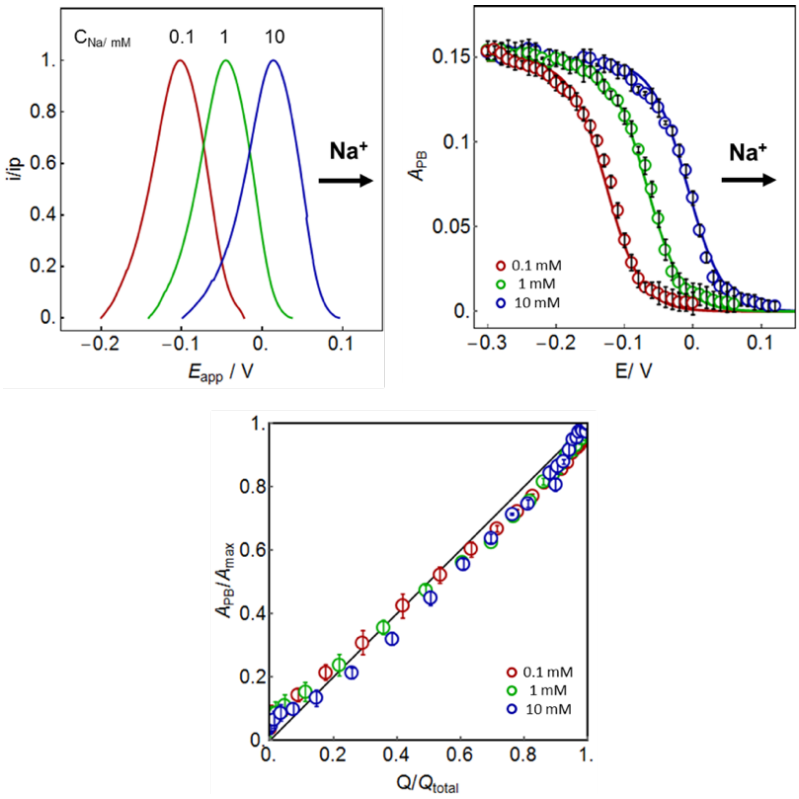

Figure 3. (a) Normalized current responses of the classical Na-BPE. The scan rate is 1 mV s^{-1}. (b) Observed absorbance in the detection compartment at each applied potential and with the increase sodium concentrations of 0.1, 1 and 10 mM NaCl in sample compartment. The calibration curves are simulated by using eq. 6. (c) A linear relationship between the PB absorbance and PB charge in Na-BPE. Error bars are standard deviations (n=3).

Figure 3a shows the normalized current responses of a Na^+-selective BPE with a 10-fold increase in sample concentration. The bell-shape current response demonstrates that the current is limited by the conversion of PW/PB. The peak shifts to a more anodic potential with increasing sodium activity (slope of 59.2 mV per 10-fold sodium activity change in sample compartment). Figure 3b demonstrates the corresponding absorbance change and confirms the potential modulation at the detection cell by the ion-selective probe. The sigmodal calibration curves are described by eq. 6. The absorbance change of redox indicator PB correlates linearly with the charge passed through the cell, see Figure 3c.

The corresponding current responses for K^+-selective and Ca^{2+}-selective BPEs are shown in Figure S7 (Top). The peak is found to shift by 61.6 and 32.0 mV per 10-fold potassium and calcium activity change, respectively, which agrees with the Nernstian slope. The absorbance-based calibration curves shift in the same manner to more anodic potentials with increasing ion activity in the sample, Figure S7 (Bottom). This anodic shift demonstrates that the measuring range of the optical PB indicator can be electrochemically tuned.

IV) Characterization of the closed BPE array. Cation-selective electrodes for K^+, Na^+ and Ca^{2+} were combined to a BPE sensor array as schematically shown in Scheme 1b.

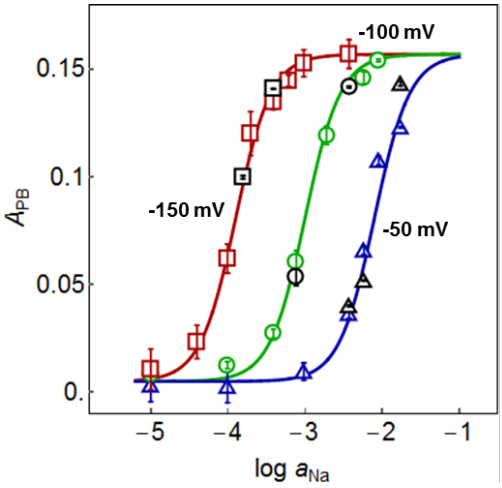

Figure 4. PB absorbance and logarithmic sodium activity of Na-BPE in classical BPE (colored symbols) and multiple BPE array (black symbols) at three different constant applied potentials. The sigmodal calibration curves are fitted by using Boltzmann equation.

Figure 4 shows the resulting absorbance-based calibration curves for Na-BPE in a single configuration (colored symbols) and multiple electrode array (black symbols), using applied potentials of -150, -100 and -50 mV for the three calibration curves as shown. No discrepancy for the observed absorbance values in single and multiple electrode configuration was observed, which suggested a lack of cross-talk between the three bipolar electrodes. For best analytical results, the absorbance-based calibration curves are here fitted sigmoidals based on the Boltzmann equation.[51] The corresponding calibration curves of the K-BPE (Figure S8, Left) and Ca-BPE (Figure S8, Right) in both single and BPEs array configuration are shown in the Supporting Information. In all cases, the PB absorbance values correspond well to the fitted calibration curves, which suggested that a single image of the PB array can be used to assess multiple cations in the sample.

The stability and reproducibility of the BPE was characterized by altering the applied potential values. Figure S9 shows the reversibility of the PB electrode in the bipolar arrangement by switching the applied potential between -120 mV and -150 mV in the Na-BPE, with the sample cell containing 0.1 mM NaCl. This resulted in an absorbance change between 0.038 ±0.05% (1.4% uncertainty in activity) and 0.095 ±0.1% (1% uncertainty in activity), respectively. In the BPE arrangement, the optical signal responds more slowly than for the detection cell only ($t_{95\%}$ = 65 s, compare with Figure 2). This slower equilibration is explained with the transient potential at the ion-selective electrode upon the passage of current, see above. This does not influence the final absorbance, as the analysis is performed after electrochemical equilibrium is established where the current again approaches zero.

V) Selectivity in multiple BPEs array. In the BPE array, the cations of interest are simultaneously determined in mixtures of KCl, NaCl and $CaCl_2$. The selectivity coefficients of the ISEs have been reported in our previous work,[32] so here each individual BPE in the sensor array was analyzed to ensure that the optical response of each channel remains selective to its associated target ion.

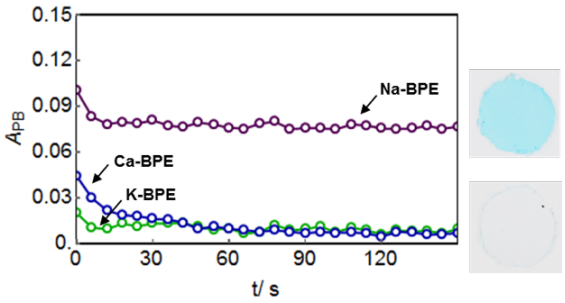

Figure 5. Absorbance values of Na-BPE (purple), K-BPE (green) and Ca-BPE (blue) are changed, when a constant potential of -100 mV is imposed in multiple BPEs array. The sample solution contains only 1 mM NaCl.

Figure 5 traces the absorbance values of three different channels in the multiple cation-BPE array containing the three ISEs selective for Na^+, K^+ and Ca^{2+} with an applied potential of -100 mV. The introduction of 1 mM NaCl into the sample cell results in a higher PB absorbance only for the Na-BPE, while remaining unchanged at the K^+ and Ca^{2+}-BPEs. Similarly, higher PB absorbance was only observed for the K-BPE (Figure S10, Left) and Ca-BPE (Figure S10, Right), when the sample contained only 1 mM KCl and 1 mM $CaCl_2$, respectively. Figure S11 show the corresponding images of the PB spots in the detection compartment. This experiment confirms that each individual BPE in the BPE array is highly selective toward its target ion.

VI) Analysis of real-world samples by the cation-BPE array. The cation-selective BPE array was used to simultaneously determine the concentrations of potassium, sodium and calcium ions in colored juice samples, including orange, grape, multifruit and coconut juices. Different constant potentials were applied to the cation-selective BPE array in order to obtain appropriate absorbance changes that reflect the dynamic range for the samples. When an applied potential of -100 mV was imposed to the BPE array, the PB absorbance for the Na-BPE and K-BPE was found to change, allowing ones to simultaneously measure the sodium content in grape and multifruit juices and the potassium level in coconut juice. When a constant potential of -50 mV was imposed, the K-BPE could be used to assay potassium in orange, grape and multifruit juices and sodium in coconut juice by the Na-BPE. With a more cathodic potential of -150 mV the PB absorbance changed for the Na-BPE in orange juice. Calcium ions for all samples were measured by applying a potential of -170 mV.

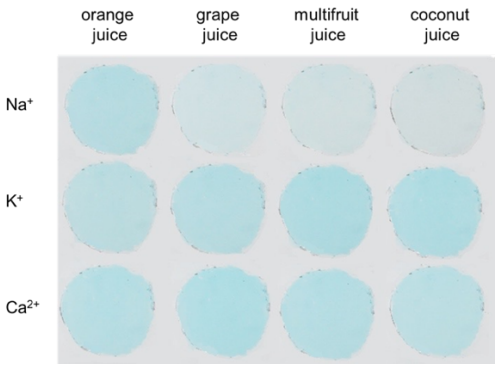

Figure 6. Images of the colorimetric sensor array acquired in the detection compartment for different samples coupled to their respective cation-selective BPEs. For this experiment, different constant potentials are imposed and the absorbance values correlating to sodium, potassium and calcium concentration are compared to the respective calibration curves as shown in Figure S12.

The corresponding images captured in the detection compartment are shown in Figure 6. The absorbance values for sodium, potassium and calcium are plotted on the sigmodal calibration curves at the corresponding applied potential, as shown in Figure S12. The observed absorbance is converted to the predicted concentration as shown in Table 1. The results correlate well with those from direct potentiometry, used here as reference method.

The ISE exhibits great stability and reproducibility and it can be stored for at least 30 days.[32] The PB film also shows good reproducibility and can be used for at least 85 cycles (Figure S13) The PB deposited on the ITO electrode can be easily disposed of by rinsing with 10 mM NaOH. The ITO electrode can be reused again for the new PB film deposition.

Table 1. Determination of sodium, potassium and calcium concentration (mM) in various juices using the multiple cation-selective BPE array (SD, n=3). Potentiometry is used as a reference method.

Samples	**Na / mM**	**K / mM**	**Ca / mM**
orange juice: BPE	0.85 ±0.09	43.0 ±0.8	4.09 ±0.09
potentiometry	0.86 ±0.00$_2$	45.7 ±0.02	4.4 ±0.2
grape juice: BPE	2.96 ±0.05	29.6 ±1.8	5.28 ±0.08
potentiometry	2.9 ±0.2	28.9 ±0.0$_1$	5.7$_4$ ±0.2$_5$
Multifruit juice: BPE	2.34 ±0.05	48.7 ±1.4	4.3 ±0.2
potentiometry	2.1 ±0.3	45.5 ±0.3	4.3 ±0.0$_5$
coconut juice: BPE	14.7 ±0.4	8.1$_5$ ±0.1	3.43 ±0.09
potentiometry	14.8 ±0.6	8.03 ±0.04	3.40 ±0.00$_4$

5.6 Conclusions

A cation-selective bipolar electrode array was successfully fabricated for the simultaneous determination of multiple cations using Prussian Blue thin films for optical readout. The work combines principles of potentiometric and optical sensors and may form the basis for new avenues in ion sensing. The approach described here makes it possible to realize optical sensors that respond in analogy to potentiometric sensing probes, with the same assumptions and the possibility for cross-correlation and traceability. The optical readout is achieved away from the sample, and does not suffer from optical interference. Consequently, colored fruit juices were chosen as examples and were adequately assessed. The technology also offers advantages over established potentiometric sensors. Any number of PB-ISE bipolar electrodes can be inserted in parallel without increasing instrumental complexity. The readout is optical and can be achieved with a convenient imaging device. Potentiometric sensing arrays require complex individual wiring or light addressability to achieve this. Last, this work forms the foundation to achieve self-powered sensing devices where the optical signal is directly generated from the potential change at

the ion-selective electrode, without the need for additional electronics or power sources, conceptually related to a recent example demonstrated by Rho et al.[52] This is currently in progress in our laboratory.

5.7 Acknowledgements

The authors thank the Swiss National Science Foundation (SNSF) for financial support. SJ special thanks the Swiss Government Excellence Fellowship in support for her doctoral studies.

5.8 Supporting Information

Theory of ion-selective bipolar electrode

The redox indicator film, Prussian blue (PB)/Prussian white (PW) deposited onto a transparent ITO electrode is connected in series to the ion-selective electrode (ISE) in the sample compartment in a closed bipolar configuration, as shown below. Each element is labeled by a number in red color.

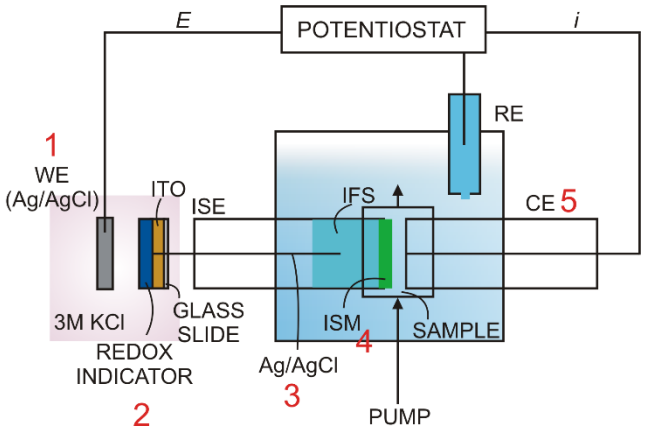

1 Working electrode connection, Ag/AgCl element in contact with detection compartment:

$$E_{AgCl/Cl} = E^{0}_{AgCl/Ag} - s \log a^{\text{det}}_{Cl} \qquad \text{(S1)}$$

2 Potential at PB film on the ITO electrode:

$$E_{\text{detection}} = E^{0}_{PW/PB} - s \log \frac{c_{PW}}{c_{PB}} + s \log a^{\text{det}}_{K} \qquad \text{(S2)}$$

or, after inserting the apparent mass balance equation for Prussian Blue :

$$E_{\text{detection}} = E^{0}_{PW/PB} - s \log \frac{c_T - c_{PB}}{c_{PB}} + s \log a^{\text{det}}_{K} \quad ; \; c_{PW} = c_T - c_{PB} \qquad \text{(S3)}$$

where c_T is the total film concentration. To approximately express the concentration in terms of absorbance based on Beer's law:

$$A_{\max} = \varepsilon_{PB} \cdot c_T \cdot l \qquad \text{(S4)}$$

$$A_{PB} = \varepsilon_{PB} \cdot c_{PB} \cdot l \qquad \text{(S5)}$$

Equations S4 and S5 are inserted into eq S3 to obtain:

$$E_{\text{detection}} = E^{0}_{PW/PB} - s\log\frac{A_{\max} - A_{PB}}{A_{PB}} + s\log a_K^{\text{det}} \quad \text{(S6)}$$

3 Potential at Ag/AgCl element in the inner solution of the ISE:

$$E^{'}_{AgCl/Cl} = E^{0'}_{AgCl/Ag} - s\log a_{Cl}^{ifs} \quad \text{(S7)}$$

4 Membrane potential at the ISE:

$$E_M = \frac{s}{z_i}\log\frac{a_i^{sample}}{a_i^{ifs}} \quad \text{(S8)}$$

5 Ag/AgCl element of the reference electrode, in contact with the reference solution (ref):

$$E^{''}_{AgCl/Cl} = E^{0''}_{AgCl/Ag} - s\log a_{Cl}^{ref} + E_J \quad \text{(S9)}$$

where EJ is the liquid junction potential.

When a constant applied potential is imposed in the bipolar electrode cell, the elements described above are combined together as follows:

$$E_{cell} = (1) - (2) + (3) + (4) - (5)$$

Specifically,

$$E_{cell} = E^{0}_{AgCl/Ag} - E^{0}_{PW/PB} - s\log\left(a_{Cl}^{\text{det}} a_K^{\text{det}} \frac{a_{Cl}^{ifs}}{a_{Cl}^{ref}}\right) + s\log\frac{A_{\max} - A_{PB}}{A_{PB}} + \frac{s}{z_i}\log\frac{a_i^{sample}}{a_i^{ifs}} - E_J \quad \text{(S10)}$$

or, simplified:

$$E_{cell} = E_{\text{const}} + s\log\frac{A_{\max} - A_{PB}}{A_{PB}} + \frac{s}{z_i}\log a_i^{sample} \quad \text{(S11)}$$

This equation is rewritten as follows to express the absorbance change as a function of sample activity:

$$\frac{A_{\max} - A_{PB}}{A_{PB}} = (a_i^{sample})^{-1/z_i}\cdot\psi \text{ with } \psi = 10^{\frac{E_{cell} - E_{const}}{s}} \quad \text{(S12)}$$

The Prussian Blue film absorbance is given by solving eq S12 as follows:

$$A_{PB} = A_{\max}\left(\frac{\psi}{a_i^{1/z_i}} + 1\right)^{-1} \quad \text{(S13)}$$

Photograph of experimental setup

The closed bipolar electrode sensor array contains two separate compartments. One is the detection compartment and the other is the sample compartment. Ion-selective electrodes (ISEs) are in contact with the sample compartment and connected to the PB electrodes in the detection compartment, as shown in the photograph below. The detection compartment contains 3 M KCl into which the PB electrodes are immersed. In the bipolar configuration, a constant potential is imposed in the bipolar cell between the working electrode (Ag/AgCl wire) in detection compartment and Ag electrode (CE) in sample compartment, where the double junction reference electrode (RE) is in a bulk solution in sample compartment. The camera is placed in front of the detection compartment to record consecutive images.

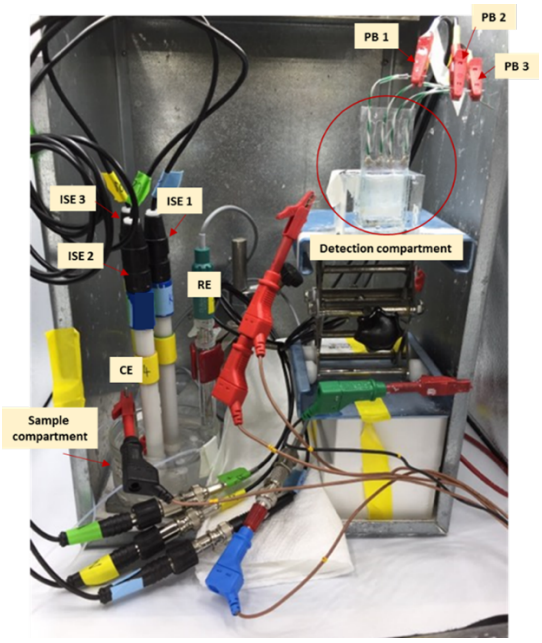

Schematic illustration

This scheme shows the connection between each individual ISE and the PB electrode in a closed bipolar sensor array configuration.

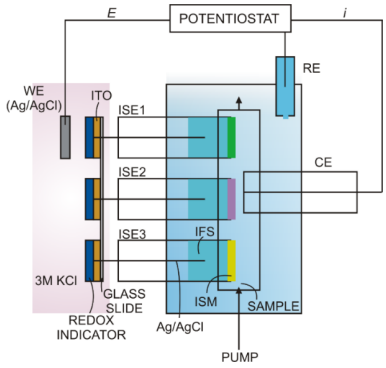

Flow cell in the sample compartment for inserting numerous ISEs

The flow cell contains openings for inserting three ion-selective electrodes as labeled with ISE 1, ISE 2 and ISE 3 (Ostec electrode bodies). Visible are the inlet and outlet holes, by which the sample is guided into and out to the bulk solution by peristaltic pumping. An Ag electrode is inserted into the flow cell at CE to serve as a counter electrode. The reference electrode is placed just outside the outlet in a beaker filled with electrolyte solution.

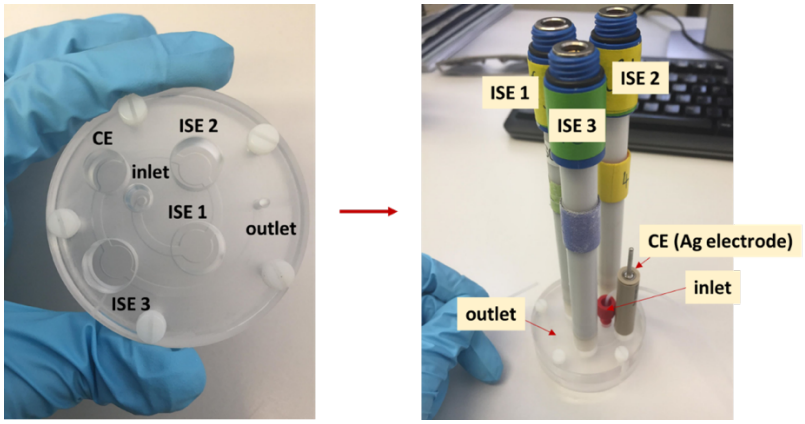

Fabrication of patterned PB array

The conductive ITO film coated glass slide (25×25×1.1mm) is etched into 3 channels as an example. The entire ITO glass surface was first covered by insulating tape. To remove the ITO film, the tape was cut by a cutter. The exposed ITO film was removed by immersing in concentrated HCl for 10-20 minutes. Complete removal was confirmed by measuring with an Ohmmeter, confirming insulation. In this design there are three ITO electrodes on the same glass slide.

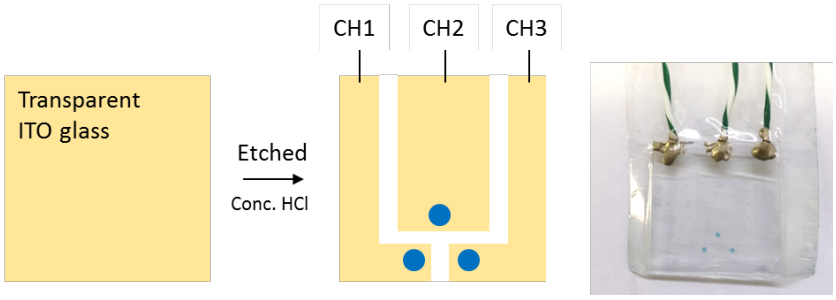

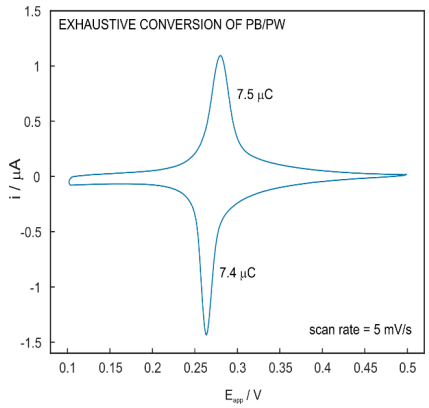

Figure S1. Cyclic voltammogram of the PB electrode in 3 M KCl (pH 2). The scan rate is 5 mV s^{-1}. An Ag/AgCl element is used as the reference/counter electrode.

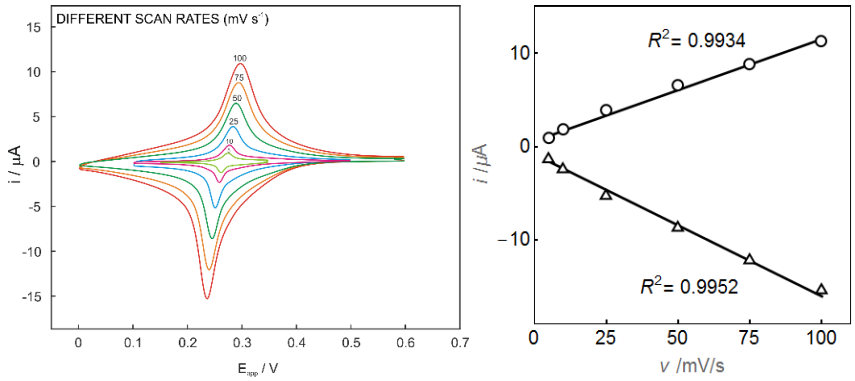

Figure S2. (Left) Cyclic voltammogram of PB electrode in a solution of 3 M KCl (pH 2) at different scan rates. (Right) Linear relationship between peak height and scan rate for the PB film.

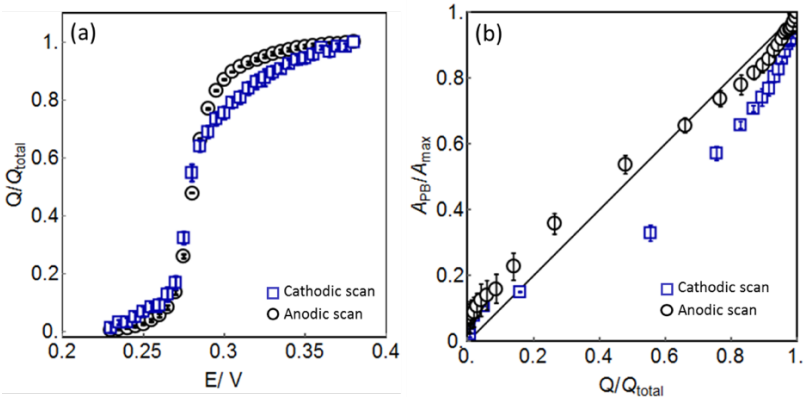

Figure S3. Anodic and cathodic potentials are imposed (scan rate of 0.5 mV s^{-1}) to the PB electrode in the detection cell only. (a) Integrated charge of PB film observed for different applied potentials. (b) The relationship of PB absorbance with integrated PB charge.

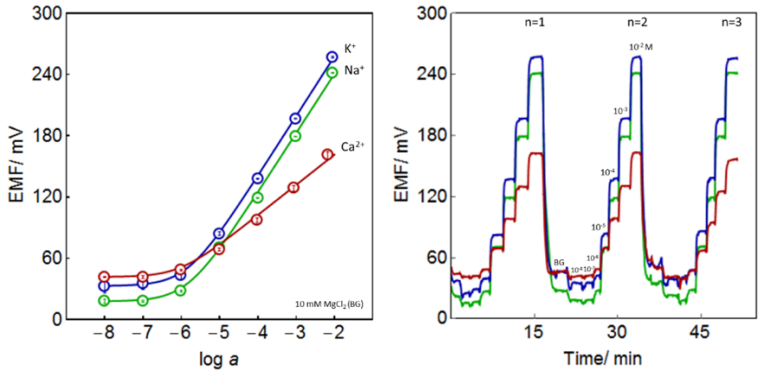

Figure S4. (Left) Calibration curves of three different potentiometric probes based on the liquid PVC membranes in the flow cell. (Right) Observation of potentiometric time traces (n=3) upon simultaneously changes of K+ (blue), Na+ (green) and Ca2+ (red) concentrations.

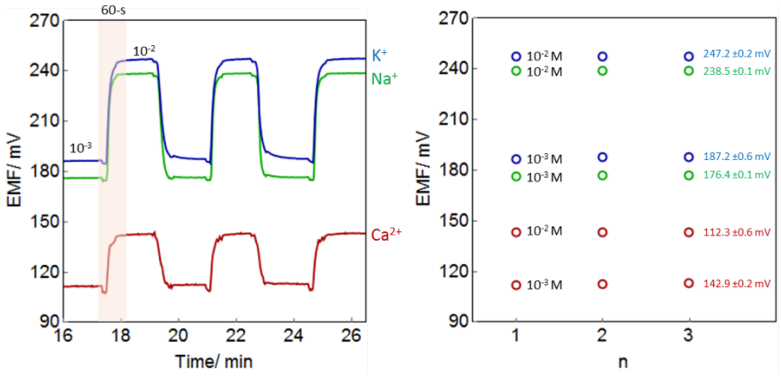

Figure S5. (Left) Reproducibility of potential-time trace of K-ISE, Na-ISE and Ca-ISE in the sample compartment at high concentrations between 1 and 10 mM of the KCl (blue), NaCl (green) and $CaCl_2$ (red). (Right) Corresponding EMF values of K-ISE, Na-ISE and Ca-ISE (n=3) at each concentration.

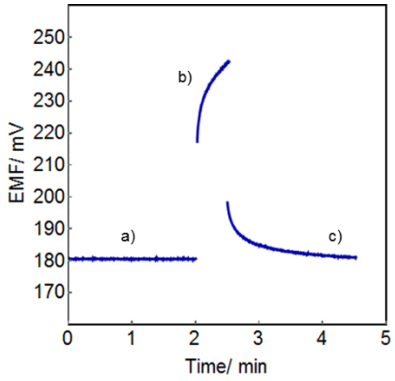

Figure S6. Electrochemical perturbation only at Na-ISE probe containing 1 mM NaCl in sample compartment. A constant current amplitude of 0.25 µA for a period of 30-s or 7.5 µC is imposed. The potential (OCP) readout; a) before perturbation, b) during perturbation and c) after perturbation are observed.

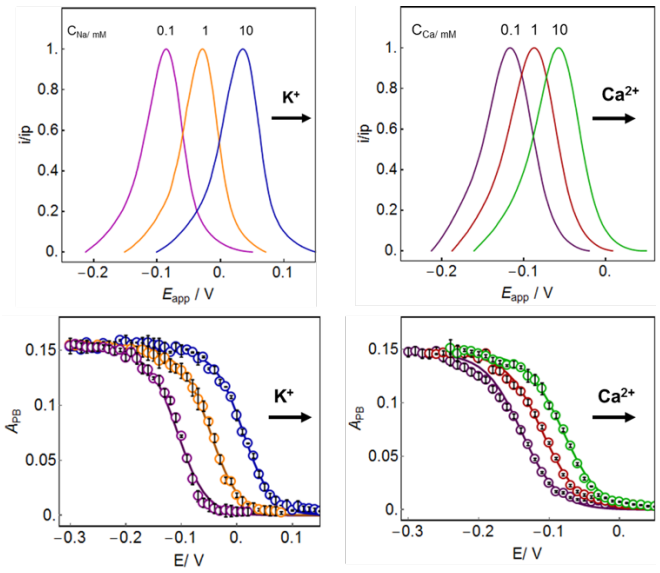

Figure S7. (Top) Normalized current responses of the classical BPE of (Left) K^+-selective BPE, and (Right) Ca^{2+}-selective BPE. The scan rate is 1 mV s^{-1}. (Bottom) Corresponding absorbance changes in the detection compartment at each applied potential and with increasing concentration in sample compartment. Error bars are standard deviations (n=3). The absorbance calibration curves are fitted with eq 6.

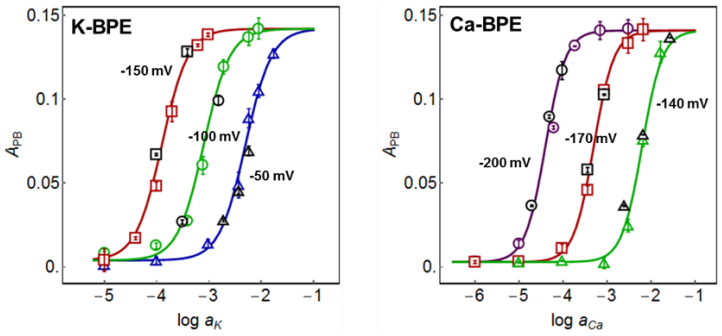

Figure S8. A relationship between absorbance and logarithmic ion activities of (Left) K-BPE and (Right) Ca-BPE in classical (colored symbols) and multiple BPEs (black symbols) platforms at three different constant applied potentials. The sigmoidal curves are calculated with the Boltzmann equation.

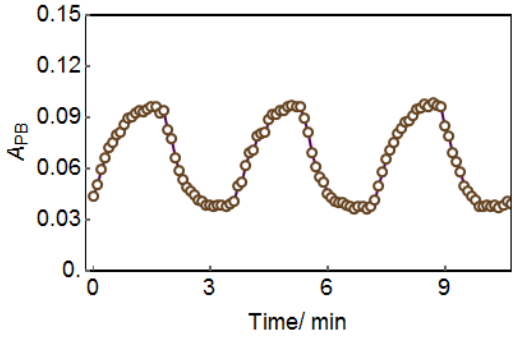

Figure S9. Colorimetric reproducibility of a Prussian Blue film responding to a Na-BPE. Different applied potentials of -150 and -120 mV are imposed with 0.1 mM NaCl in the sample compartment.

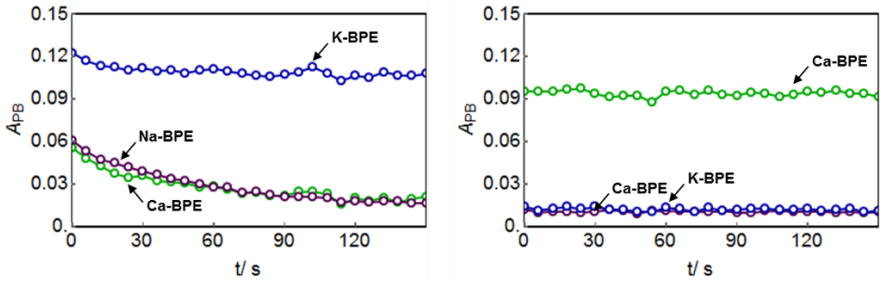

Figure S10. Selectivity of K-BPE (Left) and Ca-BPE (Right) in the BPE sensor array. (Left) A constant potential of -100 mV is imposed to the cell, where the sample contains only 1 mM KCl. (Right) A constant potential of -170 mV is imposed, where the sample contains only 1 mM $CaCl_2$.

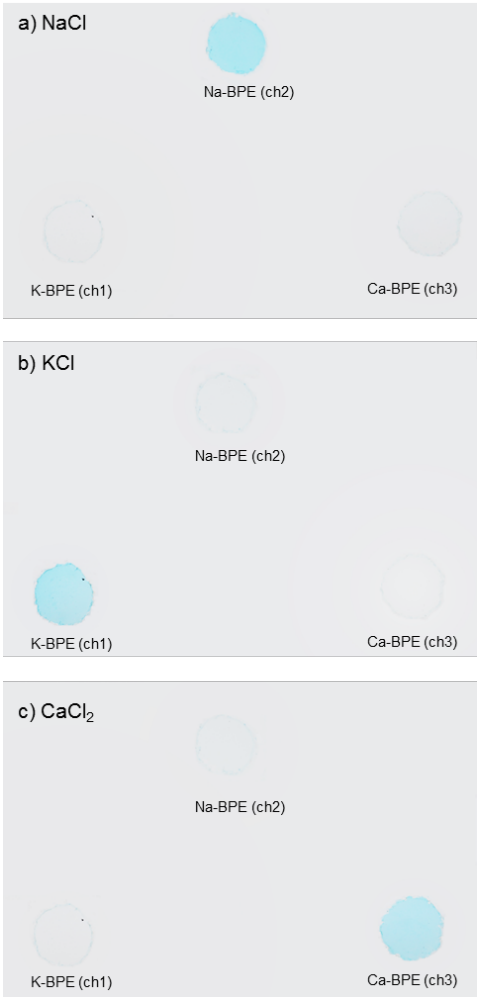

Figure S11. Photographs of the multiple cation-selective BPEs array composed of K-BPE (ch1), Na-BPE (ch2) and Ca-BPE (ch3). The absorbance values are observed at a fixed potential, at which the sample solution contains only (a) 1 mM NaCl (E_{app}= -100 mV), (b) 1 mM KCl (E_{app}= -100 mV) and (c) 1 mM $CaCl_2$ (E_{app}= -170 mV).

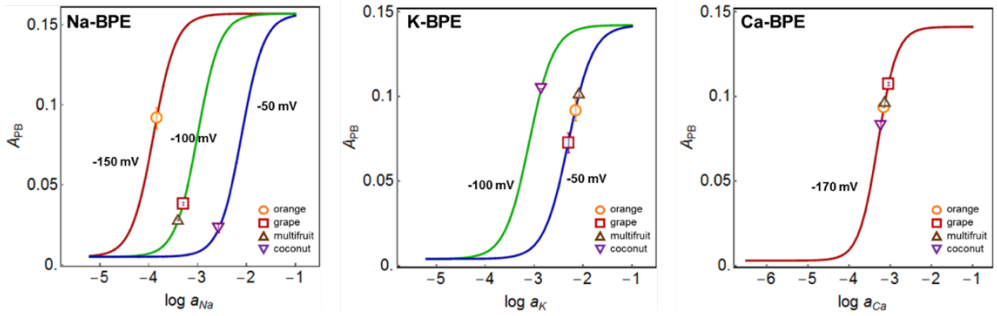

Figure S12. Observed colorimetric PB absorbances that are plotted on the calibration curves for Na-BPE, K-BPE and Ca-BPE. Quantitative analysis of sodium (left), potassium (middle) and calcium (right) contents in real-world samples are shown using the multiple cation selective BPEs sensor array.

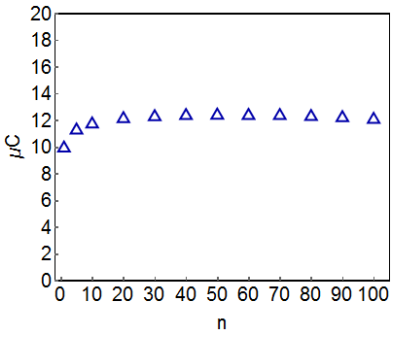

Figure S13. The integrated charge of PB film (anodic peak) with increasing number of cycles, as indicated. The PB film was deposited for 30-s by passing a cathodic current density of 2.0 A m^{-2} through the ITO electrode. For this experiment, the film is in contact with 3 M KCl (pH 2). The potential is applied through the PB electrode by alternating between 0.4 and 0.2 V vs Ag/AgCl.

5.9 References

1. Zheng, G.; Patolsky, F.; Cui, Y.; Wang, W. U.; Lieber, C. M., Multiplexed electrical detection of cancer markers with nanowire sensor arrays. *Nat. Biotechnol.* **2005,** *23* (10), 1294-1301.
2. Gao, W.; Emaminejad, S.; Nyein, H. Y. Y.; Challa, S.; Chen, K.; Peck, A.; Fahad, H. M.; Ota, H.; Shiraki, H.; Kiriya, D.; Lien, D.-H.; Brooks, G. A.; Davis, R. W.; Javey, A., Fully integrated wearable sensor arrays for multiplexed in situ perspiration analysis. *Nature* **2016,** *529* (7587), 509-514.
3. Albert, K. J.; Lewis, N. S.; Schauer, C. L.; Sotzing, G. A.; Stitzel, S. E.; Vaid, T. P.; Walt, D. R., Cross-Reactive Chemical Sensor Arrays. *Chem. Rev.* **2000,** *100* (7), 2595-2626.
4. Martinez-Olmos, A.; Capel-Cuevas, S.; López-Ruiz, N.; Palma, A. J.; de Orbe, I.; Capitán-Vallvey, L. F., Sensor array-based optical portable instrument for determination of pH. *Sens. Actuators B Chem.* **2011,** *156* (2), 840-848.
5. Lapresta-Fernández, A.; Capitán-Vallvey, L. F., Environmental monitoring using a conventional photographic digital camera for multianalyte disposable optical sensors. *Anal. Chim. Acta* **2011,** *706* (2), 328-337.
6. Lapresta-Fernández, A.; Huertas, R.; Melgosa, M.; Capitán-Vallvey, L. F., Multianalyte imaging in one-shot format sensors for natural waters. *Anal. Chim. Acta* **2009,** *636* (2), 210-217.
7. Bakker, E.; Pretsch, E., Modern Potentiometry. *Angew. Chem. Int. Ed.* **2007,** *46* (30), 5660-5668.
8. Zdrachek, E.; Bakker, E., Potentiometric Sensing. *Anal. Chem.* **2019,** *91* (1), 2-26.
9. Alexander, P. W.; Dimitrakopoulos, T.; Hibbert, D. B., A Six Sensor Array of Coated-Wire Electrodes for Use in a Portable Flow Injection Analyzer. *Electroanalysis* **1998,** *10* (10), 707-712.
10. Mourzina, Y. G.; Schubert, J.; Zander, W.; Legin, A.; Vlasov, Y. G.; Lüth, H.; Schöning, M. J., Development of multisensor systems based on chalcogenide thin film chemical sensors for the simultaneous multicomponent analysis of metal ions in complex solutions. *Electrochim. Acta* **2001,** *47* (1), 251-258.
11. Rudnitskaya, A.; Ehlert, A.; Legin, A.; Vlasov, Y.; Büttgenbach, S., Multisensor system on the basis of an array of non-specific chemical sensors and artificial neural networks for determination of inorganic pollutants in a model groundwater. *Talanta* **2001,** *55* (2), 425-431.
12. Bratov, A.; Abramova, N.; Ipatov, A., Recent trends in potentiometric sensor arrays—A review. *Anal. Chim. Acta* **2010,** *678* (2), 149-159.
13. Dimitrakopoulos, T.; Alexander, P. W.; Hibbert, D. B., A serial array of ISEs for use in a portable battery-powered flow injection analyzer. *Electroanalysis* **1996,** *8* (5), 438-442.
14. Mueller, A. V.; Hemond, H. F., Extended artificial neural networks: Incorporation of a priori chemical knowledge enables use of ion selective electrodes for in-situ measurement of ions at environmentally relevant levels. *Talanta* **2013,** *117*, 112-118.
15. Pankratova, N.; Crespo, G. A.; Afshar, M. G.; Crespi, M. C.; Jeanneret, S.; Cherubini, T.; Tercier-Waeber, M.-L.; Pomati, F.; Bakker, E., Potentiometric sensing array for monitoring aquatic systems. *Environ. Sci.: Process. Impacts* **2015,** *17* (5), 906-914.
16. Le Goff, T.; Braven, J.; Ebdon, L.; Chilcott, N. P.; Scholefield, D.; Wood, J. W., An accurate and stable nitrate-selective electrode for the in situ determination of nitrate in agricultural drainage waters. *Analyst* **2002,** *127* (4), 507-511.
17. Martínez-Barrachina, S. l.; del Valle, M.; Matia, L.; Prats, R.; Alonso, J., Potentiometric flow injection system for the determination of polyethoxylate nonionic surfactants using tubular ion-selective electrodes. *Anal. Chim. Acta* **2001,** *438* (1), 305-313.
18. Di Benedetto, L. T.; Dimitrakopoulos, T., Evaluation of a new wall-jet flow-through cell for commercial ion-selective electrodes in flow injection potentiometry. *Electroanalysis* **1997,** *9* (2), 179-182.
19. Gutiérrez, M.; Alegret, S.; del Valle, M., Potentiometric bioelectronic tongue for the analysis of urea and alkaline ions in clinical samples. *Biosens. Bioelectron* **2007,** *22* (9), 2171-2178.
20. Gallardo, J.; Alegret, S.; Muñoz, R.; De-Román, M.; Leija, L.; Hernández, P. R.; del Valle, M., An electronic tongue using potentiometric all-solid-state PVC-membrane sensors for the simultaneous quantification of ammonium and potassium ions in water. *Anal. Bioanal. Chem* **2003,** *377* (2), 248-256.
21. Askim, J. R.; Mahmoudi, M.; Suslick, K. S., Optical sensor arrays for chemical sensing: the optoelectronic nose. *Chem. Soc. Rev.* **2013,** *42* (22), 8649-8682.
22. Rakow, N. A.; Suslick, K. S., A colorimetric sensor array for odour visualization. *Nature* **2000,** *406* (6797), 710-713.
23. Johnson, S. R.; Sutter, J. M.; Engelhardt, H. L.; Jurs, P. C.; White, J.; Kauer, J. S.; Dickinson, T. A.; Walt, D. R., Identification of Multiple Analytes Using an Optical Sensor Array and Pattern Recognition Neural Networks. *Anal. Chem.* **1997,** *69* (22), 4641-4648.
24. Anzenbacher, J. P.; Lubal, P.; Buček, P.; Palacios, M. A.; Kozelkova, M. E., A practical approach to optical cross-reactive sensor arrays. *Chem. Soc. Rev.* **2010,** *39* (10), 3954-3979.
25. Wu, M.-S.; Liu, Z.; Shi, H.-W.; Chen, H.-Y.; Xu, J.-J., Visual Electrochemiluminescence Detection of Cancer Biomarkers on a Closed Bipolar Electrode Array Chip. *Anal. Chem.* **2015,** *87* (1), 530-537.
26. Liu, C.; Wang, D.; Zhang, C., A novel paperfluidic closed bipolar electrode-electrochemiluminescence sensing platform: Potential for multiplex detection at crossing-channel closed bipolar electrodes. *Sens. Actuators B Chem.* **2018,** *270*, 341-352.
27. Xu, W.; Fu, K.; Ma, C.; Bohn, P. W., Closed bipolar electrode-enabled dual-cell electrochromic detectors for chemical sensing. *Analyst* **2016,** *141* (21), 6018-6024.
28. Crespo, G. A.; Mistlberger, G.; Bakker, E., Electrogenerated Chemiluminescence for Potentiometric Sensors. *J. Am. Chem. Soc.* **2012,** *134* (1), 205-207.
29. Zhai, J.; Yang, L.; Du, X.; Xie, X., Electrochemical-to-Optical Signal Transduction for Ion-Selective Electrodes with Light-Emitting Diodes. *Anal. Chem.* **2018,** *90* (21), 12791-12795.
30. Jaworska, E.; Michalska, A.; Maksymiuk, K., Fluorimetric readout of ion-selective electrode potential changes. *Electrochim. Acta* **2018,** *284*, 321-327.
31. Jansod, S.; Cuartero, M.; Cherubini, T.; Bakker, E., Colorimetric Readout for Potentiometric Sensors with Closed Bipolar Electrodes. *Anal. Chem.* **2018,** *90* (11), 6376-6379.
32. Jansod, S.; Bakker, E., Tunable Optical Sensing with PVC Membrane Based Ion-Selective Bipolar Electrodes. *ACS Sens.* **2019,** *4*, 1008-1016.
33. Niklasson, G. A.; Granqvist, C. G., Electrochromics for smart windows: thin films of tungsten oxide and nickel oxide, and devices based on these. *J. Mater. Chem* **2007,** *17* (2), 127-156.
34. Hoshino, K.; Okuma, M.; Terashima, K., Electrochromic Properties of Metal Oxide Nanoparticles/Viologen Composite Film Electrodes. *J. Phys. Chem. C* **2018,** *122* (39), 22577-22587.
35. Hoshino, K.; Nakajima, R.; Okuma, M., Improved electrochromic performance of viologen at an ITO-nanoparticle film electrode. *Appl. Surf. Sci.* **2014,** *313*, 569-576.

36. Cutler, C. A.; Bouguettaya, M.; Reynolds, J. R., PEDOT Polyelectrolyte Based Electrochromic Films via Electrostatic Adsorption. *Adv. Mater* **2002,** *14* (9), 684-688.
37. Nossol, E.; Zarbin, A. J. G., Electrochromic properties of carbon nanotubes/Prussian blue nanocomposite films. *Sol. Energy Mater. Sol. Cells* **2013,** *109*, 40-46.
38. Liu, X.; Zhou, A.; Dou, Y.; Pan, T.; Shao, M.; Han, J.; Wei, M., Ultrafast switching of an electrochromic device based on layered double hydroxide/Prussian blue multilayered films. *Nanoscale* **2015,** *7* (40), 17088-17095.
39. Liana, D. D.; Raguse, B.; Gooding, J. J.; Chow, E., Toward Paper-Based Sensors: Turning Electrical Signals into an Optical Readout System. *ACS Appl. Mater. Interfaces* **2015,** *7* (34), 19201-19209.
40. Chow, E.; Liana, D. D.; Raguse, B.; Gooding, J. J., A Potentiometric Sensor for pH Monitoring with an Integrated Electrochromic Readout on Paper. *Aust. J. Chem.* **2017,** *70* (9), 979-984.
41. Itaya, K.; Shibayama, K.; Akahoshi, H.; Toshima, S., Prussian-blue-modified electrodes: An application for a stable electrochromic display device. *J. Appl. Phys.* **1982,** *53* (1), 804-805.
42. Robin, M. B., The Color and Electronic Configurations of Prussian Blue. *Inorg. Chem.* **1962,** *1* (2), 337-342.
43. Neff, V. D., Electrochemical Oxidation and Reduction of Thin Films of Prussian Blue. *J. Electrochem. Soc.* **1978,** *125* (6), 886.
44. Kim, L. T. T.; Gabrielli, C.; Perrot, H.; Garcia-Jareno, J.; Vicente, F., Redox switching of Prussian blue thin films investigated by ac-electrogravimetry. *Electrochim. Acta* **2012,** *84*, 35-48.
45. Ho, K.-C.; Lin, C.-L., A novel potassium ion sensing based on Prussian blue thin films. *Sens. Actuators B Chem.* **2001,** *76* (1), 512-518.
46. Nguyen, B. T. T.; Ang, J. Q.; Toh, C.-S., Sensitive detection of potassium ion using Prussian blue nanotube sensor. *Electrochem. commun.* **2009,** *11* (10), 1861-1864.
47. Ghosh, T.; Chung, H.-J.; Rieger, J., All-Solid-State Sodium-Selective Electrode with a Solid Contact of Chitosan/Prussian Blue Nanocomposite. *Sensors (Basel)* **2017,** *17* (11), 2536.
48. Krishnan, V.; Xidis, A. L.; Neff, V. D., Prussian blue solid-state films and membranes as potassium ion-selective electrodes. *Anal. Chim. Acta* **1990,** *239*, 7-12.
49. Itaya, K.; Uchida, I.; Neff, V. D., Electrochemistry of polynuclear transition metal cyanides: Prussian blue and its analogues. *Acc. Chem. Res.* **1986,** *19* (6), 162-168.
50. Soda, Y.; Bakker, E., Quantification of Colorimetric Data for Paper-Based Analytical Devices. *ACS Sens.* **2019,** *4* (12), 3093-3101.
51. Erenas, M. M.; de Orbe-Payá, I.; Capitan-Vallvey, L. F., Surface Modified Thread-Based Microfluidic Analytical Device for Selective Potassium Analysis. *Anal. Chem.* **2016,** *88* (10), 5331-5337.
52. Rho, J.; Yeon, S. Y.; Chung, T. D., Sensitivity-Tunable and Disposable Ion-Sensing Platform Based on Reverse Electrodialysis. *Anal. Chem.* **2020,** *92*, 8776-8783.

Chapter 6: Self-powered colorimetric sensing array based on ion-selective electrodes.

This work has been submitted.

6.1 Abstract

A self-powered absorbance-based colorimetric sensor array empowered by ion-selective electrodes (ISE) in short circuiting system is first presented. The cell voltage is maintained at zero, an adequate potentiometric response serves as a power generator directly transfer the power by the same amplitude to a potential-dependent Prussian Blue (PB) film in contacting electrolyte in a separate compartment. This allows one to activate a color change of the PB film without a use of an external power supply, where a redox potential of PB indicator is enabled between 50 and 250 mV (vs. Ag/AgCl). This potentiometric energy originated by membrane potential is proportional to ion activity in sample with respect to Nernst equation. Higher cation activity in sample generates more power and right enhances the PB absorbance, which serves as an analytical signal. Self-powered optical sensor array indicated by hydrogen-ISEs is utilized as a model. A measuring range is chemically tuned by varying pH of an aqueous inner solution of the ISE, allowing one to spontaneously determine the pH from 3 to 10.5. In optimal condition, this sensor is independent of ionic strength effect and successfully applicable for quantitative analysis in turbid/colored real samples including red wine, coke, coffee, baking soda and antacid. These colorimetric outputs are well-correlated to reference methods (potentiometry and pH meter). PB film exhibits excellent reproducibility and faster response time up to 21 s compared to one where the cell potential is dictated by the external power source.

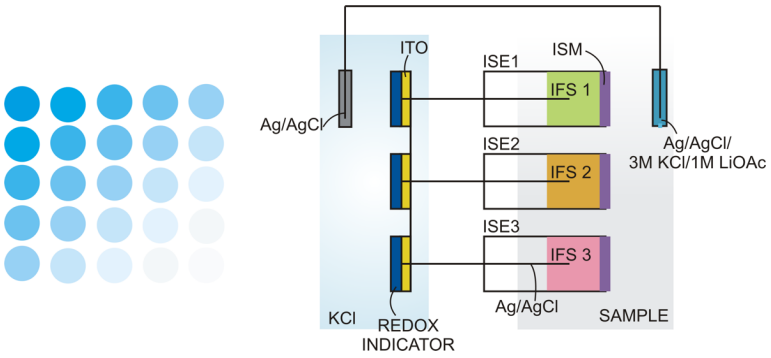

6.1 Introduction

Potentiometric ion-selective electrodes (ISEs) are well-established analytical tools for measuring a range of target ions.[1,2] While the pH probe is ubiquitous in most analyses involving aqueous solutions, sensors for other ions are most widely established in the area of clinical diagnostics of blood electrolytes.[3] More recently, they also found their way into environmental analysis as well as paper-based and wearable sensors.[4] These advances are partially driven by the need for remote or wearable sensing systems to draw as little power as possible.

To achieve integrated systems that are even more convenient, low cost, and small, one would require to integrate the power source into the device itself. If so, they would become a much lesser burden to the environment after being disposed of. Therefore, the design of integrated sensing systems without an external power source would be highly desired so that simple, low cost devices can be achieved.

Self-powered systems draw the energy needed for their operation without requiring an external power supply. Amperometric sensors, especially enzyme biosensors, have been shown to be spontaneously driven by the underlying galvanic cell reaction. They draw the required power from the sample itself, blurring the lines between a fuel cell and a sensor for a combined approach. Katz et al. developed an enzyme-based self-powered glucose sensor, generating different open circuit potential values dependent on glucose concentration.[5] The glucose utilized as a fuel is simultaneously oxidized at an anode while oxygen is reduced at a cathode. In the absence of fuel, the system did not generate a voltage. The OCP increased logarithmically showing a Nernstian dependence as expected. This concept has been expanded to other analytes, for example lactate[6] and ascorbic acid.[7] In other work, Miyake et al. demonstrated a fructose sensing device consisting of a biofuel cell coupled to an light-emitting diode (LED) system by using a capacitor as a transducer.[8] The charging rate of the capacitor that served as the power source was proportional to the fructose concentration. This capacitor discharged though the optical indicator, resulting in a characteristic blinking interval of the LED.

In contrast, potentiometric sensors are operated under zero current conditions. It is therefore not immediately obvious how they could be powered by the energy stored in the contacting aqueous solutions. Yet, a number of advances have recently appeared in the literature where ion-selective electrodes undergo transient currents after which a new electrochemical equilibrium state is reached. In this way, potentiometric measurements are possible while allowing work to be performed. So far, most of these concepts still require a power source to keep the cell potential to a constant value. Bobacka, for example, used this strategy to compensate the spontaneous membrane potential change of the sensor over a capacitive conducting polymer layer placed behind the ion-selective membrane.[9] This results in a current spike that can be integrated to give a charge as readout. Our group has recently adapted this approach to work with capacitive electronic components, giving even better-defined transients. The resulting sensors may exhibit an extremely high sensitivity that largely surpass that of potentiometric probes.[10]

Transient currents at constant potential have also been used to achieve a colorimetric readout from ion-selective electrodes. For this, an electrochromic material is placed in series with the ISE and, similar to above, the membrane potential change must be compensated over the electrochromic cell component to allow for the cell potential to remain constant. This results in a potential-dependent color change that indicates the sample ion activity directly

from the potentiometric sensor. Examples of this approach include the use of molecular redox indicators in a thin layer cell,[11,12] as well as polyaniline (PANI)[13] and Prussian Blue (PB) films.[14]

A limiting case of the concept described above involves the application of a constant potential of zero volts, which can be achieved without added power by short circuiting the cell. For example, an electronic capacitive component may be directly connected to the potentiometric cell to transfer the energy of the cell to the capacitor to perform work or to read it out later.

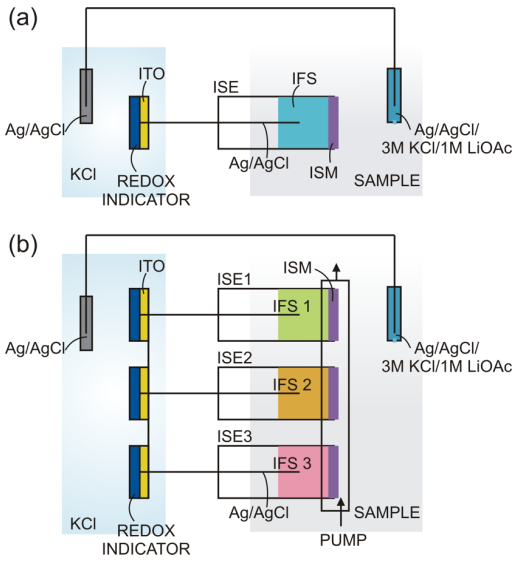

Scheme 1. Self-powered colorimetric ion-selective electrode platform, where the physically separated colorimetric signal is driven by the potential change at the sensing membrane. (a) A single sensor consists of a redox indicator (Prussian Blue film) coupled to an ion-selective electrode (ISE) by directly connecting the two reference elements as shown. This short circuiting imposes a constant potential of zero across the cell. (b) A corresponding self-powered colorimetric sensing array contains multiple electrochromic elements, each coupled to an ISE. IFS: inner filling solution. ISM: ion-selective membrane. ITO: transparent indium tin oxide electrode.

A self-powered sensing approach removes the instrumental tunability of the system by the amplitude of the applied potential. Consequently, it now requires chemical optimization. Here, the magnitude of the current transient depends on the charge required to change the potential of the electrochromic element to a value that compensates the potential of the ion-selective electrode. The energy originates in the membrane potential of the ISE: with aqueous inner solutions, the ion activity ratio on either side of the membrane is the driving force for the electrochromic transition reaction. To achieve this, the current transient imposes a discrete ion flux across the membrane. It is important for this ion flux not to change the value of the membrane potential once the transient current decays sufficiently to give the new electrochemical equilibrium state.

Only a few literature examples exist on self-powered readouts of potentiometric sensors. Rho et al. recently described a hue-based color generation of electrochromic PANI film activated by a potentiometric signal based on self-powered system.[13] The driving energy was increased proportionally by stacking ion-selective membranes, the concept of which was called reverse electrodialysis. This concept is promising and is still awaiting a thorough characterization. Another self-powered system was reported by Jaworska et al. where a reference element of high driving potential[15] in a cell containing a closed bipolar electrode was chosen to oxidize and release zinc ions into solution that in turn were assayed by fluorescence measurements. While this work uses an ion-selective membrane,

the concept is perhaps more analogous to an amperometric sensor because a continuous current is flowing through the cell.

Here, a self-powered optical sensor array is introduced where the power source is directly provided by an ISE. The cell voltage is maintained at zero by short circuiting, see Scheme 1. A pH responsive ISE is chosen as a model system that is connected in series to a Prussian Blue film in contact with a detection compartment that is separate from the sample solution. The reference electrodes of the two elements are connected together to complete the cell. The potentiometric response of the ISE directly drives the color change of the PB film, which reaches a new electrochemical equilibrium value upon each pH change in the sample. This allows one to measure colorimetric absorbance, which serves as the analytical signal. The measuring range is chemically tunable by varying the pH of the inner filling solution of the ISE, the membrane composition, and the electrolyte concentration in contact with the Prussian Blue element. This approach is shown to be applicable to the realization of optical sensor arrays, as demonstrated here in the direct colorimetric visualization of pH in the range of 3 to 10.5.

6.2 Results and Discussion

The cathodic conversion of Prussian Blue (PB) is known to produce Prussian White (PW), a process that is coupled to the insertion of potassium ion from the contacting electrolyte solution.[16] A color change of this film can be driven by a cation activity change in the sample as follows. A decreasing cation activity in the sample solution results in a potential decrease at the ion-selective membrane (ISM). Because the short-circuited cell remains at zero volts, the potential over the electrochromic PB film must change by the same amplitude. To achieve this, a net quantity of sample cations is transported from the inner solution across the ISM in direction of the sample. This is coupled to a partial oxidation of the inner Ag/AgCl element of the ISE, which removes sufficient chloride from the inner filling solution to maintain charge balance. The released electron from this process triggers the reduction of PB, resulting in turn in an extraction of potassium ion into solution.[14] The reference electrodes of the two compartments are connected to complete the circuit and maintain the potential. The electrochemical cell for the self-powered colorimetric detection of ion activity used here is written here for the detection of pH:

Ag | AgCl | KCl(ds) | **PB film** | ITO | Ag | AgCl | NaCl(is), pH(is) | **ISE membrane** | pH(sample) || 3M KCl | AgCl | Ag (1)

where ds, is, sample and rs stand for detection solution (in contact with the Prussian Blue film), inner solution (of the ion-selective electrode), sample solution and reference solution, respectively. As established, ITO is an indium tin oxide-based transparent electrode. The approach should be applicable for any ion for which a suitable ISE can be found. Closer inspection of eq 1 shows that the right hand side of the cell is in complete analogy to a potentiometric pH probe:

Ag | AgCl | NaCl(is), pH(is) | **ISE membrane** | pH(sample) || 3M KCl | AgCl | Ag (2)

For which the open circuit potential is established to obey the following equation:

$$E_{ISE} = s\log\frac{a_{Cl}^{aq}(rs)}{a_{H}(is)a_{Cl}^{aq}(is)} - s\,pH(sample) \quad (3)$$

The first potential term for the ISE may be varied by the composition of the inner solution to shift the potential as desired. For pH probes, the reference electrolyte is commonly fixed at 3M KCl and therefore not variable unless a double junction electrolyte system is chosen.

The left side of eq 1 depicts the colorimetric detection compartment,

$$\text{Ag | AgCl | KCl(ds) | } \textbf{PB film} \text{ | ITO | Ag} \quad (4)$$

and the half-reaction for the reduction of the PB film may be written as:[18]

$$KFe^{III}[Fe^{II}(CN)_6]_{film} + K^{+}_{(aq)} + e^- \rightleftharpoons K_2Fe^{II}[Fe^{II}(CN)_6]_{film} \quad (5)$$

(PB) (PW)

with its standard reduction potential reported as 0.238 V *vs.* Ag/AgCl at 25°C.[17] The absorbance change of the PB redox indicator in contact with KCl concentration as a function of potential has been confirmed to give near-Nernstian behaviour.[14] Consequently, the relationship between the electromotive force (EMF) and PB absorbance may be approximately described as:

$$E_{PB} = E^0_{PB} - s\log\frac{c_{PW}}{c_{PB}a_K^{aq}(ds)} \approx E^0_{PB} - s\log\frac{A_{\max} - A_{PB}}{A_{PB}a_K^{aq}(ds)} \quad (6)$$

where c_{PW} and c_{PB} are the concentrations of Prussian White and Prussian Blue in the electrochromic film, A_{max} and A_{PB} are the PB film absorbances at maximum and at a given equilibrium, respectively, and $a_K^{aq}(ds)$ is the potassium activity in the detection solution. As the electrochromic PB film acts as a potassium ion transfer mediator in the detection compartment the associated potential depends on the potassium ion activity. The potential of the complete detection cell also comprises an Ag/AgCl element and can therefore be described as:

$$E_{Detection} \approx E^0_{PB} + E^0_{AgCl/Ag} - s\log\frac{A_{\max} - A_{PB}}{A_{PB}a_K^{aq}(ds)^2} \quad (7)$$

Note that in pure KCl solution chloride and potassium activity are the same, explaining the square of the potassium activity in eq 7. This is here confirmed by a linear potential scan of just the detection cell. The peak potential shifts to more negative values with increasing KCl activity with a slope of 120.3 mV (Figure 1a) in agreement with eq 7 (see Supporting Information, Figure S1).

In principle, the KCl activity in the detection compartment may be used to help shift the potential to the desired value so that the colour change occurs in the range of desired sample concentration. As shown in Figure 1b, however, a 10 mM concentration gives unstable voltammetric behaviour and is not recommended. The PB film in contact with 0.1 M KCl or higher gave good stability for at least 15 cycles (Figure 1b), which should give a limited range of tunability of about 150 mV. Because a low reduction potential was desirable in this work, 0.1 M KCl was

chosen. The average peak potential of the PB cyclic voltammogram ($E_{1/2}$), where the concentration of PB and PW are approximately equal was found as 111 mV *vs.* Ag/AgCl (Supporting Information, Figure S2 left). This value agrees with the potential giving half maximum absorbance observed at 115 mV (Supporting Information, Figure S2 right). The total charge required to convert between PB and PW was found as 9.48 ± 0.03 µC and 9.55 ± 0.03 µC for the reduction and oxidation reactions, respectively.

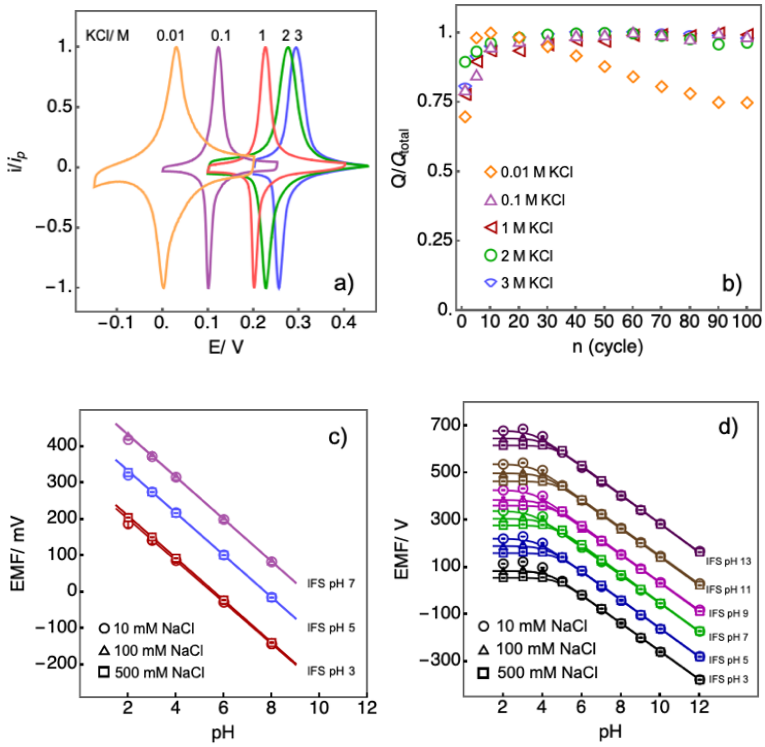

Figure 1. Top row: PB film in contact with different KCl concentrations (pH 2) in an isolated detection compartment. a) Normalized cyclic voltammograms *vs.* Ag/AgCl (cycle number 50) at a scan rate of 10 mV s^{-1}. b) Normalized integrated charges (anodic peaks) with increasing number of cycles. Bottom row: Potentiometric responses of H-ISEs *vs.* double junction reference electrode as a function of pH with different NaCl backgrounds, as indicated, in a 10 mM universal buffer. The ISMs are doped by c) hydrogen ionophore II and d) hydrogen ionophore I. IFS is the inner filling solution.

The energy required for the colour change of the PB film is driven by the membrane potential, which depends on the ion activity in the sample solution. Since the cell is short circuited, the two potentials in eq. 3 and 7 must sum to zero, giving a direct relationship between colorimetric response in the detection compartment and the pH of the sample:

$$pH(sample) = Constant + \log\frac{A_{\max} - A_{PB}}{A_{PB}} \qquad (8)$$

The constant shown may be chiefly optimized by pH of the inner solution, which can be varied in a wide range.

Figure 1c and 1d show the potentiometric responses (EMF) of polymeric pH probes containing the hydrogen ionophores I and II, optimized for different pH ranges (see Supporting Information for membrane compositions). As shown in Table S1, near-Nernstian slopes are found throughout. Changing the pH of the inner solution shifts the pH calibration curves in agreement with eq 3. The experimental E^0 values obtained from Figure 1c and 1d agree

with theoretical expectations (Supporting Information, Figure S3). This important characteristic allows one to match the potential ranges for the sensor and detection compartment in order to obtain a color response precisely in the pH range of interest. The possible shift is substantial, on the order of 600 mV.

Increasing the background electrolyte concentration in the sample is known to negatively affect the upper detection limit of the pH probe, which is especially pronounced with membranes containing tridodecylamine as ionophore (hydrogen ionophore I) (Figure 1d). This ionophore is more basic than hydrogen ionophore II, promoting electrolyte coextraction at low pH.[19] For this membrane the inner solutions of pH 7, 9 and 11 are best suited they give EMF responses that are independent from high salt concentration of NaCl between 50 and 250 mV. High salt concentrations of NaCl in the sample does not significantly affect the upper detection limit when doping the membrane with hydrogen ionophore II (Supporting Information, Figure S4), which is explained by the lower basicity of the ionophore.

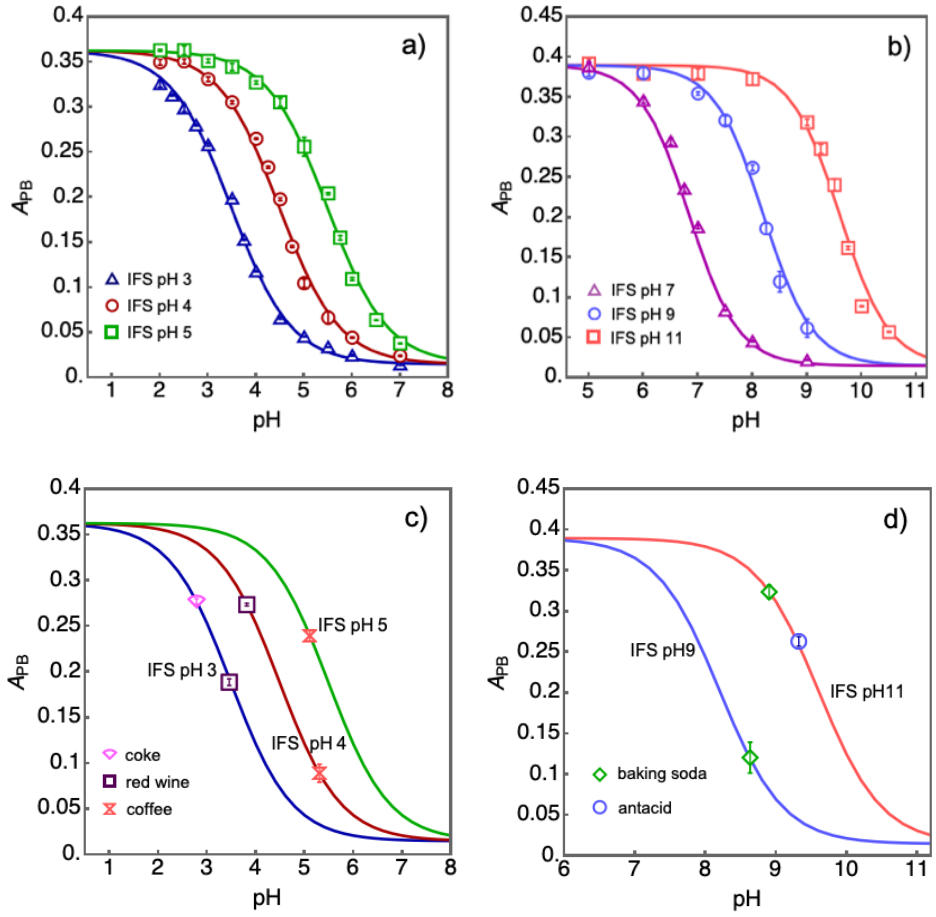

Figure 2. Self-powered optical calibration curves driven by H-ISEs, where the ion-selective membranes are doped by a) hydrogen ionophore II for acidic measurement and b) hydrogen ionophore I for alkaline determinations. IFS is the inner filling solution. The solutions contain 10 mM universal buffer with 10 mM NaCl and the PB array is in contact with an electrolyte of 0.1 M KCl (pH 2). Sigmodal calibration curves are fitted by the Boltzmann equation.[20] Observed PB absorbance of unmodified real samples in c) acidic region and d) alkaline region, as indicated.

A unique feature of this optical pH readout principle is that the color change is directly driven by the potentiometric pH probe. By definition, the practical pH is in fact defined as the output of such a calibrated potentiometric pH sensor. The self-powered colorimetric principle introduced here should therefore be free of the common biases that

are associated with indicator-based optical pH measurements. For example, ionic strength of the solution influences the activity coefficient of the charged indicator used in optical pH measurements, which has a direct impact on the value of the apparent dissociation constant and the associated pH, resulting in limited pH traceability. This aspect was evaluated by comparing the pH response of a bromothymol blue indicator as a function of ionic strength with that from the self-powered optical pH sensor proposed here, using a traditional potentiometric pH probe to cross-correlate, see Figure S5 in Supporting Information. Indeed, the ionic strength has no influence on the correlation with the bipolar sensing approach introduced here. In contrast, the apparent pH from the bromothymol blue measurements is found to shift to more acidic values with increasing NaCl concentration, as expected.

Under optimized conditions, the self-powered optical sensor is not markedly sensitive to high salt concentration one may typically find in the environment. The absorbance-based calibrations for the quantitative analysis of pH under acidic conditions are shown in Figure 2a (pH 3 – 6.5) while the alkaline range is evaluated in Figure 2b (pH 6.5 – 10.5). In both cases, the optical readout correlates well to the EMF signal from just the ISE (Supporting information, Figure S4). Unlike earlier work involving a potentiostat to maintain the potential, the energy used to trigger the absorbance does not originate from the external power supply[14] but from the sample itself.

Table 1. pH determination in unmodified real-world samples using self-powered colorimetric hydrogen ion selective electrodes (SD, *n*=3). The membrane electrode (H-ISE) and a commercial pH probe (pH meter) serve as reference methods.

samples	IFS (pH)	self-powered PB-ISE	H-ISE	pH meter	ΔpH	
					Self-powered *vs.* ISE	Self-powered *vs.* pH meter
coke	3	2.78 ±0.03	2.49 ±0.07	2.44 ±0.01	0.29	0.34
red wine	3	3.45 ±0.02	3.49 ±0.04	3.61 ±0.01	0.04	0.16
	4	3.81 ±0.01	3.50 ±0.02		0.31	0.20
coffee	4	5.30 ±0.10	4.92 ±0.01	5.01 ±0.01	0.38	0.29
	5	5.10 ±0.04	4.96 ±0.01		0.14	0.09
baking soda	9	8.63 ±0.11	8.60 ±0.35	8.51 ±0.03	0.03	0.12
	11	8.90 ±0.07	8.72 ±0.24		0.18	0.39
antacid	11	9.32 ±0.03	9.38 ±0.29	9.15 ±0.02	0.06	0.17

The self-powered colorimetric pH sensing array is confirmed to be highly selective and allows one to measure pH in a wide range of 3 – 10.5. Because the colorimetric absorbance is spatially separated from that of the sample, the pH of colored/turbid real samples covering coffee, coke, red wine, baking soda and antacid are successfully investigated as demonstrated in Figure 2c-d, see photographs of the colorimetric PB array in the Supporting Information. The results correlate well to the reference method (potentiometry using a pH meter) as shown in Table 1. The proposed self-powered device is a major advance over our previous work involving a potentiostat because the absorbance values are here generated without an external power source. Perhaps surprisingly, the response time

for PB conversion (charge of 9.5 μC) in the short-circuited cell was found as $t_{95\%}$ = 44 s (Figure S6), which is 20 s faster than in the previous work.[14]

6.3 Conclusion

A self-powered colorimetric readout based on ion-selective electrode has been introduced without requiring an external power supply. The potential of the pH probe must be adjusted chemically to the desired value imposed by the colorimetric redox indicator element, which is here chiefly performed by a suitable choice of the pH of the inner solution. The technique is robust and can spontaneously measure pH values from 3 to 10.5 in an array format with two different membrane compositions and appropriate pH values in the inner filling solution. Importantly, the device is insensitive to variations in ionic strength because the gold standard for pH measurements is the potentiometric probe upon which this principle is based. Of course, the approach may be combined with many other ISEs for the detection of other analytes of interest.

6.4 Acknowledgements

We thank the Swiss National Science Foundation (SNSF) for financially support. Dr. Sunil Kumar Sailapu and Stéphane Jeanneret are acknowledged for their assistance with the electronics aspects of the work. S.J. especially thanks the Swiss Government Excellence Scholarship.

6.5 Supporting information

Experimental section

Materials, reagents, and instrumentation. Hydrogen ionophore I (tridodecylamine), hydrogen ionophore II (ETH 1907), poly(vinyl-chloride) (PVC, high molecular weight), 2-nitrophenyl octyl ether (NPOE), sodium tetrakis-[3,5-bis- (trifluoromethyl)phenyl]borate (NaTFPB), tetradodecylam- monium tetrakis(4-chlorophenyl)borate salt (ETH 500), tetrahydrofuran (THF), potassium chloride (KCl), sodium chloride (NaCl), boric acid (H_3BO_3), phosphoric acid (H_3PO_4), acetic acid (CH_3COOH), hydrochloric acid (HCl), sodium hydroxide (NaOH), indium tin oxide (ITO glass slide 25×25×1.1 mm, surface resistivity 1.28–1.92 Ω cm^{-2}), iron(III) chloride hexahydrate ($FeCl_3 \cdot 6H_2O$) and potassium hexacyanoferrate(III) ($K_3[Fe(CN)_6]$) were purchased from Sigma- Aldrich. Real samples including coke, red wine, coffee, baking soda and antacid were purchased at a local market. An insulating transparent Scotch 3 M tape (50 μm thickness) and a metallic hole punch tool (0.8 mm diameter) were used. An IPC ISMATEC peristaltic pump (model ISM935C, Clattbrug, Switzerland), TYGON tubing (inner diameter 1.42 mm, wall 0.86 mm), and PTFE tubing (L × OD × ID = 300 mm × 1/16 × 100 μm, Supelco) were used in the flow system. The electrochemical measurement of cyclic voltammetry was performed in a faraday cage with a potentiostat/galvanostat PGSTAT 204 (Metrohm Autolab, Utrecht, The Netherlands) that was controlled by Nova 2.1.2 software. A tethered digital camera (Canon EOS 5D Mark II) equipped with a MP-E 60 mm macro lens and matching ring flash was used to capture the images from the detection cell. The solutions were prepared in Milli-Q water. The background electrolyte was 10 mM universal buffer (a mixture of 10 mM of boric acid, phosphoric acid and acetic acid) with 10 mM NaCl. A studio shooting tent box was purchased from PULUZ Technology Limited (Shenzhen, China).

The pH meter, platinum electrode rod and double junction reference electrode were sourced by Metrohm. Ostec electrode body was purchased from Oesch Sensor Technology, Sargans, Switzerland.

Preparation of hydrogen ion-selective membrane (H-ISM). The membrane was doped by an ionophore (15 mmol kg^{-1}), either hydrogen ionophore I or hydrogen ionophore II. The membrane also contained NaTFPB (5 mmol kg^{-1}), ETH 500 (90 mmol kg^{-1}), PVC, and NPOE plasticizer (1:2 by weight; total mass 200 mg). All components were completely dissolved in THF (2 mL). This cocktail solution was poured into a glass ring (22 mm i.d.) tightly fixed on a glass slide with rubber bands. The solution was evaporated overnight at room temperature. The homogeneous master membrane was punched into disks of 8 mm diameter. The membranes were conditioned in different pH values of 10 mM universal buffer for at least 3–4 h. The membrane was mounted in an Ostec electrode body. The inner filling solution of the ion-selective electrode was 10 mM universal buffer with 10 mM NaCl.

Potentiometric measurement. The potentiometric measurement of ISE-based PVC membranes was carried out against a commercial double junction reference electrode in a Faraday cage using a 16-channel EMF interface (Lawson Laboratories, Inc., Malvern, PA). The ion is transported to the ISEs by a peristaltic pump through the inlet and waste to bulk solution through the outlet. The reference electrode was placed in the bulk solution in the beaker.

Fabrication of patterned ITO array.[1] A conductive ITO film-coated glass electrode was etched into smaller channels. The glass electrode was entirely placed by the insulating tape. A liner gap was disclosed by a cutter, this exposed ITO film vanished by immersion in concentrated HCl for 10–20 min. The entire tape was removed. The patterned ITO array was rinsed many times by Milli-Q water until there was no acid residue left on the electrode. It was then dried at room temperature. The surface resistivity of the etched tiny gap was measured by a digital ohmmeter. If these channels were disconnected or isolated from each other, the resistance value of this exposed area should not be found. The patterned ITO array contained multi-channels in the same glass.

Electrochemical PB film deposition. The insulating tape was punched by a metallic hole (0.8 mm dia.) to form recesses. The tape was firmly placed on the pattern ITO array. The ITO electrode (working electrode) was immersed in the mixed solution of 20 mM $K_3Fe(CN)_6$, 20 mM $FeCl_3{\cdot}6HO$, and 10 mM HCl. The Ag/AgCl wire and platinum electrode rod were used as the reference and counter electrodes, respectively. The PB film was electrochemically deposited for 30 s by passing a cathodic current density of 2.0 A m^{-2} through the ITO electrode. Each channel was separately deposited. The PB film array was washed by 10 mM HCl before use.

Cyclic stability of PB film. The optical PB array in contact with 0.1 M KCl (pH 2) was stabilized by applied reversibly potential between 0 and 0.25 V (*vs*. Ag/AgCl) by cyclic voltammetry for at least 15 cycles before use in the self-powered system. The scan rate was 0.01 V s^{-1}. The PB electrode served as the working electrode and the Ag/AgCl acted as the counter/reference electrodes.

PB film disposal. The PB film deposited on the ITO electrode was discarded by rinsing with 10 mM NaOH followed by an abundance of Milli-Q water. The ITO electrode was dried at room temperature before use.

Camera settings and computational color analysis. The image was captured in the white bright studio shooting tent at ISO 800, f/6.3, flash power 1/128. The camera was set in front of the tent. The optical signals were recorded

with a tethered digital camera (Canon EOS 5D Mark II) equipped with a Canon MP-E 60 mm macro lens and a ring flash. Only the macro lens with the ring flash was in the tent. The camera captured all images in JPEG format, which were analyzed for absorbance. This involved importing each image, automatic cropping for the detection compartment area, and computing the absorbance from the red channel. The colorimetric absorbance (A) for any of three R, G or B was measured as shown;[1,2]

For the red channel: $A(R) = -\frac{1}{\gamma}\log\frac{I(R)}{I_0(R)}$

where I(R) and I_0(R) are the recorded red channel intensities of the PB film and the background, respectively. γ is the gamma correction (γ = 1/2) applied in the camera to make the image output more realistic to the human eye. The observed absorbance (A) from the image was obtained after removing gamma correction.

Boltzmann equation.

$$A = \frac{A1 - A2}{1 + e^{loga_i - x_0/dx}} + A2$$

where A1 is an initial absorbance, A2 is a final absorbance, X_0 is a center of the curve, dx is an ion activity constant

Real samples. Unmodified real samples including red wine, coffee, coke, baking soda and antacid were directly measured.

References

(1) Jansod, S.; Cherubini, T.; Soda, Y.; Bakker, E. Optical Sensing with a Potentiometric Sensing Array by Prussian Blue Film Integrated Closed Bipolar Electrodes. *Anal. Chem.* 2020, *92* (13), 9138–9145.

(2) Soda, Y.; Bakker, E. Quantification of Colorimetric Data for Paper-Based Analytical Devices. *ACS Sens.* 2019, *4* (12), 3093–3101.

Table S1. Experimental slopes of H-ISEs with different pH values of the inner filling solution and ionic strength of NaCl at 25°C.

Hydrogen ionophore	Inner filling solution (pH)	Ionic strength of NaCl (mM)	Slope (n=3) (mV pH^{-1})
I	3	10	59.73
		100	60.37
		500	59.69
I	5	10	60.38
		100	60.84
		500	60.35
I	7	10	59.28
		100	61.53
		500	60.62
I	9	10	60.04
		100	60.78
		500	58.97
I	11	10	59.93
		100	60.44
		500	59.87
I	13	10	60.66
		100	61.80
		500	60.78
II	3	10	57.17
		100	57.99
		500	57.99
II	5	10	57.99
		100	58.02
		500	58.02
II	7	10	58.02
		100	58.13
		500	58.13

Photographs of PB redox indicator in detection compartment for different samples using self-powered colorimetric hydrogen ion-selective electrodes platform.

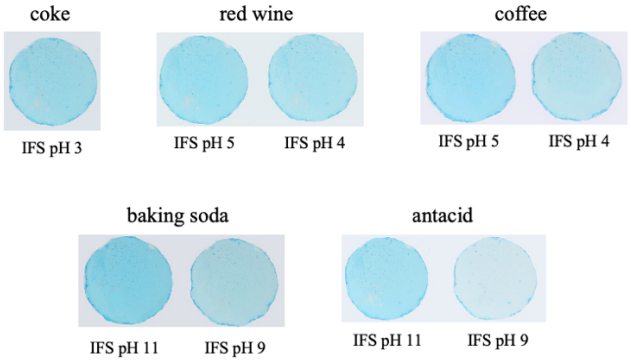

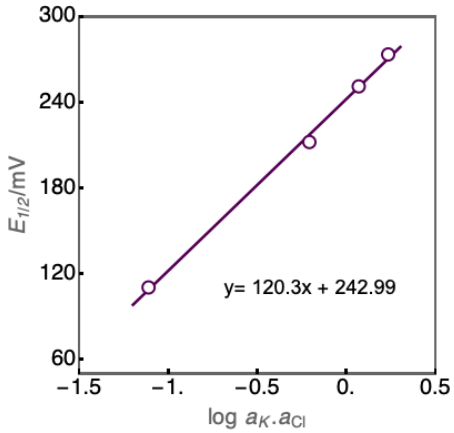

Figure S1. Linear relationship between peak potential ($E_{1/2}$) *vs.* Ag/AgCl element of PB film and logarithmic of potassium and chloride activities in the detection compartment only. The PB electrode in contact with KCl concentrations (pH 2) acted as the working electrode. The Ag/AgCl element served a counter/reference electrode.

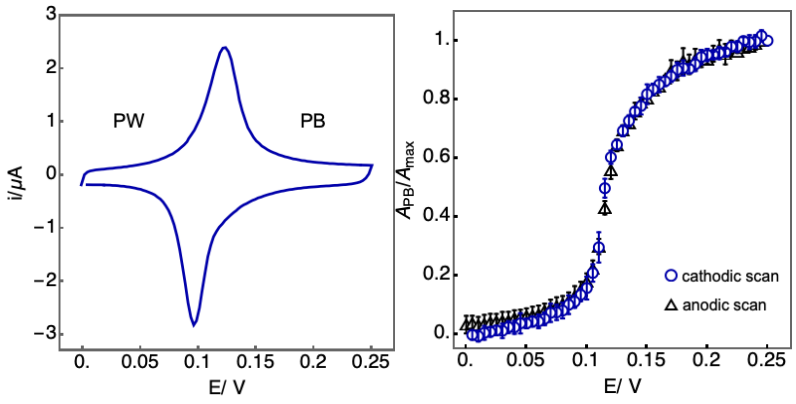

Figure S2. The potential-dependent of PB converses to PW in 0.1 M KCl (pH 2) *vs.* Ag/AgCl element. The experiments were performed in the detection compartment only. (left) CV response of the PB film (v =10 mV s^{-1}). (right) Corresponding PB absorbance with different constant applied potentials (SD, n=3).

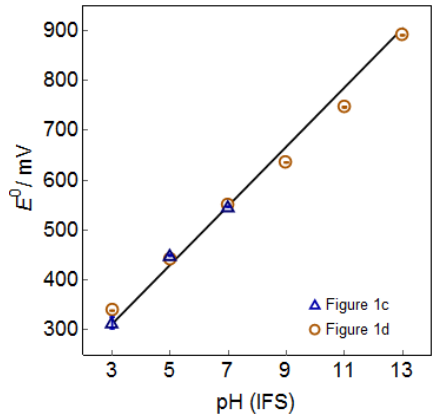

Figure S3. Comparison of the experimentally obtained E^0 values with pH of the inner filling solutions from Figure 1c and Figure 1d and comparison with theoretical expectation (solid line) in agreement with eq. 3.

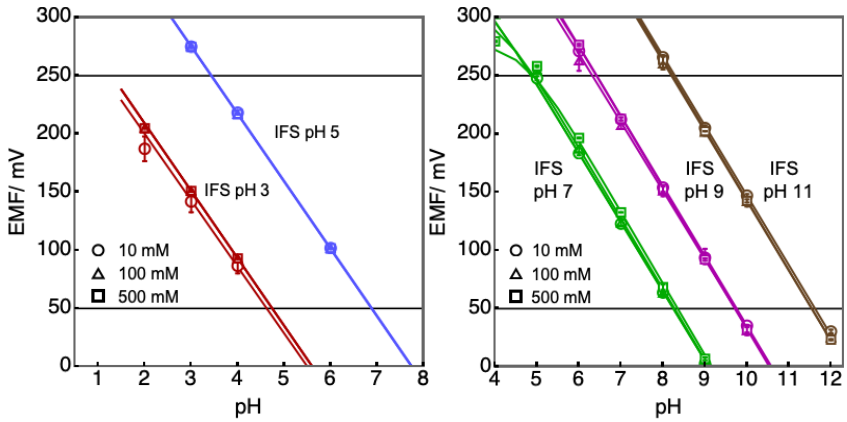

Figure S4. Potentiometric responses (*vs.* double junction reference electrode) of H-ISEs, where the hydrogen ion-selective membranes are doped with hydrogen ionophore II (left) and hydrogen ionophore I (right). IFS is the inner filling solution. The background electrolyte was 10 mM universal buffer with NaCl concentration of 10, 100 and 500 mM. The potential window between 50 – 250 mV is shown.

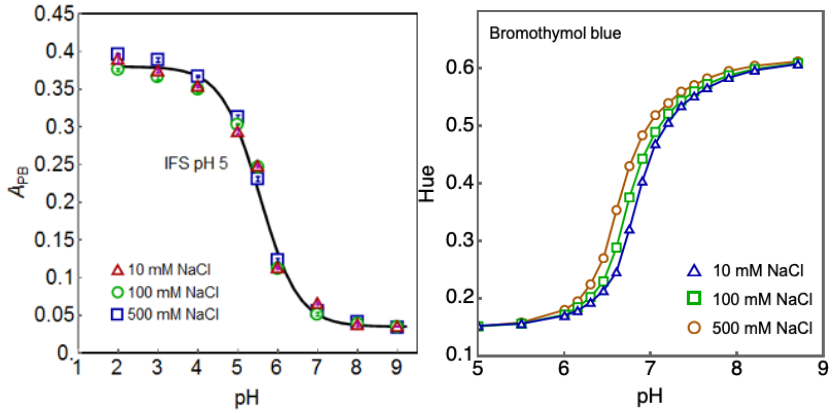

Figure S5. The effect of ionic strength of NaCl in background electrolyte of 10 mM universal buffer. (left) PB absorbance-based calibration, where the cell voltage was maintained at zero by short circuiting cell (self-powered). The PB film was immersed in 0.1 M KCl (pH 2) and the sensing membrane was prepared by using hydrogen ionophore II. The IFS was 10 mM universal buffer (pH 5) with 10 mM NaCl. (right) Hue-based calibration curves of water-soluble pH indicator dye (bromothymol blue).

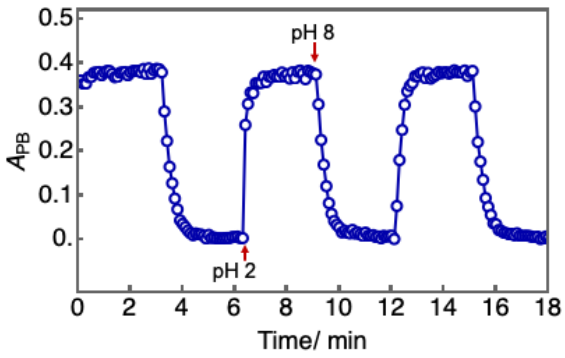

Figure S6. PB conversion by alternating the pH solution between pH 2 and 8 in the short-circuiting cell, where the PB film in 0.1 M KCl (pH 2) coupled to the H-ISE (inner solution of pH 5). The optical signal (blue dot) was recorded every 6 s by the digital camera.

6.6 References

[1] E. Bakker, P. Bühlmann, E. Pretsch, *Chem. Rev.* **1997**, *97*, 3083–3132.
[2] E. Bakker, E. Pretsch, *Angew. Chem. Int. Ed.* **2007**, *46*, 5660–5668.
[3] C. C. Young, *J. Chem. Educ.* **1997**, *74*, 177.
[4] L. Wang, D. Chen, K. Jiang, G. Shen, *Chem. Soc. Rev.* **2017**, *46*, 6764–6815.
[5] E. Katz, A. F. Bückmann, I. Willner, *J. Am. Chem. Soc.* **2001**, *123*, 10752–10753.
[6] C.-H. Chen, P.-W. Lee, Y.-H. Tsao, Z.-H. Lin, *Nano Energy* **2017**, *42*, 241–248.
[7] A. Zloczewska, A. Celebanska, K. Szot, D. Tomaszewska, M. Opallo, M. Jönsson-Niedziolka, *Biosens. Bioelectron.* **2014**, *54*, 455–461.
[8] T. Miyake, K. Haneda, N. Nagai, Y. Yatagawa, H. Onami, S. Yoshino, T. Abe, M. Nishizawa, *Energy Environ. Sci.* **2011**, *4*, 5008.
[9] E. Hupa, U. Vanamo, J. Bobacka, *Electroanalysis* **2015**, *27*, 591–594.
[10] P. Kraikaew, S. Jeanneret, Y. Soda, T. Cherubini, E. Bakker, *ACS Sens.* **2020**, *5*, 650–654.
[11] S. Jansod, M. Cuartero, T. Cherubini, E. Bakker, *Anal. Chem.* **2018**, *90*, 6376–6379.
[12] S. Jansod, E. Bakker, *ACS Sens.* **2019**, *4*, 1008–1016.
[13] J. Rho, S. Y. Yeon, T. D. Chung, *Anal. Chem.* **2020**, *92*, 8776–8783.
[14] S. Jansod, T. Cherubini, Y. Soda, E. Bakker, *Anal. Chem.* **2020**, *92*, 9138–9145.
[15] E. Jaworska, A. Michalska, K. Maksymiuk, *Anal. Chem.* **2019**, *91*, 15525–15531.
[16] K. Itaya, T. Ataka, S. Toshima, *J. Am. Chem. Soc.* **1982**, *104*, 4767–4772.
[17] V. Krishnan, A. L. Xidis, V. D. Neff, *Anal. Chim. Acta* **1990**, *239*, 7–12.
[18] K. Itaya, I. Uchida, V. D. Neff, *Acc. Chem. Res.* **1986**, *19*, 162–168.
[19] E. Bakker, A. Xu, E. Pretsch, *Anal. Chim. Acta* **1994**, *295*, 253–262.
[20] M. M. Erenas, I. de Orbe-Payá, L. F. Capitan-Vallvey, *Anal. Chem.* **2016**, *88*, 5331–5337.

Chapter 7: Conclusions and Outlook

The main goals of the thesis have been the fabrication and development of integrated devices by coupling optical sensing and potentiometric sensing systems into a closed bipolar electrode configuration where the detection compartment is physically separated from the sample solution. Some major limitations of traditional optical sensors (i.e., optical interferences, requirement of extra-thermodynamic assumptions, narrow working range) may be overcome. The final goal of the work was to fabricate self-powered integrated devices by removing the external instrumental tunability. Here, the potentiometric probe in the bipolar electrode draws the energy at the ion-selective membrane, which is exploited as a self-generated power to trigger the optical readout at detection compartment, which is utilized as analytical signal. The proposed integrated systems are successfully established for achieving quantitative analysis.

Optical sensors are very attractive tools owing to their simple readout, ease of miniaturization and the possibility of naked eye detection that requires no power. Unfortunately, optical sensors for the detection of ions (ion optodes) require extra-thermodynamic assumptions that are often difficult to understand and that make them difficult to compare to other established sensing principles. Variations in ionic strength of the sample, for example, give deviations because the optical readout typically depends on concentration while the underlying sensor principle responds to ion activities. Moreover, the optical readout may be hampered by turbid, opaque or colored samples, which places practical limits on their applicability. The working range is normally quite narrow in comparison with electrochemical probes.

The principal aim of this thesis was to overcome to above mentioned limitations by integrating optical and potentiometric sensors (ion-selective electrodes, ISEs) by means of a closed bipolar electrode platform. In this manner, the detection compartment is spatially separated from the sample solution. The signal of most optical sensors is based on a change of spectral properties, whereas the membranes of potentiometric probes are established to directly respond to the ion activity of the analyte. Potentiometric principles have been widely integrated into other readouts. The examples include chronopotentiometric, coulometric, voltametric and optical readouts (e.g., ECL, LEDs, fluorescence). However, none of them have translated the potentiometric response into an optical indicator readout.

The concept was first introduced by using a chloride responsive Ag/AgCl element as model example. The color of the water-soluble tris(1,10-phenanthroline) Fe(II) complex (ferroin) reversibly changes between red (reduced form) and blue (oxidized form). When the overall potential, controlled by the potentiostat in the assembled cell containing the bipolar electrode is kept constant, a change at the potentiometric probe must be compensated by the potential of the redox indicator. This results in a change of the redox species concentrations until the new equilibrium is reached. In case of measuring the analyte anion chloride, for example, the peak-shaped current response of the ferroin is found to shift to a more negative potential with increasing chloride activity. This results in an increase of the oxidized form of the redox indicator. A liquid membrane-based calcium-selective probe on the basis of a doped porous polypropylene (PP) membrane was then successfully constructed in the same bipolar electrode configuration (Chapter 3). This approach successfully expanded to traditional, more robust ISEs based on

plasticized PVC membranes. The sensors were used to demonstrate the successfully measurement of potassium concentration in real world samples such as commercial beverages and river and lake samples. The results from the proposed bipolar optode agreed with data from reference methods (Chapter 4). This approach has been applicable for a range of traditional ISEs. Still, the sensors may be limited by the available number of commercially available ionophores. The points that are of potential concern and may require improvement include the following: (i) the current transient (and associated charge) required to obtain the color change of the ferroin indicator. If the amount of charge is too high, it may result in ion fluxes across the membrane and associated potential drifts; (ii) the resistance of the sensing membrane and/or solution may affect the response time of the optical readout; (iii) the stability of the water-soluble ferroin indicator in the thin layer cell may be leaking and/or water evaporating; (iv) using hue values for readout is less quantitative than absorbance and may be influence by changes in ambient light; (v) the approach was found to be difficult to implement for the simultaneous determination of analytes because separate thin layer cells would need to be built for each potentiometric probe; (vi) mass transport of ferroin in the thin layer cell at detection compartment is found to be rate-limiting, giving relatively slow response times.

The drawbacks of the approach mentioned above were addressed by improving every key element in the bipolar measurement cell. The sensing membrane was doped with an inert lipophilic electrolyte (ETH 500) in order to reduce the resistance of the ion-selective membrane electrode, so that traditional potentiometric probes can be used. In the detection compartment, it was attempted to reduce the charge of ferroin indicator by dilution. Unfortunately, this resulted in a dramatic decrease of the sensitivity of the optical response. An electrochromic Prussian Blue (PB) film was therefore explored in order to replace the water-soluble ferroin indicator (Chapter 5). The PB thin film electrochemically deposited on the ITO demonstrated a better physical and chemical stability (no leaking, dispersing or/and evaporating), and an improved ease of fabrication by electrodeposition. The PB charge was stable and could be used for at least 85 cycles. The thin layer behaviour of the PB membrane was confirmed by cyclic voltammetry, suggesting that mass transport was not rate-limiting under the optimized conditions. Furthermore, the amount of PB maximum charge turnover could be controlled during electrodeposition of the PB film. The PB charge of 7.5 μC was found to be about six times smaller than with ferroin indicator (44 μC). This total charge of the PB may still perturb/polarize the ISE to some extent, but this was alleviated by reading out the optical signal of the PB film only after the transient current returned to zero, which took about 2 min. To make the readout more robust for quantitative analysis, the optical signal of the PB was computed into colorimetric absorbance. These steps made PB a more attractive electrochromic material for use as the optical sensor display. We further integrated the approach into a potentiometric sensing array by still using the closed-bipolar electrode platform. This allowed us to simultaneously measure different ions at the same location or/and samples. The selectivity of the sensors reflected the selectivity coefficients of the ISEs. Consequently, we demonstrated that each individual bipolar electrode in the sensor array was highly selective to its associated target ion. A miniaturized array of three array of three PB film spots deposited on ITO were shown as example. This handmade PB pattern may limit the number of PB spots on the ITO, and state-of-the-art microfabrication techniques or patterns may be beneficial in the future. The working ranges of the sensors introduced above (Chapter 3-5) were electrochemically modulated by using the potentiostat. However, while this system already has numerous advantages, it may not be elegant if the optical readout needs an assistance from a potentiostat.

A self-powered colorimetric absorbance-based PB array powered by the ISEs in a short circuited system was introduced for the first time without requiring an external power source (Chapter 6). This approach showed that ISEs can be made self-contained and self-powered. The energy at the ISE probe was directly transferred to the opposite pole in the bipolar electrode in the detection compartment, which contained the PB film in contact with electrolyte. The reference electrodes of the two compartments were completed the circuit and helped maintain a stable cell potential of zero. Since the power was generated only at the potentiometric probe, it was predictable how one could activate and change the color of the PB film between blue and transparent. We developed the theoretical framework and demonstrated the associated experimental results, which were a good match. Any number of PB-ISE bipolar electrodes can be inserted in parallel without instrumental complications. The working range was wide because it could be chemically modulated (instead of using electrochemical control) by adjusting the composition of the inner filling solution of the ISEs, the KCl concentration in contact with PB film and the ion-selective membrane composition. This possibility is very much unlike traditional optical sensors. To have an even wider working range, other optical materials may be needed. Other colorimetric materials may be promising to be used as the optical readout if their redox potential is low. This approach is applicable to other ISEs and may also be promising for the fabrication of self-powered wearable sensors in the future.

In a separate project not directly related to the above, we introduced a new molecular redox probe for ion-transfer voltammetry at ISEs (Chapter 2). This molecular redox probe was a lipophilic Os(II)/Os(III) complex and was dissolved into the sensing membrane. Because of the homogeneity of the membrane film their separate transducing layer as for example found with POT or PEDOT layers. The Os(II)/Os(III) redox probe was used to mediate ion transfer during its oxidation/reduction. The sensors could be made to measure cations or/and anions, depending on the membrane composition, which was easier than using POT or PEDOT as mediators. We found that in the presence of an asymmetric quaternary ammonium salt, a kinetic enhancement of the ion transfer process was observed because the peak separation and peak widths of Os(II)/Os(III) probe were reduced, which were near theoretical expectations. At this stage of the work, the selectivity of the sensors followed the lipophilicity order (Hofmeister series) because there was no ionophore in the sensing membranes. An addition of an ionophore would be important to develop practically useful sensors. Moreover, polyurethane as membrane material would help to increase the stability of the sensor.